



UNIVERSITÀ DEGLI STUDI DI PADOVA
Facoltà di Scienze MM.FF.NN.

Laurea Magistrale in Scienze della Natura

TESI DI LAUREA

**Holocene surface ocean conditions of the Norwegian Sea as
recorded by *Globigerina bulloides* (Mg/Ca ratios and $\delta^{18}\text{O}$)**

**Temperature superficiali del Mare di Norvegia nell'Olocene desunte dall'analisi
del Mg/Ca e degli isotopi stabili dell'ossigeno in *Globigerina bulloides***

Relatore: Dr. Luca Giusberti

Co-relatore: Dr.ssa Carin Andersson Dahl
The Bjerknes Centre for Climate Research
University of Bergen (Norway)

Laureanda: Luana Dei Tos

Anno Accademico 2010/2011

ACKNOWLEDGMENTS

I would like to express my gratitude to Dr. Carin Andersson Dahl and Dr. Bjørg Risebrobakken for the precious suggestions, discussions, supervision, improvements, critical reading and reviews on my thesis. The Bjerknes Centre of Climate Research and the University of Bergen are thanked for offer me the possibility to use their laboratories, facilities and resources.

A sincere thanks to my supervisor Dr. Luca Giusberti that carefully followed my work, reviewed it and that kindly helped me with the bureaucracy.

Vincent Scao is thanked for the technical assistance and training on the Mg/Ca cleaning method, for help during the analyses. Moreover I want to thank Rune Søråas for technical assistance for the preparation and measurements of the stable isotopes.

Alyssa Daigle, Mimy Wang and Kristina Elmer are thanked for correcting the English language and the grammar of this manuscript. Sara Borsoi is thanked for helping in developing the sites map.

RIASSUNTO

Durante il tirocinio svolto presso il Bjerknes Centre dell'Università di Bergen (Norvegia) mi sono occupata di ricostruzioni di paleotemperature nel Mar di Norvegia durante l'Olocene. Nello specifico sono stati analizzati esemplari di *Globigerina bulloides* (d'Orbigny, 1826) presenti nella carota di fondo MD95-2011 estratta dal fondale del Vøring Plateau (66.97 °N, 7.64 °E) a largo della Norvegia. *G. bulloides* è un foraminifero planctonico e il carbonato di calcio (calcite) del suo guscio viene generalmente secreto in equilibrio con l'ambiente circostante. La composizione del suo guscio riflette quindi le condizioni dell'acqua in cui la calcite è precipitata (es. temperatura e salinità). Tre *proxy* sono stati utilizzati per ricostruire le paleotemperature nell'intervallo studiato: composizione isotopica dell'ossigeno ($\delta^{18}\text{O}/^{16}\text{O}$), composizione isotopica del carbonio ($\delta^{13}\text{C}/^{12}\text{C}$) e rapporto tra Mg e Ca (Mg/Ca). Le paleotemperature ricostruite grazie a questi *proxy* mostrano un aumento di temperatura dalla base dell'Olocene (11.7 ka) fino a 0.5 ka. Quest'aumento di temperatura è stato già osservato in molti studi nel Nord Atlantico che ne confermano quindi l'attendibilità, ed è spiegato dall'aumento dell'insolazione invernale nello stesso periodo. Il primo Olocene (11.7-8 ka) è caratterizzato da un periodo freddo, centrato a 9.1 ka. Questo evento è presente anche in altri record nel Nord Atlantico (Came *et al.*, 2007) e testimonia che il famoso "8.2 ka event" non è l'unico abbassamento di temperatura di tale portata nel primo Olocene. Nella carota studiata *G. bulloides* registra nell'Olocene medio (8-3.6 ka) temperature relativamente stabili mentre i *proxy* basati su organismi fitoplanctonici (diatomee e alchenoni) evidenziano una fase calda nota come *Holocene Thermal Maximum* (HTM). Quest'anomalia è spiegata dall'aumento di insolazione estiva durante l'Olocene inferiore-medio: il fitoplancton che abita la zona eufotica registra maggiormente i cambiamenti di insolazione rispetto allo zooplancton che abita la parte sottostante della colonna d'acqua. Il tardo Olocene al Vøring Plateau (3.6-0 ka) è caratterizzato da un aumento di temperature ($\delta^{18}\text{O}$ record), come confermato da altri *proxy* misurati nella carota studiata e in altre carote del Nord Atlantico. Quest'aumento di temperature è spiegato da un intensificarsi dell'influsso delle acque Atlantiche e/o da un indebolimento delle acque Artiche. Nel complesso l'andamento dei *proxy* studiati nella carota MD95-2011 dimostra che *G. bulloides* registra in modo affidabile

l'evoluzione climatica dell'Olocene. Il lavoro svolto ha evidenziato tuttavia nei gusci di *G. bulloides* concentrazioni di Mg anomale che si traducono in temperature mediamente più alte rispetto a quelle ottenute da altri *proxy* (es. Mg/Ca su *Neogloboquadrina pachyderma* dx; Nyland *et al.*, 2006). Quanto emerso rende quindi necessarie ulteriori indagini sulle modalità di calcificazione in *G. bulloides*.

ABSTRACT

During my master project I have performed stable isotopes and Mg/Ca analyses of the foraminifera *Globigerina bulloides* (d'Orbigny, 1826) from the core MD95-2011 located in the Vøring Plateau in the eastern Norwegian Sea (66.97 °N, 7.64 °E at 1048 m water depth).

The North Atlantic represents a key area for the study of climate: here the warm Atlantic Water loses most of its heat, sinks and flow back southwards as part of the North Atlantic Deep Water. The Nordic Seas are strongly influenced by Atlantic, Arctic and Polar water. When the Atlantic water flux through the Norwegian Current is stronger, warmer conditions occur in the eastern Nordic Seas (the Norwegian Sea). The Holocene is the period that starts after the last glacial period at 11.7 ka BP and continues until the Present. This is the most recent warm period that has not been influenced by the human activity, for this reason the climate dynamics of this Epoch can reveal useful information to understand climate change dynamics and future climate.

Globigerina bulloides is a planktic dwelling foraminifer that populates the upper 50 m of the water column. It has a calcite test that is built in equilibrium with the surrounding water conditions. Therefore the isotopic content of the test reflects the water conditions in which the biogenic calcite precipitated. Shallow water dwelling foraminifera were thought to reflect insolation conditions like alkenones and diatoms (Jansen *et al.*, 2008), however recent studies (i.e. Thornalley *et al.*, 2009) show that *G. bulloides* reflect temperature and salinity more than insolation, however the interpretations of the information stored in the tests of this species are still not completely clear. This dissertation aims at clarifying the possible uses of this species as a paleotemperature and paleoinsolation proxy. This target is achieved by comparing the stable isotopes and Mg/Ca results with other paleo achieves from the same core and other cores in the North Atlantic. The results show a warming trend throughout the whole Holocene in agreement with the observations made in many other studies of cores of North Atlantic. The early Holocene shows a warming trend in the oxygen isotope record. The Mg/Ca record indeed displays a warm peak at 10.8 ka followed by a cold period that has its minimum at 9.1 ka BP. This cold period is assumed to be caused by the input of melt-water in the Nordic Seas during the beginning of the deglaciation. Slowly the fresh

water input stabilised and the actual circulation start to form at about 8 ka. The middle Holocene (4-8 ka BP) in the core MD95-2011 record is indeed characterised by a stable period. The late Holocene shows a slightly warming trend in the oxygen isotopes record that can be explained with a regression northwards of the Arctic front and an increase in heat and/or increased transport northwards. The Mg/Ca record is characterised by an odd warm period with mean temperature of about 15°C. This warm period recorded by Mg/Ca is seen in other records from the same core, although with lower amplitude (Andersson *et al.*, 2003; Risebrobakke *et al.*, 2003). This warm period is interrupted by a cooling period between 600-800 yr BP, which overlaps with colder foraminiferal SSTs.

The record of *Globigerina bulloides* in this study shows high variability in both the stable isotopes and Mg/Ca ratios. The Mg/Ca analysis of *Neogloboquadrina pachyderma* from the same core shows high variability. Many hypotheses were considered to explain this high variability. According to the more reliable hypothesis the changes in the water column during the calcification season can partly explain the observed variability. In such an unstable environment the water compositions may differ a lot from year to year, and this reflects on the test isotopic content. Temperature values higher than expected are seen throughout the whole Holocene in this record. This abnormality reflects higher assimilation of Mg in the test of *G. bulloides*. In other studies this is not seen, therefore it is not a normal behaviour of this species, but can have been forced from environmental causes. To answer this question more detailed studies are needed both on the paleontological record and on biological behaviour of the species.

INDEX

1. INTRODUCTION	p. 1
1.1 The Holocene	p. 2
1.1.1 Holocene climate	p. 4
1.1.2 Holocene climate in the MD95-2011 record	p. 7
2. OCEANOGRAPHY	p. 8
3. MATERIALS AND METHODS	p. 12
3.1 Core MD95-2011	p. 12
3.2 Chronology	p. 13
3.3 The Planktic Foraminifer <i>Globigerina bulloides</i>	p. 14
3.3.1 Taxonomy	p. 14
3.3.2 Stratigraphic and geographic distribution	p. 15
3.4 Paleotemperature Proxies Based On Stable Isotope Composition And The Mg/Ca Ratios	p. 16
3.5 Laboratory Procedure	p. 19
3.5.1 Picking procedure	p. 19
3.5.2 Stable isotopes analyses	p. 20
3.5.3 Mg/Ca analysis	p. 21
3.5.3.1 Tests cleaning	p. 22
3.5.3.2 Measurements	p. 24
3.6 Laboratory Instruments	p. 25
3.6.1 Mass spectrometer	p. 25
3.6.2 Inductively Coupled Plasma Spectrometer	p. 27
4. RESULTS	p. 29
4.1 Carbon Isotopes	p. 29
4.2 Oxygen Isotopes	p. 29
4.3 Mg/Ca Ratios	p. 29

5. DISCUSSION	p. 31
5.1 Carbon Isotopes	p. 31
5.2 Oxygen Isotopes	p. 31
5.3 Mg/Ca Ratios	p. 33
5.4 Comparison With North Atlantic Records	p. 36
5.5 High Frequency Variability	p. 39
6. CONCLUSIONS	p. 41

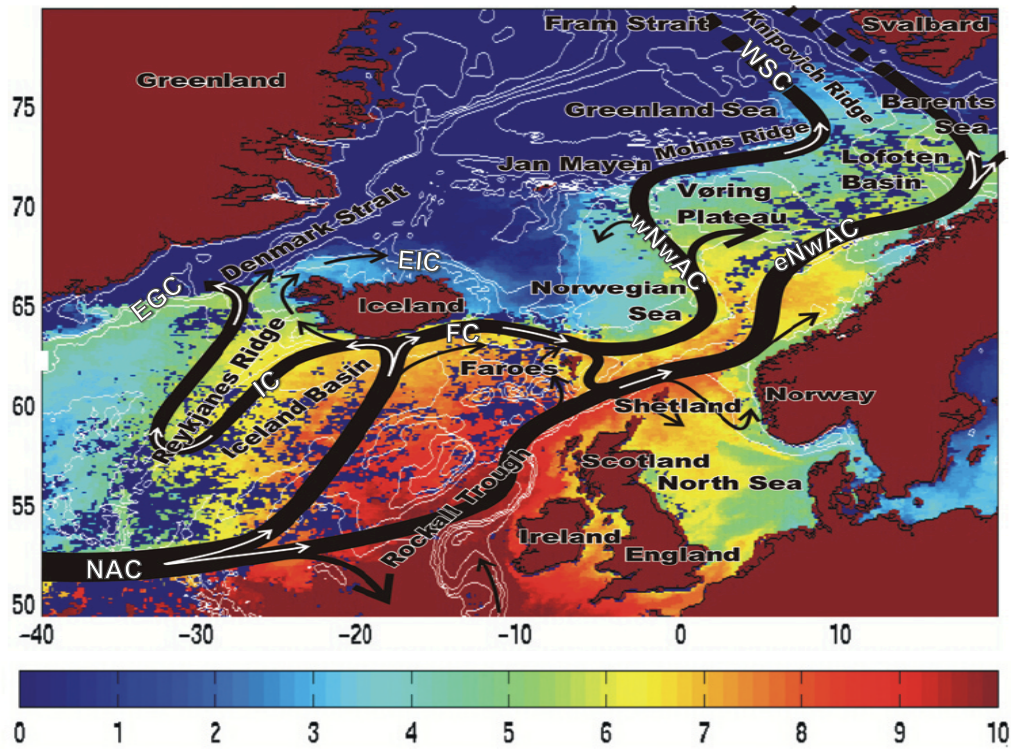
BIBLIOGRAPHY

APPENDIX I

1. INTRODUCTION

A better understanding of the key mechanisms driving climate change is crucial in order to predict future changes and assess human impacts on climate (Alley *et al.*, 2003; Gleckler and Weare, 1997; Sala *et al.*, 2000). Many studies and many models have been generated in order to predict the future climate conditions, e.g. the possible consequences of a warming in the North Atlantic (Barreiro *et al.*, 2008; IPCC, 2007; Rahmstorf, 1995; Stouffer *et al.*, 2006). None of the current climate models predicts an abrupt weakening or collapse of the Atlantic Meridional Overturning Circulation (AMOC) in the 21st century (Delworth *et al.*, 2008), but many drastic changes are expected. These changes include sea level rise in the North Atlantic of 80 centimetres and an increased probability of hurricane activity (Delworth *et al.*, 2008). IPCC (2007) climate models predict a mean global warming of 1.5-3°C during the next century. Depending on the future greenhouse gas level at high latitudes in future years, such an increase in temperature may have an impact up to twice the global mean temperature. In order to have an overview of the complex relations of all the factors that rule and influence the climatic variability, it is necessary to monitor the present conditions, and to also compare them with the geological past. Instrumental measurements of temperature and salinity in the North Atlantic date back to the late 19th century (Blindheim and Østerhus, 2005). Therefore, paleo archives are studied to obtain information on climatic records prior to the 19th century. Understanding the past natural variability helps in understanding the future variability and therefore the possible effects of future climate change. Recent studies amplify the knowledge on climate change dynamics, however many mechanisms and feedbacks of the climate system are still unknown and many investigations are focused on this topic. The most studied Epoch for paleoclimate reconstructions is the Holocene, the study of the climatic dynamics during this warm period can help to understand the future climatic dynamics. Consequently, the best period for paleoclimatic studies is the Holocene: the climatic conditions do not perfectly match present conditions, but they give knowledge on natural climate variability without human influence. Moreover, generally high resolution data can be obtained from sedimentary record for the Holocene and a number of studies have tried to understand and explain the Holocene climate variability (e.g. Came *et al.*, 2007; CCSP 2008; Farmer *et al.*, 2008; Houghton *et al.*, 1995; Jansen *et al.*, 2008).

A



B

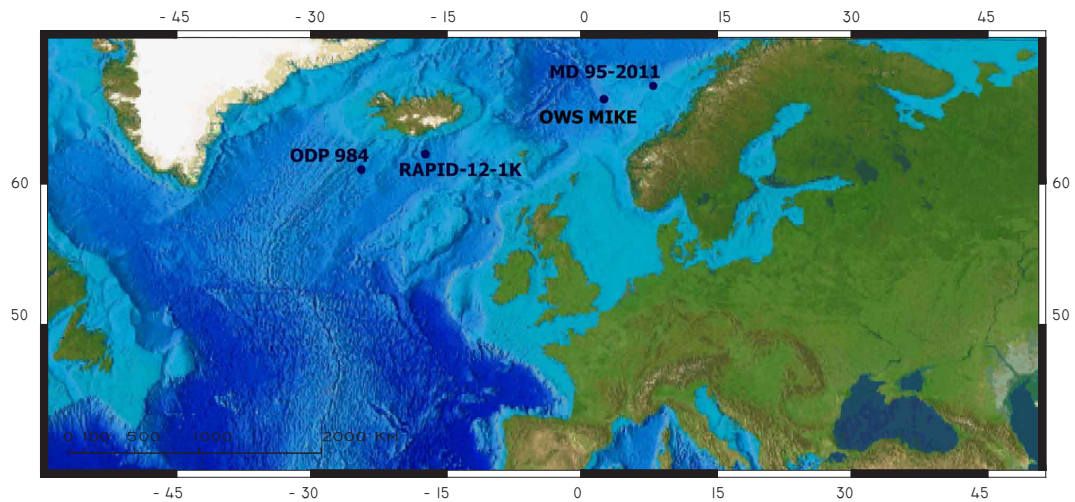


Fig. 1.1. Figure A, shows a schematic representation of the major near-surface currents in the Nordic Seas (dark arrows), the colours indicate sea surface temperature differences image in March 1991 (from Orvik *et al.*, 2002). Abbreviations: NAC = North Atlantic Current, EGC = East Greenland Current, EIC = East Icelandic Current, IC = Irminger Current, FC = Faroe Current, eNwAC = east Norwegian Current, wNwAC = west Norwegian Current, WSC = West Spitsberg Current.

Figure B, location of the cores MD95-2011 (this study), ODP Site 984 (Thornalley *et al.*, 2009), RAPiD-12-K1 (Came *et al.*, 2007), and Ocean Weather Ship MIKE (modified from NOAA, www.noaa.gov).

The Atlantic is crossed by the Gulf Stream. As one of the strongest currents in the world, the Gulf current moves huge quantities of water and heat towards higher latitudes in the North Atlantic, influencing temperatures in the North of Europe (Fig. 1.1A). While flowing northward this currents gradually loses its heat and sinks. At high latitudes the Atlantic water mixes with the Arctic waters and flows back southwards. The Nordic Seas, that include the Greenland Sea, the Icelandic Sea and the Norwegian Sea, represent a transitional zone between Atlantic and Arctic. Therefore the study of this area can provide helpful information in the study of the Atlantic currents dynamics, on the relation between Arctic and Atlantic influences on the water masses and its influence on the climate in the North Atlantic region.

1.1. The Holocene

Since 1759 when Giovanni Arduino coined the term Quaternary, the usage and the time span of this chronological unit have been unclear and together with Pleistocene it has been used as a synonym of Ice age for a long time. According to Lyell (1839) these two periods differed because the Quaternary (that he called 'Recent Epoch') includes the 'post-glacial' period that was later called Holocene. The Quaternary Period is included in the Phanerozoic Eon and it is the last of the three periods of the Cenozoic Era in the Geological Time Scale of the International Commission on Stratigraphy (ICS; Fig. 1.2). The Quaternary Period includes two Series/Epochs the Pleistocene and the Holocene, which is the most recent of the world history (Fig. 1.2). Gervais (1867-1869) was the first to use the term Holocene, which originates from the Greek words '*holo*' (whole-entire) and '*kainos*' (new), together meaning 'entirely new'. According to Gervais definition the Holocene was the 'post-diluvial deposits approximately corresponding to the post-glacial period'. The International Geological Congress (IGC) officially adopted the term Holocene in 1885. Three terms are still used as synonyms of Holocene: Recent, Post-glacial and Flanders. Recent and Post-glacial were mainly used in the past, but they are not recognised by the IGC. Thus these terms have no validity (Gibbard and van Kolfshoten, 2005). Flandrian indicates the temperate stages of the Quaternary, and accordingly to some interpretations it includes the present temperate episode (Walker *et al.*, 2009). However, this interpretation is not accepted worldwide. Accordingly, the term Holocene is preferred. Generally the Holocene is thought to have begun 10000 radiocarbon years before 1950 AD (Wolff, 2008). The Pleistocene-Holocene boundary

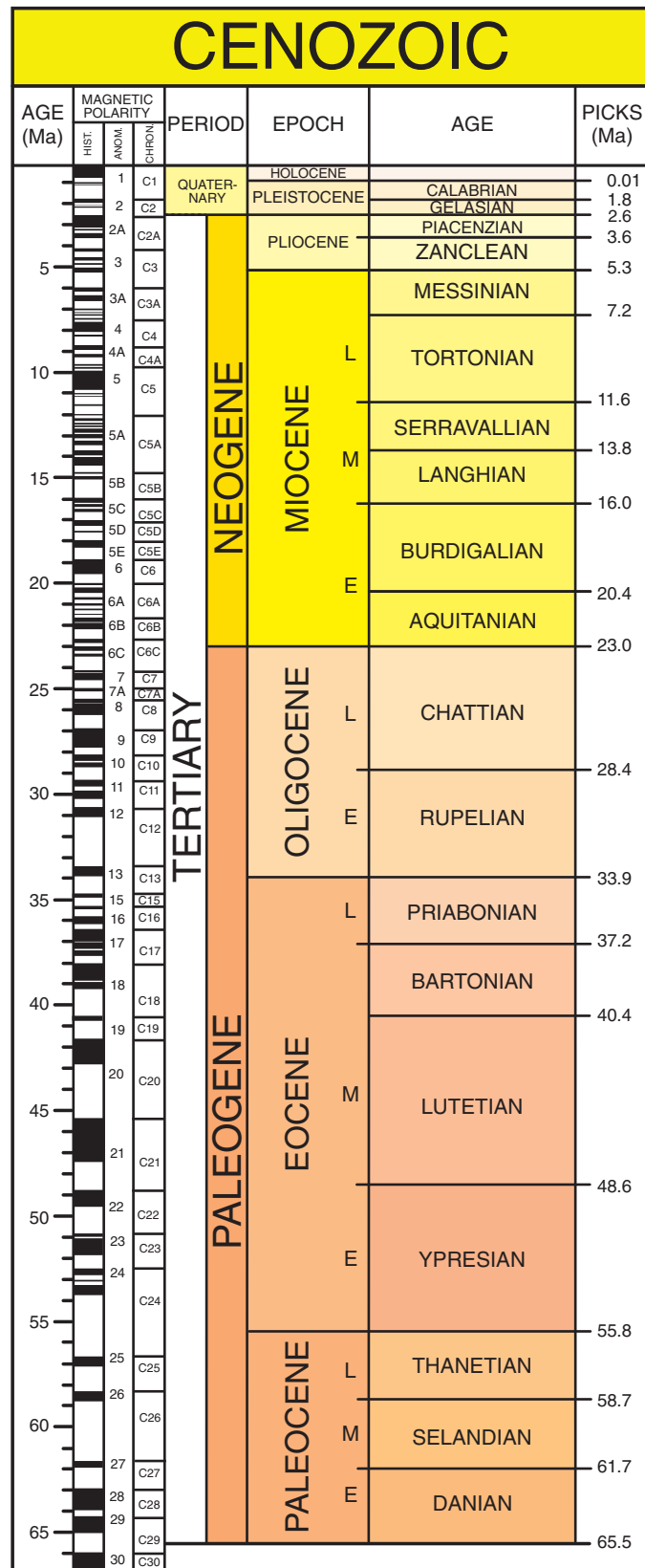


Fig. 1.2. Geological Time Scale of the Cenozoic (International Commission on Stratigraphy, ICS) from Walker and Geissman, 2009.

is identified by the Global Stratotype Section and Point (GSSP) defined by Walker *et al.* (2008, 2009) within the Greenland ice core NorthGRIP (NGRIP) located at 75.10° N, 42.32° W (Rasmussen *et al.*, 2006). This GSSP is unique since it is the only one defined on an ice core. For this peculiarity other auxiliary stratotypes have been defined, e.g. Litt *et al.* (2001). The Pleistocene-Holocene boundary is defined as ‘*the horizon that shows the clearest signal of climatic warming*’ and ‘*an abrupt shift in deuterium excess values, accompanied by more gradual changes in $\delta^{18}O$, dust concentration, a range of chemical species, and annual layer thickness*’ (Walker *et al.*, 2008, 2009) and it indicates the end of the last cold event of the Pleistocene. The Holocene starts at the end of the cold phase at the end of the Younger Dryas/Greenland Stadial 1 (GS-1). The Greenland Stadial 1 is an anomalous cold event that interrupted the postglacial warming displayed in the Greenland ice core NGRIP. The beginning of the Holocene was dated on the base of a multi-parameter annual layer counting and it is approximately 11700 years BP. The whole Quaternary tends to be subdivided by contrasting climatic events (geo-climatic units). Mangerud *et al.* (1974) on the base of the classification proposed by Blytt-Sernander a chrono-stratigraphic subdivision of the Holocene Epoch was suggested (Fig. 1.3). This allows the correlation between the different biological, climatic and morphostratigraphic divisions with metachronous boundaries valid for the north of Europe (Norway, Iceland, Sweden, Finland and Denmark). The Holocene has been divided into five chronozones with ^{14}C dated boundaries (Fig. 1.3). This subdivision has been applied not only in the north and centre of Europe but also in other parts of the world, although it was not originally designed for those regions. Recently a new unit following the Holocene has been proposed: the Anthropocene (Crutzen, 2002). The term Anthropocene indicates the current period characterised by global environmental changes. The Anthropocene has no precise beginning date, but may be considered to start with the Industrial Revolution (late XVIII century), an event strong enough to leave a worldwide track (Gibbard and Cohen, 2008).

In the following dissertation I adopted the terms early, middle and late Holocene. The early Holocene is the period between 10.5-8 ka BP, the middle Holocene the period between 8-4 ka BP and the late Holocene 4 ka-present.

Chronozone	Sub-division	Radiocarbon years B.P.
Subatlantic	Late	1000
	Middle	2000
	Early	2500
Subboreal	Late	3000
	Middle	4000
	Early	5000
Atlantic	Late	6000
	Middle	7000
	Early	8000
Boreal	Late	8500
	Early	9000
Preboreal	Late	9500
	Early	10,000

Fig. 1.3. Holocene subdivisions by Magerud *et al.* (2006).

1.1.1. Holocene climate

The Holocene was for long time considered a period with relatively stable climate (Grooties *et al.*, 1993), in comparison to the huge climatic variations that characterised the last glacial period. However, recent and more detailed studies have shown evidences of variability on decadal, centennial and millennial timescale (e.g. Bond *et al.*, 1997, 2001; Chapman and Shackelton, 2000; Cronin *et al.*, 2003; Denton and Karlén, 1973; Hurrell, 1995). Decadal time scale variability is still poorly documented, mainly because high resolution marine records are scarce. One of the main features of Early Holocene climate at middle and high latitudes in the Northern Hemisphere is the Holocene Thermal Maximum (HTM). The Holocene Thermal Maximum is characterized by warmer than present conditions. The sea surface temperature (SST) reconstructions for the North Atlantic based on alkenones and diatoms show warmer conditions than the present at 9-6 ka BP (Fig 1.4; e.g. Birks and Koç, 2002; Calvo *et al.*, 2002; Koç and Jansen 1992). Norwegian glaciers reach their minimum volume during the early and mid-Holocene (e.g. Nesje *et al.*, 2005). Ice core analysis of the Greenland ice cover shows a decrease in temperatures during the Holocene, with warmest conditions between 5-10 ka BP (e.g. Dahl-Jensen *et al.*, 1998; Vinther *et al.*, 2009). The Holocene Thermal Maximum was considered as a mere oceanic response to the Holocene orbital forcing, but timing and magnitude of this warm period vary between regions, moreover during this period the summer radiation decreased, indicating the involvement of other feedbacks and forcing (Renssen *et al.*, 2009 and references therein). During the Holocene sea surface dwellers show a decreasing trend in temperatures correlated with the decreased summer radiation (e.g. Calvo *et al.*, 2002). After the Holocene Thermal Maximum the temperatures show a lowering (Fig. 1.4), contrary to the cooling trend seen by the phytoplankton-based proxies, during the Holocene at high latitudes in the North Atlantic foraminiferal based proxies recorded a warming trend (e.g. Came *et al.*, 2007; Marchal *et al.*, 2002; Risebrobakken *et al.*, 2003). This difference was explained as due to variations in depth habitat and blooming seasons (Moros *et al.*, 2004) of these two groups. Alkenones and diatoms record summer temperatures in the euphotic zone and may record the response to the summer insolation, that decreases during the Holocene. Foraminifera and radiolarians indeed live in deeper water and can therefore record the response to winter insolation that slightly increases during the Holocene (Came *et al.*, 2007; Liu *et al.*, 2003). The deglaciation of large ice sheets started after the Younger Dryas cold phase at 11.7 ka BP

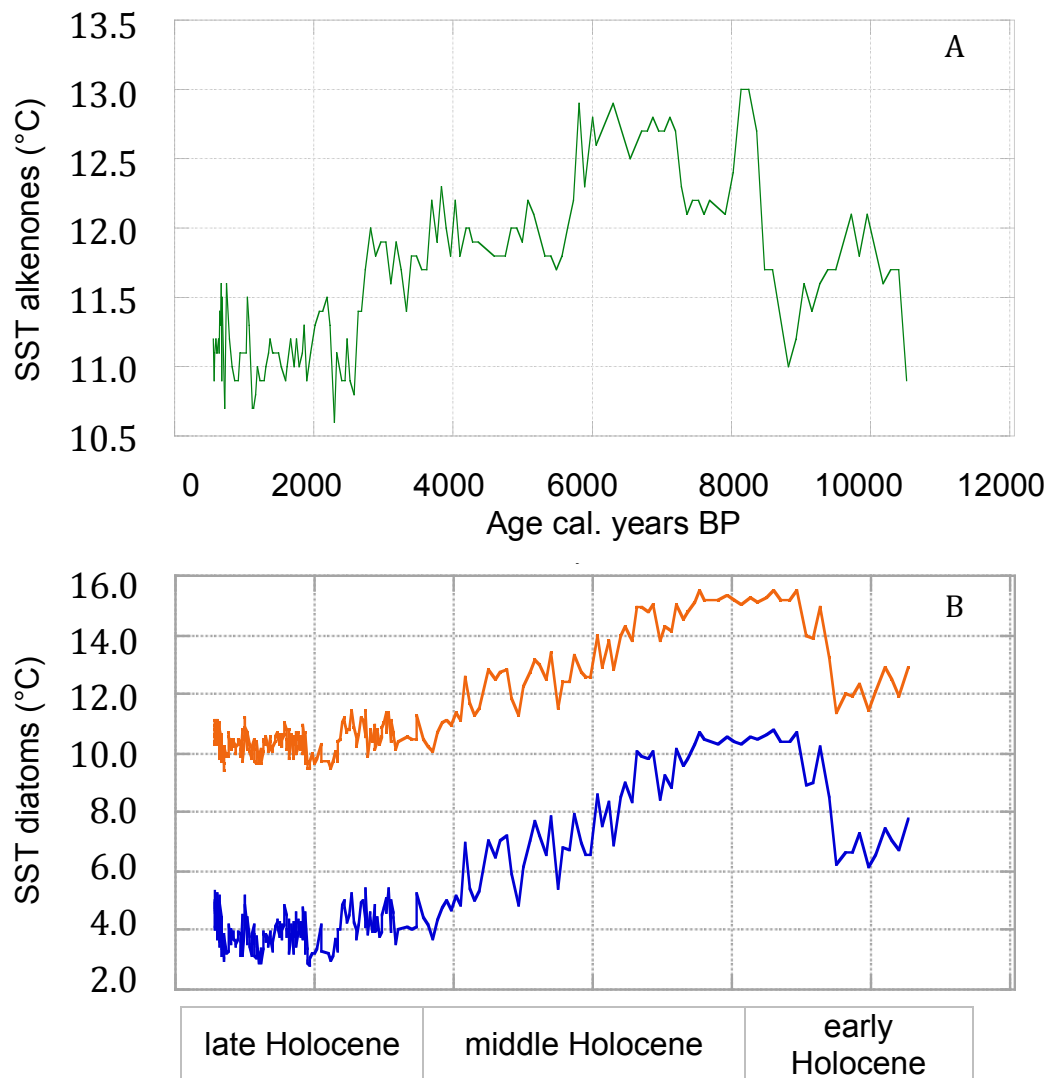


Fig 1.4. Alkenones and diatoms (Birks *et al.*, 2002) sea surface temperatures (SST) from the core MD95-2011 (Norwegian Sea). A, the green line represents the SST of alkenones (Calvo *et al.*, 2002). B, the orange line shows the SST of August and the blue the SST of February of diatoms (Birks *et al.*, 2002).

continued for several millennia after the Younger Dryas in the Northern Hemisphere (e.g. Peltier, 2004). The main part of the Laurentide ice sheet (LIS) persisted until 7 ka BP (Carlson *et al.*, 2008), the Fennoscandinavian ice sheet persisted until 9 ka BP (Linden *et al.*, 2006). The input of melted water during the early Holocene had a cooling effect at regional scale and reduced its impact of the increased summer insolation (e.g. Kutzbach and Webb, 1993). The Laurentide ice sheet is responsible for a delayed HTM in the northeast of Canada (Kaufman *et al.*, 2004), however the impact outside North America is still unclear (Renssen *et al.*, 2009). Risebrobakken *et al.* (submitted) suggests that during the early Holocene the high insolation was reflected in the high temperatures into the summer mixed layer (SML) at high northern latitudes. However, the insolation-driven warming did not affect the water temperature underneath the SML: for this reason the record from deeper dwellers do not show such high temperatures during the HTM. These are only hypotheses and the reasons for this offset are still not well understood.

A simplistic representation of the climate changes in the last millennium evidences a warm period called Medieval Warm Period (MWP). The MWP was interpreted as an effect of the Atlantic Meridional Overturning Circulation (AMOC; Lund *et al.*, 2006). A cold period called Little Ice Age (LIA) follows the MWP. The precise duration of these two periods is uncertain, and it changes according to the proxies and the standards that are used for the dating (Nesje *et al.*, 2005). The Medieval Warm Period is usually thought to last from X to XIII century (Lamb 1977, 1982). The LIA followed the MWP, and initially it was thought that these warm conditions had global distribution, with marked effects in the Northern Europe according to the recent studies (Mann, 2002). The LIA was, initially thought to be a single cold event, the latest of a series of ‘neoglaciations’ (Porter and Denton, 1967). In the Northern Hemisphere the LIA lasted from about 1460 to 1920, but it was divided in many cold events divided by several warm periods (Mann, 2002; Mann and Jones, 2003; Nordli *et al.*, 2003). Andersson *et al.* (2003) reported at least two cool events occurring during the year 400 and 100 BP at the Vøring Plateau. The AMOC is thought to have caused these events, although at the present state the only proved link between climate and AMOC is given by Lund *et al.* (2006). The present knowledge and resolution in the analyses does not allow a clear separation between the influence of the AMOC and the winds. In this study the LIA is not present, because not included in the analysed time span.

Many climatic records from different proxies recorded a cooling and freshening event, which occurred at around 8.2 ka BP (e.g. Alley and Ágústðóttir, 2005; Dahl and Nesje, 1994; Denton and Karlén, 1973). This event was initially named ‘*Finse event*’ (Dahl and Nesje, 1994). Later on it was seen in a widespread number of paleo-climatic archives, and now it is generally referred as the ‘8.2 event’. This is the terminology adopted in the following dissertation. This cooling event is not as severe as the Younger Dryas (YD) cold event, but more severe than the one occurred during the Little Ice Age (LIA; CCSP, 2008). This abrupt climate change brought cooling, freshening and dry conditions in the North Atlantic region (Alley and Ágústðóttir, 2005; Alley *et al.*, 1997). The sudden dragging of the proglacial Lake Agassiz in North America at about 8.3-8.4ka BP is assumed to be the cause of the 8.2 event BP (e.g. Clarke *et al.*, 2004; Ellison *et al.*, 2006; Klitgaard-Kristensen *et al.*, 1998). The fresh, cold water from the Lake Agassiz had a huge impact on the North Atlantic oceanic circulation, causing abrupt changes in the THC (e.g. Alley and Ágústðóttir, 2005). In the Northern Hemisphere the 8.2 ka event also represents a significant exception to the HTM. The presence of the 8.2 event is a helpful comparison point in the North Atlantic records, although in this study is not as marked as in other records.

Surface dwelling foraminifera, such as *Globigerina bulloides*, may help in reconstructing shallow water dynamics, late spring-summer temperatures and insolation. The possibility of using *G. bulloides* as proxy for these tasks has been checked in the following dissertation. Analysing the isotopic information registered in the calcite tests add more information to the foraminiferal record of the North Atlantic confirming the current knowledge and may help in answering the following questions: 1) Is the summer or winter insolation or a mean water temperature the main signal registered in the tests of *G. bulloides*? 2) Is *G. bulloides* faithfully recording the temperature or is it influenced by environmental conditions? 3) How does *G. bulloides* responds to climate changes?

North Atlantic record based on *G. bulloides* showed the same warming trend as deeper dwelling species such as *Neogloboquadrina pachyderma* showed in the Nordic Seas during the Holocene (Andersson *et al.*, 2010), however new data may strengthen this observation. The main Holocene climatic events are recognised in the record of *G. bulloides* and compared with the signals from other foraminiferal species and records from other locations in the North Atlantic.

1.1.2. Holocene climate in the MD95-2011 record

The early and middle Holocene in the MD95-2011 record is characterise by cold surface conditions influenced by the strong pervasive westerlies (prevailing winds) of the Arctic Front (Risebrobakke *et al.*, 2003). The foraminiferal record, in contrast with the phytoplanktonic (Birks and Koç, 2002; Calvo *et al.*, 2002), does not show evidence of the Holocene thermal maximum, since the Arctic Waters mainly influence the uppermost part of the water column, shallow dwelling species reflect warmer Atlantic water due to the increase summer insolation (Risebrobakken *et al.*, 2003). On the contrary, deeper dwellers as foraminifera are not influenced by the increased insolation (Andersson *et al.*, 2010; Risebrobakken *et al.*, submitted).

Around 8.1 ka BP the largest percentage increase in the amount of foraminifera and coarser grains is seen in the sediment, moreover the planktic $\delta^{18}\text{O}$ values of *Neogloboquadrina pachyderma* (sin.) at about 8.1 ka BP culminate in the most extreme cold event seen in the Holocene in this core (Risebrobakken *et al.*, 2003). The cooling during this period is of $\sim 3^\circ\text{C}$ (Risebrobakken *et al.*, 2003). This event is related to the outburst of melted water from the Canadian Lakes Agassiz and Ojibway (Risebrobakken *et al.*, 2003).

The late Holocene shows decreased planktic $\delta^{18}\text{O}$, increased planktic $\Delta\delta^{18}\text{O}$, lower abundance of *Globigerina quinqueloba* (a species connected with the Arctic Front) and high SST values (Risebrobakken *et al.*, 2003). These changes reflect a decrease influence of the Arctic waters at the Vøring Plateau. Risebrobakken *et al.* (2003) suggest that this is due to a relaxation of the atmospheric forcing. The temperatures between 1200-550 yr BP were mainly warm, warmer than in the 20th century up to 0.5-1 $^\circ\text{C}$ (Nyland *et al.*, 2006); this period corresponds to the Medieval Warm Period at the Vøring plateau. This warm period was interrupted by at least 2 cooling events centred at 850 and 630 yr BP (Andersson *et al.*, 2003). At around 600-700 yr BP a cooling trend marks the beginning of the Little Ice Age (LIA; Andersson *et al.*, 2003). Other three cooling phases similar for magnitude to the LIA were observed in the combined foraminiferal fauna and stable isotopic data at the Vøring Plateau. Reconstructions on *Neogloboquadrina pachyderma* (dex.) by Nyland *et al.* (2006) showed that water masses with different $\delta^{18}\text{O}_w$ signature have influenced the site, this can cause problems in the Mg/Ca temperatures calibration.

2. OCEANOGRAPHY

The Vøring Plateau in the Eastern-Norwegian Sea is located in a crucial position: right underneath the path of the Norwegian Atlantic Current (NwAC). The climate in the Norwegian Sea is influenced by three main water masses (Fig. 1.1B): Atlantic Waters, Arctic Waters, and Polar Waters. The main currents influencing the Vøring Plateau are: the warm-salty Norwegian Atlantic Current (NwAC), the cold southward flowing East Greenland Current (ECG), and the East Icelandic Current (EIC; Blindheim *et al.*, 2000). The EGC is a cold southward flowing current which brings water masses from the Arctic Ocean, part of its water forms a dense overflow that enriches the deep western boundary current in the North Atlantic. The EIC carries some of the water from of the East Greenland Current to the Icelandic and Norwegian Seas.

The North Atlantic region has a critical importance in the whole marine circulation: here the warm saline waters rich in nutrients coming from the south release heat to the atmosphere, becoming colder and sinking down (Broecker, 1997; Clark *et al.*, 2002; Dickson and Brown, 1994; Rahmstorf, 2006). The warm Atlantic water keeps the Norwegian Sea and part of the Barents Sea free from ice. The Gulf Stream is a warm Atlantic Ocean current that is formed in the Mexico Gulf and flows throughout the Florida Straits reaching the Atlantic Ocean (Fig. 2.1). Almost at 40°N 30°W it divides in two currents: one going northwards and eastwards, crossing the Atlantic towards Europe; the second is the Azores Current moving southward towards South Africa.

The North Atlantic Current (NAC) is the northward continuation of the Gulf Stream. Above the Mid-Atlantic Ridge at about 53°N the current bifurcates in two parts (Fig. 1.1A). One branch going straight northward to Iceland following the direction of the ridge, whereas the second branch flows eastwards into the Rockall Trough, Faroe Current (FC). South of Iceland the first branch of the NAC parts in two branches, one goes eastwards the East Icelandic Current (EIC) and one westward the Irminger Current (IC). The IC first goes southwards and then northwards around the Reykjanes Ridge. At about 65°N close to Greenland this current parts again one branch flows northwards through the Denmark Strait, the second branch goes southwards adding water mass to the East Greenland Current (EGC). The FC flows north-eastward into the Norwegian Sea maintaining its characteristic high speed. The current follows the topographic characteristic of the sea bottom. Before entering the Rockall Trough the second branch

of the NAC flows south to the Canary Islands (Canary current), however the main part of this branch keeps going north following the European coastline.

When the NAC enters the Norwegian Sea it has a temperature of about 6-9° C and a salinity range of 35.1 to 35.3 PSU (Pedersen *et al.*, 2005). The Atlantic water enters the Nordic Seas through two pathways: the Faroe-Shetland Channel, and the Iceland-Faroe Ridge (Orvik and Niiler, 2002). In the proximity of the Irish-Scottish shelf the branch of the NAC, the Shetland Current (SC), increases its speed (Burrows *et al.*, 1999) and flows through the Faroe-Shetland Channel (Fig. 1.1A) entering the Norwegian Sea, his branch is called eastern Norwegian current (eNwAC). The branch of the NAC that flows through the Iceland-Faroe Ridge is the Iceland-Faroe Front (IFF), this current is faster than the one flowing through the Faroe-Shetland Channel (Orvik and Niiler, 2002). This fast meandering warm superficial current (western Norwegian Atlantic Current, wNwAC) flows further north-eastward into the Norwegian Sea following the topography (Fig. 1.1B). The western limb of the NwAC follows the topographic slope of the Vøring Plateau and flows northwards toward the Jan Mayen. In the Nordic Seas the Atlantic waters lose their heat to the atmosphere. A third current is present closer to the coast, the Norwegian Coastal Current, (NCC). The main contribution to the NCC comes from the Norwegian Coastal Water (NCW). NCW is the sum of the freshwater coming from the Baltic Sea and from the Norwegian inland. The salinity of the NCW is lower than 34.5 and the temperature is lower than 5.5°C (Pedersen *et al.*, 2005). The NwAC flows northwards following the Norwegian Trench and outside Troms County it parts again (Fig. 1.1B): one limb, the North Cape Current (NCaC), goes westwards to the Barents Sea, one other limb, the Western Spitsberg Current (WSC) flows up to the Arctic ocean west of Svalbard (Hopkins, 1991). North of Svalbard the water of the WSC sinks below the Polar Water and continues as a subsurface current into the Arctic Ocean (Hald *et al.*, 2007). The warm water from the NwAC mixes with the Polar Water from the Arctic Ocean forming Arctic Water. A minor part of the WSC waters sinks forming deep waters, and partly merges with the EGC. From the Arctic Ocean the cold EGC moves surface and deep waters southern. Close to Northern Iceland this current parts in 2 limbs, one keeps going southwards following the Greenland coast, the other goes eastwards, moving water masses into the Icelandic and Norwegian Seas (Blindheim and Østerhus, 2005). Arctic waters are characterized by reduced temperatures and salinities compared to Atlantic waters, and seasonally they are

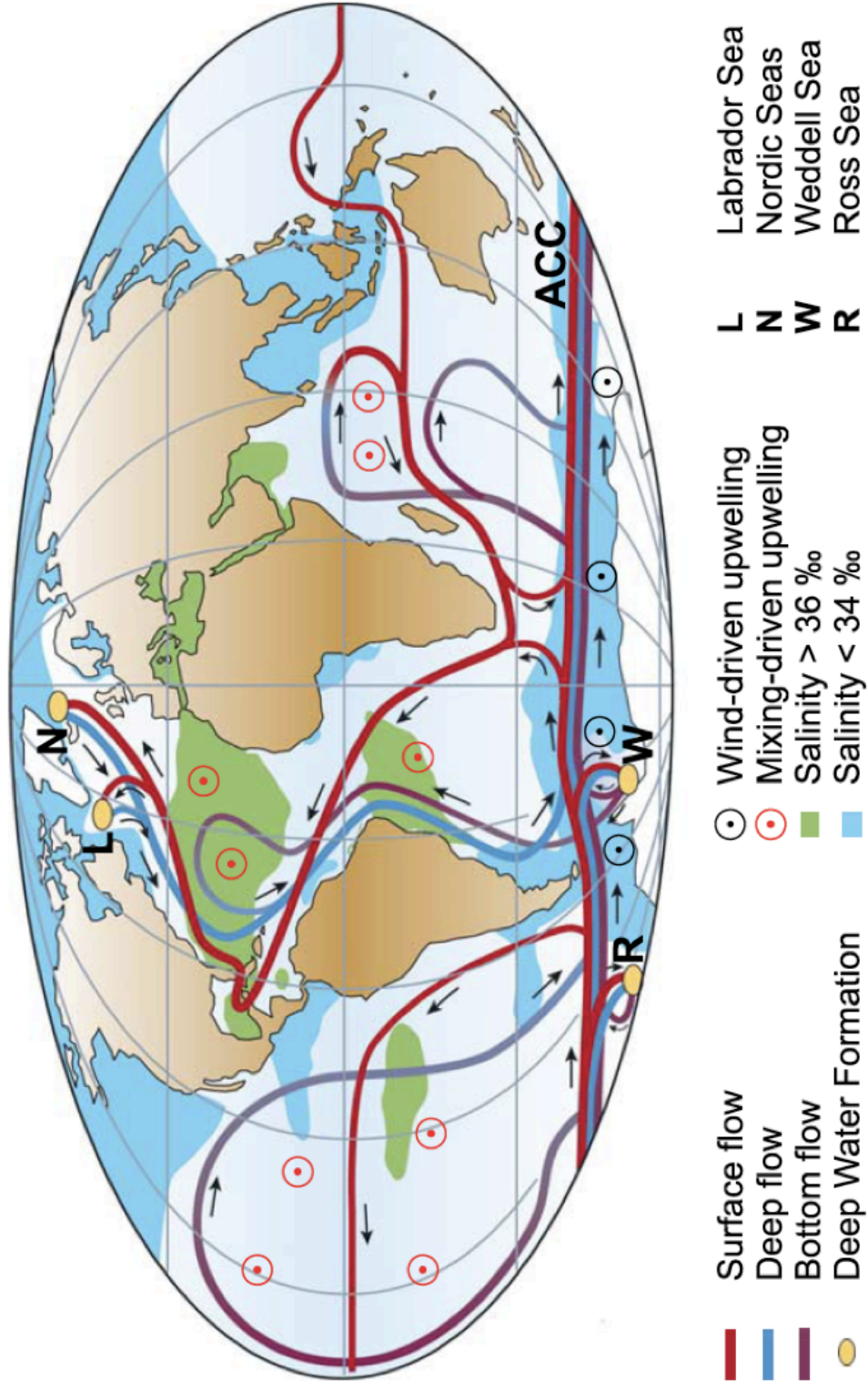


Fig. 2.1.1. Schematic overview of the global ocean circulation system (from Kuhlbrodt *et al.*, 2007).

covered by sea-ice. The Atlantic water and the Arctic water are separated by the Arctic front.

Climate and oceans are directly connected since the oceans store and redistribute the heat all around the world. Blindheim and Østerhus (2005) estimate that the total influx of Atlantic waters in the Norwegian Sea is 7,7 Sv, although the flux varies each year. The water transported by the Gulf Stream is warm and while flowing northwards it decreases its temperature, and it loses heat to atmosphere. The heat loss is higher at high latitudes where the difference in temperature between water and atmosphere is higher. Most of the heat loss from the seawater occurs in the Northern Hemisphere at a rate of 1.7 ± 0.2 PW (Ganachaud and Wunsch, 2000). Ganachaud and Wunsch (2000) calculated that the total heating lost from the water to the atmosphere in the Atlantic Ocean is 0.7 ± 0.2 PW ($1 \text{ PW} = 10^{15} \text{ W}$). The heat lost from the seawater is released into the atmosphere and this phenomenon permits a milder climate in the northeast of the North Atlantic than it would be without the AMOC. The dispersion of heat in the atmosphere creates mild conditions inland at high latitudes. The air temperature in the Nordic Seas is 10-20°C warmer than the global mean at the same latitudes (Drange *et al.*, 2005). Thanks to the Gulf Stream Scotland and Ireland have mild conditions whilst Norway and Iceland have habitable conditions. The milder conditions have effects on the whole biota in these areas, and permits the existence of species that otherwise would not survive at such high latitudes.

The oceanic currents are all connected in a global system (Fig. 2.1). Changes in water temperature and salinity force the water masses to move. Winds, differences in water density, the Coriolis effect and the input of water from the continents and the marginal basins are the main drivers of the ocean circulation. According to Delworth *et al.* (2008) the Atlantic Overturning Circulation (AMOC) is the ensemble of the water currents created by the density differences with the surrounding waters and the winds that force the water masses to move. The Thermohaline Circulation (THC), which is sometimes also called ocean conveyor belt, is defined by Rahmstorf (2006) as the complex of water fluxes driven from differences of density, heat and salinity. While the THC does not include the wind and tides component, the AMOC considers all the components, and this term will therefore be used in this thesis. The AMOC is formed by four main components: upwelling processes that pull deep water from the bottom of the ocean to the surface, surface currents that move light water at the ocean surface, deeper water formation regions where the water that becomes denser sink, and deep waters currents

(Kuhlbrodt *et al.* 2007). The four components are connected and form a current circulation that has two overturning cells at high latitudes: North Atlantic Deep Water (NADW) and Antarctic Bottom Water (AABW). NADW flows southwards at a depth of 1500-4500 meters (Delworth *et al.*, 2008). The AABW returns northwards below the depth of 4500 meters, it gradually rises until it reaches the lower part of the NADW (Delworth *et al.*, 2008). Depending on radiation frequency and water conditions the water in the upper 100 meters is heated by solar radiation (Morel and Antoine, 1994), though the majority of the radiation is absorbed in the upper 50 m (Nilsen and Falck, 2006). In the equatorial zone the heat allows the water to evaporate, the evaporation-precipitation rate is very high, so that the surface water is warm and rich in salt. This warm salty water layer is mixed by winds action and tides. The mixing creates a diapycnal gradient that spreads the warm salty water throughout the whole water column and causes internal waves in the ocean. The mixing decreases the density of the water at the bottom, and forces it to rise (Kuhlbrodt *et al.*, 2007). The anticyclonic subtropical gyre forces the resulting water to flow northwards.

3. MATERIALS AND METHODS

3.1. Core MD95-2011

Core MD95-2011 was cored during the IMAGES cruise campaign MD101 on-board the *R/V Marion Dufrense* in 1995 at 66.97 °N, 7.64 °E at 1048 m water depth (Fig. 1.1B). The core is situated at Vøring Plateau in the eastern Norwegian Sea. The core was recovered using a giant piston corer (CALYPSO), but due to over penetration of the piston corer the first centimetres of the core were lost, spanning approximately the last 500 years (Andersson *et al.*, 2010). The location of this site is right under the path of the NwAC. In this study, the upper 6,5 meters of the total 17,49 meters long core were studied. Many studies have been done on MD95-2011: diatoms assemblages (Birks and Koç, 2002), radiolarian record (Dolven *et al.*, 2002), alkenones (Calvo *et al.*, 2002), mineralogical quartz-to-plagioclase ratio (Moros *et al.*, 2004), stable oxygen records of *Neogloboquadrina pachyderma* (dex.), *Neogloboquadrina pachyderma* (sin.) and *Cassidulina teretis*, Mg/Ca ratios, foraminiferal census counts and foraminifer-based SST estimates for the Holocene (Andersson *et al.*, 2003; Andersson *et al.*, 2010; Nyland *et al.*, 2006; Riesebrøbakken *et al.*, 2003).

The studied core (MD95-2011) was sampled every cm from 0 to 745 cm (Riesebrøbakken *et al.*, 2003). The core was separated into 1 cm units. The samples were cleaned from the sand fraction and separated by using a rotating wheel for 24 hours. After the samples were sieved at 63, 125 or 150 and 500 µm using de-ionized water. The coarse and fine fractions were dried at 50°C and weighed afterwards. All the fraction-sizes are stored in vials at the Bjerknes Centre for Climate Research (BCCR) in Bergen. The samples of the core MD95-2011 are stored in vials divided on depth and dimensions. Each sample is already divided per size in < 63µm, >150 or > 125 µm and > 500µm. Foraminifera are almost all contained in the fraction between 63 and 500 µm. *Globigerina bulloides* is mainly contained in the fraction between 125-500 µm, even though some specimen can be found in the smaller fraction. Samples from every 5 cm depth were studied. In some cases it was not possible, because the coarse fraction of interest was not present or did not contain enough material, therefore nearest sample was used as a replacement.

3.2. Chronology

In order to work with the data obtained from the analysis, these have to be referred to a time data set. An age model was already calculated for this core from previous studies, but an updated age model has been preferred, thus all the dates have been recalculated. The chronology is based on linear interpolation between dated levels. The established age model for MD95-2011 for the considered interval (from 10,5 cm to 709,5 cm) rests on 23 Accelerator Mass Spectrometer (AMS) ^{14}C dated samples and the presence of the Vedde ash layer (12170 yr BP (Risebrobakken *et al.*, submitted)). The age of the Vedde ash is from Rasmussen *et al.* (2006). The levels were dated at the laboratories: Leibniz-Labor for Radiometric Dating and Isotope Research, Kiel (KIA), Centre des Faibles Radioactivite's, Gif sur Yvette (GifA), Laboratoriet for Radiologisk Datering, Trondheim (TUa) and Poznan Radiocarbon Laboratory, Poznan (Poz) (Tab 3.1). For the calculation of the calendar year the radiocarbon calibration program CALIB 6.0.0 (Stuvier *et al.*, 1998) was used. From precedent dating methods the best uncertainty (ΔR) and uncertainty error (ΔR_{error}) to build the age model in this study were used: ΔR of -3 ± 27 years (Manger *et al.*, 2006).

Four of the AMS ^{14}C dates obtained were not used, because they gave reversed ages (Tab. 3.1). The reversed dates are likely caused by resedimentation, since these five points are older than the other points close to them. The ^{14}C data of the sample 703,5 cm was not considered because there was overlapping with a Vedde ash layer. Even though the difference was not big between these two date methods, the Vedde ashes date was used, because it was considered to be more reliable than the ^{14}C dates. The ashes dates are absolute and more precise than the ^{14}C , thus the error probability is much lower. The two points do not differ significantly from one to the other so the implications on the final time scale are minimal. The program AnalySeries (Paillard *et al.*, 1996) was used to calculate ages for the sample depths of the core MD95-2011. Linear regression was used for constructing the age-depth model. Figure 3.1 highlights the points with reverse age that were cut off.

The mean sedimentation rate is about 85 cm/ka. Considering the analysed spacing of about 5 cm, the resulting mean temporal resolution is about 81 cm/ka for the *G. bulloides* isotope analysis and 90 cm/ka for the Mg/Ca analysis. The sedimentation rate changes through time. A very high late Holocene sedimentation rate is caused by the coring technique that stretches the sediment in the piston core. This has been a persistent problem with older *Marin Dufrense* cores (Nyland *et al.*, 2006; Széréméta *et*

Identifier	Core	Core depth PSH-5159N	Dated material	Sample weight (mg)	Age ¹⁴ C AMS $\pm 1\sigma$	Calibrated age range $\pm 1\sigma$ BP 1950	Relative area under probability distribution 1σ	Calibrated age range $\pm 2\sigma$ BP 1950	Calendar age BP 1950 used in age model (mid point of $\pm 1\sigma$ age range)	Used
GifA96471	MD95-2011	10.5	NPD	8.94 mg	980 \pm 60	525-623 BP	1	483-665 BP	574	
KIA 5600	MD95-2011	24.5	NPD	8.5 mg	1590 \pm 40	1097-1222 BP	1	1040-1264 BP	1159.5	NO
KIA 3925	MD95-2011	30.5	NPD	8.6 mg	1040 \pm 40	590-651 BP	0.793	526-584 BP	620	
KIA 5601	MD95-2011	47.5	NPD	8.4 mg	1160 \pm 30	663-739 BP	1	638-792 BP	701	
Poz-8244	MD95-2011	55.5	NPD	5.4 mg	1530 \pm 90	974-1180 BP	1	906-1272 BP	1077	NO
KIA 3926	MD95-2011	70.5	NPD	8.2 mg	1460 \pm 50	935-1065 BP	1	902-1153 BP	1000	
KIA 6286	MD95-2011	89.5	NPD	8.76 mg	1590 \pm 30	1106-1219 BP	1	1052-1252 BP	1162.5	
Poz-8246	MD95-2011	102	NPD	6.9 mg	1790 \pm 60	1272-1400 BP	1	1226-1502 BP	1336	
KIA 3927	MD95-2011	130.5	NPD	7.2 mg	2350 \pm 40	1905-2040 BP	1	1857-2110 BP	1972.5	NO
KIA 6287	MD95-2011	154	NPD	10.55 mg	2335 \pm 25	1894-2001 BP	1	1856-2073 BP	1947.5	
GifA96472	MD95-2011	170.5	NPD	7 mg	2620 \pm 60	2187-2378 BP	1	2115-2493 BP	2282.5	
Poz-8242	MD95-2011	225	NPD	0.14 mC	3000 \pm 50	2723-2832 BP	1	2680-2918 BP	2777.5	
Poz-8241	MD95-2011	250	NPD	8.0 mg	3380 \pm 70	3158-3346 BP	1	3039-3430 BP	3252	
KIA 10011	MD95-2011	269.5	NPD	7.7 mg	3820 \pm 35	3673-3874 BP	1	3569-3973 BP	3773.5	
Poz-8240	MD95-2011	300	NPD	0.15 mC	4080 \pm 70	4001-4232 BP	1	3909-4357 BP	4116.5	
KIA 463	MD95-2011	320.5	NPD	11 mg	4330 \pm 50	4392-4545 BP	1	4286-4644 BP	4468.5	
Poz-8238	MD95-2011	451	NPD	0.14 mC	6420 \pm 160	6732-7118 BP	1	6525-7265 BP	6925	
KIA 464	MD95-2011	520.5	NPD	6.9 mg	7260 \pm 60	7656-7797 BP	1	7588-7869 BP	7726.5	
Poz-8237	MD95-2011	528.5	NPD	0.16 mC	7690 \pm 110	8036-8279 BP	1	7936-8372 BP	8157.5	
Poz-8236	MD95-2011	533.5	?	5.0 mg	8530 \pm 160	8989-9382 BP	1	8708-9510 BP	9185.5	NO
Poz-8235	MD95-2011	541.5	?	0.24 mC	8280 \pm 140	8615-8999 BP	1	8458-9219 BP	8807	
Poz-8234	MD95-2011	570.5	?	0.16 mC	8700 \pm 90	9272-9472 BP	1	9116-9533 BP	9372	
	MD95-2011	709.5	Vedde ash						12170*	

Tab 3.1. Radiocarbon dates and ash horizon used to create the age model. The radiocarbon dates were calibrated using Calib (Stuiver and Reimer, 1993). Some dates were not used since they gave inverted ages. * Risebrobakken *et al.* (submitted).

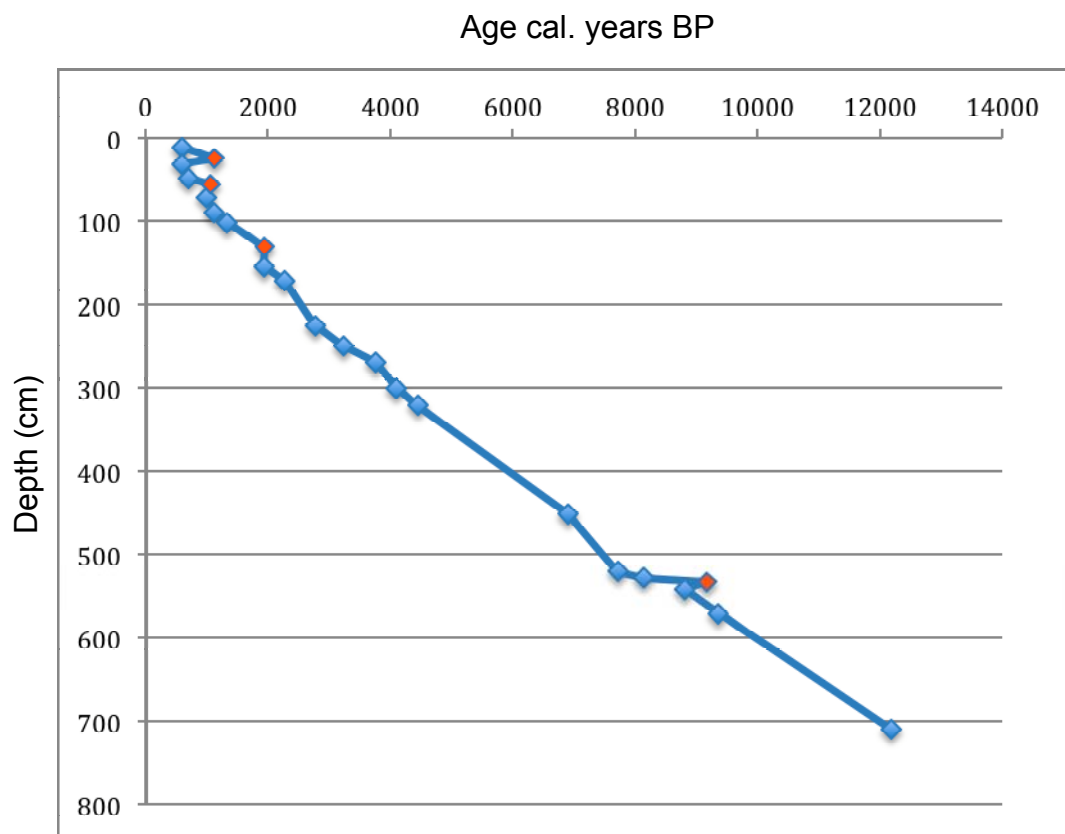


Fig. 3.1. Age model: calendar years BP 1950 versus core depth. The red points highlights the levels displaying reverse age.

al., 2004). However, mixing in the sediment was not seen, so the reliability of the result should not be affected.

Note that all the dates are reported as calendar years before present with the notation years BP, where the present is intended to be 1950.

3.3. The planktonic foraminifer *Globigerina bulloides*

Foraminifera are marine single-celled testate protozoans that are part of the marine zooplankton (e.g. Hemleben *et al.*, 1989; Kennett and Srinivasan, 1983). They inhabit all marine environments and are wide spread from equatorial to polar regions. Foraminifera can be either planktonic or benthic. Their cells are composed of soft tissue named cytoplasm enclosed and protected by a hard shell (test). The test can be built either with organic matter (membrane, polysaccharides), or minerals adsorbed from the surrounding water (calcite, aragonite, opaline silica), or agglutinate particles. The tests may be composed of an aggregation of chambers or 'loculus' separated by septa and connected to each other by an opening called foramen. The order Foraminiferida is named for this foramen structure. The first occurrence of foraminifera has been dated back to the Early Cambrian. Since then these organisms have been present in marine waters all over the world (Armstrong and Brasier, 2005). The earliest forms are all benthic and the first planktonic forms appear in the fossil record during the middle Jurassic. Due to the mineralized hard test they can have a high potential of preservation: during sedimentation the cytoplasm is dissolved, but the hard shell is preserved. It was estimated that about 5000 benthic foraminiferal species and about 100 planktic foraminifera species live in the modern oceans (Armstrong and Brasier, 2005). Due to the small size, foraminiferal tests are the most used tools in biostratigraphic and paleoenvironmental reconstructions (Loeblich and Tappan, 1988).

3.3.1. Taxonomy

Globigerina bulloides d'Orbigny, 1826 (Fig. 3.2 and 3.3), is a planktonic non-symbiotic foraminifera belonging to the superfamily *Globigerinacea*. The test (CaCO_3) is free, normally low trochospiral (can be medium trochospiral), and strongly lobulated with distinct depressed sutures. The surface is covered with pores and simple spines with

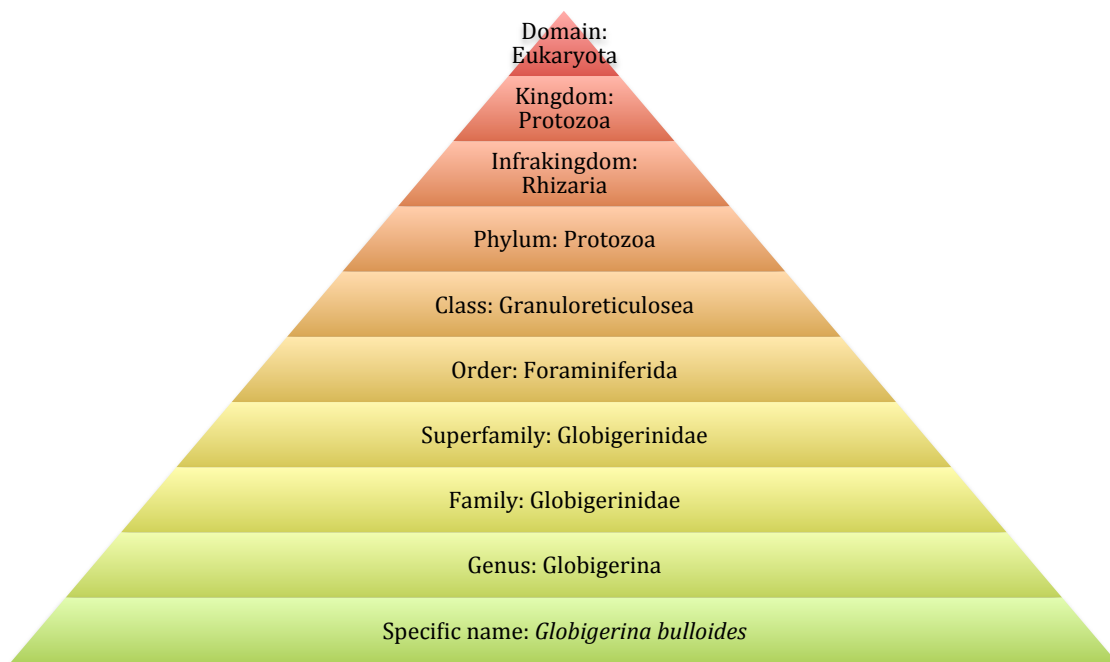


Figure 3.2: Taxonomic scheme of the classification of *Globigerina bulloides* d'Orbigny, 1826. Eukaryota -Whittaker and Margulis, 1978, Protozoa -Goldfuss, 1818, Rhizaria -Cavalier-Smith, 2002, Protozoa -(Eichwald) Margulis, 1974, Granuloreticulosea -Lee, 1990, Foraminiferida -Delage and Herouard, 1896, Globigerinacea -Carpenter *et al.*, 1862, Globigerinidae -Carpenter *et al.*, 1862, Globigerinidae -Carpenter *et al.*, 1862, Globigerina bulloides -D'Orbigny, 1826 (classification from http://zipcodezoo.com/Protozoa/G/Globigerina_bulloides/).

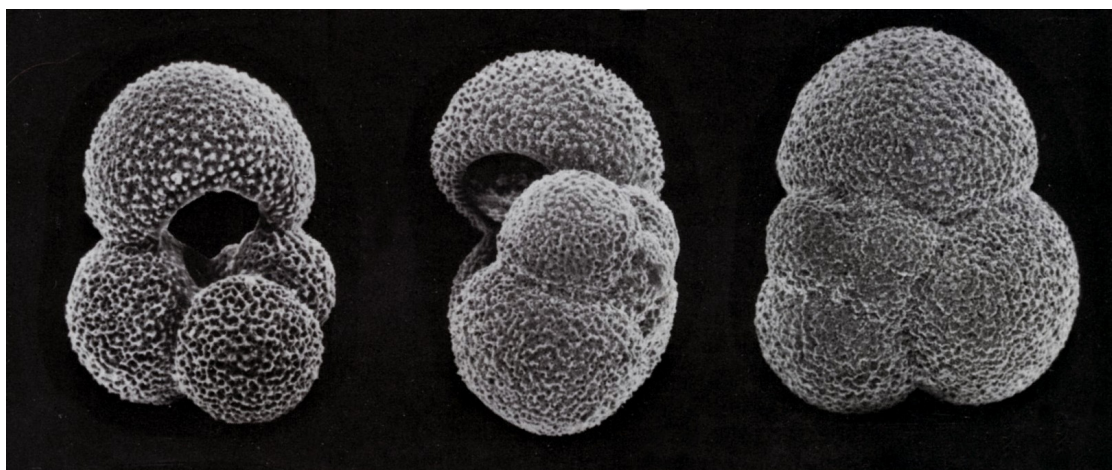


Fig. 3.3. *Globigerina bulloides* (from Kennett and Srinivasan, 1983).

circular cross-sections. From the pores the pseudopodia, called reticulopodia, extrude. Usually it has 4 chambers in the last whorl, but it can vary between 3 and 5 chambers. The chambers are spherical to subspherical, slowly increasing in size as added. The aperture is umbilical with a high symmetrical arch (Hemleben *et al.*, 1989; Kennett and Srinivasan, 1983; <http://www.eol.org/pages/489860>). Being a spinose species it possesses an atypical proloculus because it is much bigger than most other spinose species (Hemleben *et al.*, 1989).

3.3.2. Stratigraphic and geographic distribution

Globigerina bulloides is a thermophilic species, it is a typical transitional to sub-polar species that populates upwelling zones *a priori* to their latitude. It is abundant in both cool high-latitude and low-latitude upwelling regions (Hilbrecht and Thierstein, 1996). *Globigerina bulloides* stratigraphic distribution ranges from the middle Miocene to the Present (Hemleben *et al.*, 1989). In modern assemblages its maximum distribution (60%) in the North Atlantic is linked to the temperate Atlantic waters of the Irminger Current southeast of Iceland (Pflaumann *et al.*, 2003). In the Norwegian Sea the highest abundances of *G. bulloides* are found in the southeastern part, along the path of warm inflow of Atlantic Water (Hald *et al.*, 2007; Johannessen *et al.*, 1994). It is a shallow-dwelling species, usually it occupies the upper 50 m of the water column (within the seasonal mixed layer). However, it has also been found at depths as deep as 400 m (Hemleben *et al.*, 1989). *G. bulloides* highest distribution is in surface waters between 11 and 16°C (Sautter and Thunell, 1991). The $\delta^{18}\text{O}$ test composition of *Globigerina bulloides* is in equilibrium with the seasonal surface conditions (Hemleben *et al.*, 1989). The relationship isotopic content-seawater temperature is not heavily affected by the vital effect (see section in chapter 3.4 below). The calcification of *G. bulloides* is observed to take place in the first months of the year (February-March) in the sea in the southern part of Norway, and it shifts a bit later in the year (April-June) at 60°N, reflecting the movement of the spring bloom (Ganssen and Kroon, 2000). According to these observations *G. bulloides* is expected to reflect the sea surface temperature (SST) changes in the near-surface water conditions.

Being *Globigerina bulloides* a shallow waters dweller its record may help the reconstruction of shallow water dynamics, late spring-summer temperatures and

insolation. The possibility of using *G. bulloides* as proxy for these tasks has been checked in the following dissertation.

3.4. Paleotemperature proxies based on stable isotope composition and the Mg/Ca ratios

Atoms of the same element may contain different number of neutrons hence have different atomic mass. Atoms of the same species containing different number of neutrons are indicated as isotopes. Almost all the elements have at least 2 different isotopic forms, and these characterize localities and organisms. Isotopes have the same atomic number (Z), since they contain the same number of protons, but they have different number of neutrons they contain in their nucleus. The isotopes that contain more neutrons have a higher mass number (A), than the isotopes that contain fewer neutrons. More positive values are mentioned as ‘heavier’ and more negative values are called ‘lighter’ in the following dissertation. Part of the isotopes are naturally stable, most of the isotopes are naturally unstable and radiogenic. In geosciences the unstable isotopes represent an important device to calibrate the absolute geological time, stable isotopes are used in paleoclimate and paleoenvironmental reconstructions and studies. On the globe there is an unequal subdivision of isotopes (isotope fractionation), the heavier isotopes are more concentrated in the equatorial area and decrease through the poles, right the opposite happens for the lighter isotopes. Due to the cycle of evaporation, condensation and precipitation the lighter isotopes (H_2^{16}O) are readily evaporated and preferentially carried towards the poles. The isotopes fractioning causes ^{16}O -enriched precipitations over land that causes ^{16}O -enriched glacial ice and river runoff to the oceans. The surface seawater isotopic composition tends to be at the equilibrium with the atmospheric conditions, consequently the atmospheric conditions are assumed to be the same as the surface marine conditions. In the seas the different currents have different isotopic compositions, i.e. cold waters contain more heavy isotopes.

Harold Urey (1947) was the first to see the relation between precipitate oxygen isotope fraction and paleotemperatures. Today, it is commonly accepted that marine organisms like corals, foraminifera, diatoms, radiolarians, calcareous nannofossils, and pteropods isotopes composition reflects the seawater conditions (e.g. Loeblich and Tappan, 1988). Foraminifera, like many other marine organisms, record the sea isotopic composition in

their tests. Foraminifera use carbon, oxygen, calcium and minor elements (e. g. Mg, Cd) from the surrounding water to build their tests. Oxygen has three stable isotopes (^{16}O , ^{17}O and ^{18}O). The most abundant in nature is ^{16}O (~99.8%), ^{18}O is much rare (0.2004%), ^{17}O is even more rare and for this reason very difficult to be detected. The deviation from a standard (i. e. PDB) of the ratio of the isotopes of oxygen ($^{18}\text{O}/^{16}\text{O}$) can be measured in the calcite tests. This ratio is reported in δ notation, and so calculated:

$$\delta^{18}\text{O}_{\text{sample}} = 1000 ((^{18}\text{O}/^{16}\text{O})_{\text{sample}} - (^{18}\text{O}/^{16}\text{O})_{\text{standard}}) / (^{18}\text{O}/^{16}\text{O})_{\text{standard}} \quad \text{Equation 3.1}$$

The ratio of ^{18}O and ^{16}O in foraminiferal tests reflects the $\delta^{18}\text{O}$ of the seawater (δO_w) in which they calcify. δO_w changes with global ice volume, local river runoff water input and the evaporation/precipitation pattern (Katz *et al.*, 2010). In response to the Rayleigh distillation process at high latitudes snow precipitations are extremely dependent on ^{18}O (~30 ‰) (Gat, 1966). At colder conditions ^{16}O tend to evaporate more, so that more ^{18}O is stored in the seawaters. Instead during warmer periods the seawater is richer in ^{16}O , because in the system there is enough energy to allow the heavier isotope evaporate. Between $\delta^{18}\text{O}_{\text{calcite}}$ and temperatures exist an inverse relationship that allow the interpretation of $\delta^{18}\text{O}$ values of biogenic calcite. Every 1°C increase, there is about 0.23‰ decrease in the recorded $\delta^{18}\text{O}_{\text{calcite}}$ values (Katz *et al.*, 2010). Therefore the amount of water stored on land affects the δO_w value. During interglacial periods the melt-water brings to the oceans water ^{16}O -enriched water, on the contrary during glacial periods a large fraction of $\delta^{16}\text{O}$ is sequester in the ^{16}O -enriched snow and ice. The high difference composition between ice sheet (-35 to -40‰) and the mean ocean (~ 0‰) $\delta^{18}\text{O}$ values allow the reconstruction of the variations in the ice-sheet size and hence in temperature (Katz *et al.*, 2010). The analytical method to measure $\delta^{18}\text{O}$ simultaneously records the $\delta^{13}\text{C}$ content. Carbon has two stable isotopes ^{12}C and the more rare ^{13}C . The deviation from a standard (i.e. PDB) of the carbon isotopic ratio ($^{13}\text{C}/^{12}\text{C}$) is reported as for the oxygen isotope with the notation δ :

$$\delta^{13}\text{C}_{\text{sample}} = 1000 ((^{13}\text{C}/^{12}\text{C})_{\text{sample}} - (^{13}\text{C}/^{12}\text{C})_{\text{standard}}) / (^{13}\text{C}/^{12}\text{C})_{\text{standard}} \quad \text{Equation 3.2}$$

The foraminiferal $\delta^{13}\text{C}$ is primarily a function of the dissolved inorganic carbon (DIC) $\delta^{13}\text{C}$ value of the seawater (e. g. Emiliani, 1955; Urey, 1947). The ocean carbon supplies comes from hydrothermal-volcanic gasses and from weathering of continental rocks. Carbon is removed from the seawater by deposition of carbonate and organic carbon in marine sediments. The $\delta^{13}\text{C}$ recorded in planktic foraminiferal tests primarily

reflects $\delta^{13}\text{C}_{\text{DIC}}$ in the upper few hundred meters of the water column, it reflects also the influence of foraminiferal respiration and symbiont photosynthesis (e.g. Spero and Lea, 1996). Additional factors can influence the foraminifal $\delta^{13}\text{C}$ content, such as pH, test size and light intensity (Spero *et al.*, 1991). Photosynthetic organisms rather assimilate ^{12}C than ^{13}C during photosynthesis, so that they contain more ^{12}C and the surrounding seawater is enriched in ^{13}C . In high productive areas the phytoplankton can exhaust the shallow water of ^{12}C , and enrich the deeper water of ^{12}C . When marine photosynthetic organisms die they sink and enrich the sea bottom level of ^{12}C . Therefore ^{13}C foraminiferal tests content decreases with depth. In the same way photosynthetic symbionts enrich the foram-environment in $\delta^{13}\text{C}$, so that the tests of foraminifera with symbiotic relationships result enriched in $\delta^{13}\text{C}$. In upwelling conditions the cold bottom sea water is brought close to the surface and also part of the ^{12}C that is contained in the sediment.

Early studies on planktonic foraminifera did not show any correlation between temperature and stable isotopes content nor minor elements content (Delaney *et al.*, 1985). Since then a constant progress has improved the sensibility of the instruments and the method, so that nowadays stable isotopic and Mg/Ca foraminiferal content is an acknowledged and very used paleotemperatures proxy. Minor elemental ratios reported as relative to Ca (e.g. Mg/Ca) in biogenic calcite are strongly influenced by environmental parameters such as temperature (Katz *et al.*, 2010). The dependence of biogenic foraminiferal Mg on temperature has been established both in cultures and core tops. Due to modern spectrometers it is possible to obtain data from Mg/Ca and isotopes analysis from the same sample (Dekens *et al.*, 2002; Elderfield and Ganssen, 2000; Lea *et al.*, 1999; Lear *et al.*, 2002; Nürnberg, 1995; Rosenthal *et al.*, 1997) to combine the two analyses. This method can therefore be used to reconstruct changes in the oxygen isotope composition of sea water ($\delta^{18}\text{O}_w$). When the temperatures increase, larger amounts of magnesium are incorporated into foraminiferal calcite (e.g. Lea *et al.*, 1999; Nürnberg, 1995). Though there are still some problems that need further studies to be resolved; the main is that at high latitudes in cold-near surface environments the tests content of Mg/Ca is low and the changes with temperature are small. Therefore in this situation secondary factors (like salinity, pH, alkalinity, carbonate ion concentration, secondary calcification and dissolution) can have a relatively big influence on Mg/Ca ratios (Meland *et al.*, 2006). The precipitation of calcite in foraminiferal tests does not occur in equilibrium with the surrounding seawater, the disequilibrium between the

isotopic composition of the tests and the isotopic content of the seawater was reported by numerous studies on some species of foraminifera (e.g. Peeters *et al.*, 2002; Spero and Lea, 1996). This disequilibrium is called ‘vital effect’. The vital effect varies between inter- and intra-species and summarizes all the biological, chemical and physical controlled processes that cause an offset between $\delta^{13}\text{C}$ of the tests and $\delta^{13}\text{C}_{\text{dic}}$. The factors that have the main effects on foraminiferal isotopic composition are: calcification rate, photosynthesis, respiration, tests size, and seawater pH (carbonate ion concentration). Foraminifer test size and carbon isotope ratio are related: larger tests have a higher content of heavy isotopes. Mainly symbiotic foraminifera present a vital effect (Norris, 1996). In non-symbiotic species the source of intra-specific changes seems to be the respiration CO_2 . The deviation from the environmental $\delta^{13}\text{C}$ content seems to be linked to the ontogenetic development, and the deviation from the seawater $\delta^{18}\text{O}$ seems to be connected to the incorporation of metabolic CO_2 prior to full isotopic equilibrium with seawater (Spero and Lea, 1996). Peeters *et al.* (2002) calculated that *Globigerina bulloides* large tests (250-355 μm) are enriched in ^{13}C by about 0.33 ± 0.15 ‰ and about 0.23‰ in ^{18}O content, compared to small tests (150-250 μm). Minor elements partly substitute calcium or carbonate ion (CO_3^{2-}) in foraminiferal tests. *G. bulloides* suffers from vital effect. Many studies and papers aimed at the elaboration of an equation that nullifies the vital effect, but none are ready yet. Despite the vital effect the isotopic content of *G. bulloides* responds systematically to changes in the seawater temperature (Spero and Lea, 1996). However, if the disequilibrium value is known the vital effect can be annulled. *G. bulloides* has been used in many studies (e.g. Thornalley *et al.*, 2009) that attest the sensitivity of this species to the temperature variations.

3.5. Laboratory procedure

3.5.1. Picking procedure

On average 65 specimens were picked from each sample. About 50 specimens (50-60 μg) are needed to obtain reliable Mg/Ca analyses. In addition 2-4 specimens (about 20 μg) were used for the stable isotope analysis. In total 121 stable isotopes analyses and 126 from the Mg/Ca analysis were done. Sometimes the number of tests was not enough to run both Mg/Ca and stable isotopes analysis, in this case the picking was performed on different nearby samples for Mg/Ca and isotopes. The different samples

had the closest depth distance possible, in order to keep the connection between the two analyses controlled. The content of the vials were equally spread into a micropaleontological tray, and with a moist thin brush the picking was performed under an optical stereomicroscope. The picked foraminifera have been stored inside centrifuge-tubes and/or slides labelled with the sample ID (name of the core, the species, the time span, the number of the specimen and the weight).

It is important to pick specimen of almost the same size, and closest possible to the optimum size of the species (Elderfield *et al.*, 2002). The young specimens register only an incomplete record of the environmental conditions, for this reason picking adult specimens is very important. For many samples it was impossible to reach 50 specimens without picking every single specimen of *Globigerina bulloides* contained. Therefore the size fraction of the tests is included between a minimum of 125 μm and a maximum of 500 μm . It is proved that *G. bulloides* has an ontogenetic effect: it varies its isotopic content according to its size (Naidu and Niitsuma, 2004; Spero and Lea, 1996). Elderfield *et al.*, (2002) have reported differences in the content of stable isotopes, Mg/Ca and Sr/Ca between the size fractions 212-250 μm , 250-300 μm , 300-350 μm , and 350-425 μm . In this core the number of specimen was often close to the borderline to reach the number of specimens needed for both the stable isotopes and Mg/Ca analyses. Reducing the size fraction for the selection would not permit reaching the number of needed specimens. For this reason all the foraminifera in the fraction 125-500 μm were picked. It is also important to pick the cleanest specimens, even though it is not always possible to see all the particles of 'dirt' inside the chambers. Where possible the cleanest specimens were picked. Any particle of dirt can interfere with the analysis. For this reason a cleaning procedure has to be performed on the specimens before starting the analysis.

3.5.2. Stable isotopes analyses

Both stable oxygen and carbon isotopes were run using standard low-temperature techniques. The measurements were performed at the Geological Mass Spectrometry (GMS) laboratory at the Department of Earth Science, University of Bergen. All stable isotopes analyses were performed using a Finnigan MAT 253 instrument. This mass spectrometer is equipped with an automatic preparation lines, i.e. 'Kiel device'. The results were adjusted according to the Vienna Pee Dee belemnite (VPDB) standard via

NBS 19 (Coplen, 1996) and a homemade laboratory standard, NBS 18. For running the analysis 7 NBS 19 and 1 NSB 18 were used. At least 10 µg of calcite is necessary for each analysis. Around 20 µg of foraminifera were picked to allow some loss during the cleaning process. Picked samples varied between 20-28 µg, which corresponds to 2-4 specimens of *G. bulloides*. A basic rinsing was applied to the samples. The cleaning of the sample was made with methanol and ultrasonic bath. Methanol is a light alcoholic liquid and helps to bring in suspension the alien particles that may be contained in the chambers to be removed.

Due to some problems during the measurements, not all the samples gave results. The mass of the samples corresponding to the depth 176.5, 333.5, 467.5 and 567.5 cm were too small to be detected by the mass spectrometer. Moreover, the samples from depth 452.5 cm and 547.5 cm were lost during the measurements. This is probably the result of the electrostatic force that attracts the tests onto the glass walls and makes them stick there. In part one of the analysis, the acid fills just the bottom of the glasses, so not all the tests dissolve and were just partly analysed. An alternative explanation is that there was a leak in the preparation line. Errors in the resulting $\delta^{18}\text{O}$ are caused by measurement errors ($\pm 0.08\text{ ‰}$) (Barker and Elderfield, 2002). The results are reported as $\delta^{18}\text{O}$ vs. PDB and $\delta^{13}\text{C}$ in Table 3.2.

3.5.3. Mg/Ca analysis

The Mg/Ca cleaning method for foraminifera is based on the Cd/Ca and Ba/Ca cleaning methods (Boyle, 1981; Boyle and Keigwin, 1985; Lea and Boyle, 1991). These methods include sequential cleaning steps: removal of clays, removal of organic matter, removal of Mn-Fe oxide coat, optional removal of barite, and final leaching of the samples (Barker *et al.*, 2003). The debate concerning the necessity of all the phases above described for the analysis of Mg/Ca ratios is still open (Brown and Elderfield, 1996; Martin and Lea, 2002), therefore the cleaning methods change between different laboratories. In this study a cleaning procedure based on the Cambridge procedure (Barker *et al.*, 2003) has been adopted. The used procedure for cleaning and crushing partly differ from the Barker *et al.* (2003) method, to allow the comparison between the two procedures that was adopted is reported in Appendix I. The content of Mg/Ca in samples of 50 specimen, about 400 µg is in the order of part per million (ppm).

Calendar age BP 1950	Depth	$\delta^{13}\text{C}_{\text{vs VPDB}}$	$\delta^{18}\text{O}_{\text{vs VPDB}}$	Mg/Ca (mmol/mol)	Temperature °C
10922,0	647,5	-1,14	2,05	3,50	14,8
10821,3	642,5	-1,18	1,80	6,09	20,4
10720,7	637,5	-0,93	2,21	2,98	13,2
10640,2	633,5	-1,14	2,17	2,77	12,5
10519,4	627,5	-1,27	1,75	2,62	12,0
10418,7	622,5	-1,16	2,13	2,37	10,9
10318,1	617,5	-1,27	2,24	2,76	12,5
10237,6	613,5	-1,38	2,04		
10096,7	606,5	-1,68	1,76	2,63	12,0
10016,1	602,5	-1,03	1,74		
9915,5	597,5	-1,35	1,80		
9835,0	593,5	-1,03	2,15	2,27	10,5
9734,3	588,5	-0,97	1,81	2,11	9,8
9512,9	577,5	-0,54	2,23	1,88	8,6
9412,3	572,5	-0,85	1,57	2,29	10,6
9333,0	568,5	-0,53	1,98	2,22	10,3
9255,1	564,5	-0,82	2,08		
9196,7	561,5	-1,04	1,89	1,62	7,1
9118,7	557,5	-0,69	2,03	1,39	5,6
9021,3	552,5	-0,95	1,91	1,67	7,4
8943,4	548,5	-0,53	1,33		
8923,9	547,5			1,54	6,7
8846,0	543,5	-0,67	1,81	1,80	8,2
8607,2	537,5	-0,45	2,00	1,95	9,0
8407,3	533,5	-0,86	1,51	2,26	10,5
8157,5	528,5	-0,83	2,19	4,00	16,2
7942	524,5	-1,05	1,21	1,82	8,3
7691,9	517,5			2,05	9,5
7680,4	516,5	-0,97	2,07		
7634,2	512,5	-0,98	1,38	2,66	12,1
7576,6	507,5	-0,57	1,93	2,26	10,4
7518,9	502,5	-0,88	1,90	2,68	12,1
7449,7	496,5	-0,33	2,22	2,86	12,8
7403,6	492,5	-0,55	1,20	3,95	16,0
7345,9	487,5	-0,32	1,69	3,08	13,6
7299,8	483,5	-0,27	1,15	3,16	13,8
7230,6	477,5	-0,17	2,24	3,16	13,8
7172,9	472,5	-0,40	1,71	4,15	16,5
7126,8	468,5	-0,14	1,53		
7115,3	467,5			3,12	13,7
7046,1	461,5	-0,87	1,90	2,96	13,2
7000,0	457,5	-0,63	1,97	1,88	8,6
6942,3	452,5			2,44	11,2
6859,1	447,5	-0,54	1,17	2,48	11,4
6746,2	441,5	-0,37	1,76	3,27	14,1
6633,2	437,5	-1,01	1,89	3,36	14,4
6576,8	432,5	-0,75	1,83	2,36	10,9
6482,6	427,5			1,88	8,6
6463,8	426,5	-0,38	1,83		
6388,5	422,5			2,77	12,5
6369,7	421,5	-0,02	1,48		
6294,4	417,5			2,16	10,0
6275,6	416,5	-0,66	1,53		
6200,3	412,5	0,09	1,95		
6181,5	411,5			2,42	11,1
6106,2	407,5			2,58	11,8
6087,3	406,5	-0,45	1,28		
6030,9	403,5			2,47	11,4
6012,0	402,5	-0,73	1,33		
5917,9	397,5	-0,50	1,80	3,57	15,0
5823,8	392,5	-0,04	1,94	4,15	16,5
5729,7	387,5	0,08	1,47	3,82	15,7

Calendar age BP 1950	Depth	$\delta^{13}\text{C}_{\text{vs VPDB}}$	$\delta^{18}\text{O}_{\text{vs VPDB}}$	Mg/Ca (mmol/mol)	Temperature °C
5654,4	383,5	-0,21	1,66	2,91	13,0
5541,5	377,5	-0,39	1,74	1,99	9,2
5447,3	372,5	0,25	1,76	3,84	15,8
5353,2	367,5	-0,29	1,79	2,98	13,2
5259,1	362,5	-0,63	1,90	3,47	14,7
5165,0	357,5	0,10	1,75	2,47	11,3
5070,9	352,5			1,85	8,5
5052,0	351,5	-0,54	1,84		
4976,7	347,5	-0,52	1,89	2,20	10,2
4882,6	342,5	-0,62	1,58	2,38	11,0
4788,5	337,5	-0,18	1,72	3,18	13,9
4713,2	333,5			3,35	14,4
4600,3	327,5	-0,04	1,78	3,80	15,6
4543,8	324,5	-0,51	1,39		
4382,6	315,5			2,25	10,4
4314,0	311,5	0,10	1,86		
4296,8	310,5			2,56	11,7
4245,3	307,5			3,00	13,3
4228,1	306,5	-0,41	1,49		
4159,4	302,5	-0,09	1,91	2,30	10,6
4088,4	297,5	-0,38	1,78		
4077,1	296,5			2,79	12,6
4032,2	292,5	0,12	1,97	3,35	14,4
3987,2	288,5	-0,58	1,81	2,67	12,1
3919,7	282,5	-0,05	1,61	3,47	14,8
3852,2	276,5	-0,29	2,14	2,48	11,4
3818,5	273,5	-0,43	1,26	2,85	12,8
3720,0	267,5	-0,15	1,02	2,82	12,7
3586,3	262,5	0,35	1,53	2,57	11,7
3425,8	256,5	0,15	1,15	1,83	8,3
3318,9	252,5	-0,17	2,01	2,38	11,0
3204,6	247,5			3,42	14,6
3185,6	246,5	-0,28	1,88		
3128,6	243,5			1,93	8,9
3109,7	242,5			2,24	10,4
3090,7	241,5	-0,18	1,68		
3014,8	237,5			2,51	11,5
2995,8	236,5	-0,55	1,83		
2938,8	233,5			2,37	10,9
2919,9	232,5	-0,37	1,86		
2862,9	228,5			3,00	13,3
2843,9	227,5			2,21	10,2
2754,8	222,5			2,95	13,1
2745,7	221,5	-0,40	2,02		
2709,4	217,5	0,31	1,72	2,38	11,0
2673,1	213,5			2,04	9,4
2664,0	212,5	-0,49	1,58		
2618,6	207,5	-0,37	1,33	2,62	11,9
2573,1	202,5			2,35	10,9
2564,1	201,5	-0,08	2,00		
2545,9	199,5			3,55	15,0
2527,7	197,5	-0,15	1,86		
2491,4	193,5			2,96	13,2
2482,3	192,5	-0,34	1,56		
2436,9	187,5			3,64	15,2
2427,8	186,5	-0,22	1,45		
2400,6	183,5	-0,28	1,81	2,78	12,5
2337,0	176,5			3,17	13,9
2300,7	172,5	-0,37	1,86	3,62	15,2
2221,6	167,5	0,07	2,08		
2201,3	166,5			4,02	16,2
2099,8	161,5	0,08	1,68		

Calendar age BP 1950	Depth	$\delta^{13}\text{C}_{\text{vs VPDB}}$	$\delta^{18}\text{O}_{\text{vs VPDB}}$	Mg/Ca (mmol/mol)	Temperature °C
2079,5	160,5			3,89	15,9
2018,6	157,5			3,36	14,4
1998,3	156,5	-0,40	1,39		
1929,9	152,5	-0,21	1,78	4,53	17,4
1871,1	147,5	-0,41	1,89	3,41	14,6
1824,0	143,5	-1,30	1,02		
1812,3	142,5			4,45	17,2
1741,7	136,5	-0,62	1,71	4,36	17,0
1718,2	134,5			2,99	13,3
1706,4	133,5	-0,65	1,61		
1694,7	132,5			4,64	17,7
1659,4	129,5	-0,53	1,24		
1624,1	126,5			2,53	11,6
1577,1	122,5	0,01	1,97	2,66	12,1
1530,0	118,5			2,52	11,6
1518,3	117,5	0,06	1,73		
1471,2	113,5	-0,46	1,62		
1459,5	112,5			5,67	19,7
1400,7	107,5			4,42	17,2
1388,9	106,5	-0,40	1,96		
1353,6	103,5	-0,35	1,58		
1341,9	102,5			4,35	17,0
1287,4	98,5			4,44	17,2
1273,5	97,5	-0,31	1,92		
1204,1	92,5	-0,03	1,75	3,38	14,5
1145,4	87,5	-0,65	0,95	4,28	16,8
1102,6	82,5			4,09	16,4
1094,1	81,5	-0,17	1,65		
1051,3	77,5	-0,21	1,55		
1042,8	75,5			4,11	16,4
1008,6	72,5	-0,32	2,07	2,43	11,2
961	68,5	0,31	1,59		
948	66,5			3,90	15,9
883	62,5	-0,05	1,75	4,20	16,7
844	58,5			2,63	12,0
818	57,5	-0,47	1,51		
792	53,5			2,39	11,0
766	52,5	0,04	1,65		
740	49,5			2,46	11,3
714	48,5	-0,44	1,24		
691,5	44,5			2,79	12,6
682,1	43,5	0,27	1,83		
644,2	35,5	0,05	1,81		
639,4	34,5			2,37	10,9
630,0	32,5			2,49	11,4
625,2	31,5	-0,06	1,87		
613,5	27,5			2,58	11,8
611,2	26,5	-0,39	1,20		
606,6	24,5			3,51	14,9
599,6	21,5	0,02	1,80		
592,6	18,5			2,67	12,1
590,3	17,5	-0,33	1,39		
578,7	12,5	-0,83	1,75		
576,3	11,5			2,61	11,9

Tab 3.2: Analysis results: oxygen and carbon isotopes are reported as $\delta^{18}\text{O}$ vs VPDB and $\delta^{13}\text{C}$ vs VPDB and expressed as ‰; Mg/Ca data are listed as content in mmol/mol and as temperatures expressed in Celsius degrees. Mg/Ca temperatures were calculated using the equation 3.2 (Thornalley *et al.* 2009).

It is necessary to open each single chamber and extract all alien particles to avoid any contaminations in the analysis. This is done by crushing all the chambers. So that the different substances dissolved the dirt inside and bring it into suspension, allowing the separation from the tests fragments. The crushed fragments must not be too small, otherwise the action of the acids used for the cleaning process will dissolve most of the CaCO_3 and will not leave enough substrate for the analysis. The crushing procedure requires two glass plates. The tests were poured on a tray and every alien particle visible was removed. When no particles were present on the tray anymore, the tests were moved onto the glass plate. The tests with an excess of de-ionised water were kindly pressed between the two glass plates till when all the chambers of each test were open. After each removal the brush, the tray and the plates have to be sterilised. They were washed with ethanol, rinsed with water (to avoid that the ethanol will contaminate the tests), and then used for the next sample. The fragments of the tests have been stored in centrifuge-tubes. Except for polytetrafluoroethylene (PTFE, commonly named Teflon) all the plastic materials contain some tracks of magnesium even though in scarce quantities. Thus to avoid contaminations, the centrifuge-tubes have been sterilised with a strong acid. Two baths of 24 hours each in HNO_3 0,1 M were used. Regarding the strength of the acid this has to be totally removed after the bath, otherwise it will dissolve the tests fragments.

3.5.3.1. Test cleaning

With all the chambers open the clays that fill the test is lost and brought in suspension much easier. Maximum one series of 12 or 24 samples was cleaned per time. In each section there must be at least one blank. The function of the blank is to check the presence of contaminant in the series and to calibrate and adjust the data avoiding the background noises. Thus, each section had 11 or 23 samples and 1 blank. The clay removal process is divided in two parts, the first with water as reagent, and the second with ethanol. In the first part the tubes were rinsed with ultra-high quality (UHQ) water alternating to ultrasonic baths to increase the separation of alien particles and the fragments of the tests. According to the minimal settling technique the fragments of tests had a brief time to settle. Then the overlying solution (supernatant) was removed and about 10-20 μl of water were left in the centrifuge-tube. The alien particles are visible as a milky part at the bottom of the centrifuge-tubes. This rinsing-ultrasonicate

sequence has to be repeated about 6 times. The number of repetitions changed according to the aspect of the liquid in the tubes: if the milky part was still evident after the sixth rinsing the rinsing was repeated another couple of times alternatively if instead the milky part was already not visible before then the rinsing could be stopped earlier. In the second part of the rinsing it is required to use methanol. Ethanol is more secure to use, because it has lower probability to pollute the samples. Methanol or ethanol is used because of the lower viscosity that the alcohols reagents have. Due to this characteristic the thinner material still attached to the tests surface will be detached. The tests fragments were put into a methanol bath and then into an ultrasonic bath and rocked at a vortex to bring the clays into suspension. After the minimal time for settling the supernatant ethanol was removed. The washing with ethanol was repeated twice, after the second time all the ethanol was removed and the tubes were rinsed with 500 μ l of UHQ water.

The organic matter was removed using the alkali oxidizing solution H_2O_2 1% (H_2O_2 and NaOH 0.1 M (100 μ l: 10ml)). The centrifuge-tubes with this solution were put in a bath of boiling water for ten minutes. Within this time they were shaken manually (twice) and ultrasonicate (one time) to make sure that the reagent was always in contacts with the fragments of the tests. Then the tubes were run in the centrifuge at 10000 rpm for one minute. Subsequently the supernatant liquid was than removed. This procedure was repeated twice. At the end of the process the centrifuge-tubes were rinsed twice with UHQ water.

After the settlement of the tests at the sea bottom, the tests can be enriched in CaCO_3 . This secondary crust (gametogenic crust) contains some tracks of Mg (Elderfield and Ganssen, 2000). This crust is built before the foraminifera reproduce in deep waters, and the isotopes contained can compromise the analysis, interfere with the Mg of the tests and move the results towards a colder environment. A dilute acid leaching is done in order to take off the secondary crust that lies around the tests. A dilute acid (0.001 M of HNO_3) is used to remove the adsorbed contaminants from the walls of the test. 250 μ l of this acid were added into each centrifuge-tube that was then ultrasonicated for 30 seconds. After a minimal settle time the supernatant was removed. The rinsing with UHQ water was repeated twice. The acid solution was removed as soon as possible, otherwise the acid would totally dissolve the fragments. The tubes were rinsed twice with UHQ water. Approximately all the solution was removed in this way the

possibility of contamination is almost null and the samples can be stored for some weeks before they have to be run.

To run the analysis through an ICP-AES (Vista Inc.) the fragments of the tests have to be dissolved in a liquid, for this reason a strong acid (0,1 M HNO₃) was added to the centrifuge-tubes. This process (Barker *et al.* 2003) has to be carried out on the same day of the analysis. Each addition of 0,1 M HNO₃ was followed by an ultrasonic bath of at least 5 minutes to facilitate the dissolution of the fragments of the tests. The centrifuge-tubes were then centrifuged for 5 minutes at 10000 rpm so that if some silicate particles were still in the centrifuge-tubes they would sink to the bottom. Quickly 300 µl of solution were transferred into a clean centrifuge-tube, leaving any big particles in the residual 50 µl. If silicate particles remain in the tube with the acid there is a high risk that they will partly dissolve and contaminate the solution.

3.5.3.2. Measurements

The samples were run in twice. During the first analysis the percentage of Ca contained in each sample was detected. During the second analysis with a fix percentage of Ca was used to check how the content of Mg changed in relation to the Ca. For this reason two different dilutions were used.

1. 280 µl of HNO₃ 0,1 M were added to 70 µl of the sample-solution. The analysis results show the percentage of Ca present in the samples, so it is possible to calculate how much of the sample-solution must be added to have a solution with 40 ppm of Ca.
2. in each centrifuge-tube the right volume of solution is poured and HNO₃ 0,1 M is added to reach 500 µl.

E.g. for the solution obtained from the samples picked at 11-12 cm there were 112.23 ppm of Ca in 350 µl of solution, in order to have only 40 ppm 35.6 µl of solution were poured in a new centrifuge-tube and 464 µl of HNO₃ 0,1 M were added. When all the solutions contain 40 ppm of Ca they are ready for being analysed.

The standards were run to regulate the instrument. Between each sample run the tubes were cleaned and rinse with a blank solutions of HNO₃ 0,1 M.

The basic equation that correlates oceanic temperature and Mg/Ca ratios is:

$$\text{Mg/Ca} = A \exp^{(B \times T)} \quad \text{Equation 3.3}$$

In this equation T is the calcification temperature express in °C; A and B are two constants related to the species. The values that better than others reflect the conditions of *Globigerina bulloides* at the Vøring Plateau are the ones used by Thornalley *et al.* (2009):

A = 0,794 (based on a calcification depth of 0-50 m and a temperature between 11 and 7,8 °C);

B = 0,1 (based on the north Atlantic core top calibration of Elderfield and Ganssen (2000).

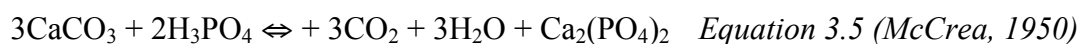
The results in the following equation:

$$\text{Mg/Ca} = 0,794 \exp^{(0,1 \times T)} \quad \text{Equation 3.4 (Thornalley et al., 2009)}$$

3.6. Laboratory instruments

3.6.1. Mass spectrometer

All the samples of *Globigerina bulloides* were measured on the Finnegan MAT 253 at the Geological Mass Spectrometry (GMS) laboratory at BCCR. The Finnegan MAT 253 is a devised to analyses of carbonates with two Nier type dual inlet gas source Isotope Ratio Mass Spectrometers (IRMS). The Finnegan MAT 253 is combined with a Kiel carbonate preparation device developed by McCrea (1950). To be analysed the carbonate (C and O in this case) have to be converted to gas. The Kiel device permits the formation of CO₂ gas from the carbonate tests by dissolving the carbonate in 100% phosphoric acid (H₃PO₄) at 70°C accordingly to the following chemical reaction (Eq. 3.5).



In this reaction all the carbon present in the test CaCO₃ is converted in the gaseous CO₂, therefore no fractionation of carbon occurs, thus only two out of three atoms of O are present in the gaseous CO₂, which means that a fractionation of oxygen occurs. If the fractionation is constant at a constant temperature (McCrea 1950), the fractionation is easily corrected. The optimal sample weight for the MAT 253 mass spectrometer is 30µg. Since the presence of the studied species in this core is low, an average weight of 25µg was analysed.

The Kiel device pumps the CO₂ into the inlet system of the mass spectrometer. Two inlets sites for gas are present in the mass spectrometer: one for the sample and one for the standard-reference gas. The isotopic fraction has to be avoided, for this reason the flow of the gasses has to be viscous and not molecular. In a molecular flow the lighter isotopes acquire faster speed than the heavier ones, therefore they will reach the mass spectrometer first and create a fractionation that will bias the isotopic signal. Indeed the viscous flow ensures that the isotopic fractionation does not occur in the capillary (Sharp, 2007). The viscous flow is created forcing the gasses to flow inside a crimp. After passing through the crimp both the gasses reach the switching block, here the sample and the standard gas flow alternate. This allows the measure of the isotopic content of both the gasses within a quick time eliminating the noise cause by electronic instability and other factors (Sharp, 2007) and allows the alternating measure of the isotopic fraction of standard and sample. When the gas leaves the switching box it flows into the ion source, where it is bombarded with electrons. These electrons stripes off the outer electrons of the ions and creates positively charged ions. The charged ions are then forced to pass in single beam through a strong magnetic field. The magnetic field deflects the positively charged ions into a circular trajectory, the deflection is controlled by the mass of the isotopes: lighter isotopes are deflected more strongly than heavier ones. The deflected ions are collected by several Faraday cups simultaneously, the difference between the isotopic ratio (δ) of the sample and the standard ratio is calculated. The CO₂ molecules that reach the Faraday cups have different weights, depending on the isotopic components. In nature molecules with more than one rare (heavy) isotope are extremely rare, so that for approximation the isotopic forms present are:

¹²C₁₆O₂, molecular weight 12 + (16 x 2) = 44, mass 44

¹³C₁₆O₂, molecular weight 13 + (16 x 2) = 45, mass 45

¹²C₁₆O₁₈O, molecular weight 12 + 16 + 18 = 46, mass 46

The mass spectrometer measures the molecular weight differences. Generally light isotopes and molecules (44) are way more abundant than the heavy ones (46). Heavy isotopes (¹³C and ¹⁸O) are almost impossible to be express in terms of absolute abundance. Therefore in paleoclimatology and paleoceanography the isotopes are not measured as isotopes concentration, but as the isotopic concentration is compared with the isotopic concentration of a standard reference sample (Hoefs, 1997). For this reason the results of the mass spectrometer analyses are express with a delta (δ), that represent

the difference between the sample and the standard measurements:

$$\delta_{\text{sample}} = ((R_x - R_{\text{standard}}) / R_{\text{standard}}) \times 10^3 \quad \text{Equation 3.6}$$

where x is a generic element and R is the isotopic ratio (e. g. $^{13}\text{C}/^{12}\text{C}$). δ values are expressed in parts per mill (‰). More positive δ_{sample} values correspond to an enrichment in heavy isotopes in the sample compared to the standard ($R_x > R_{\text{standard}}$) and *vice versa* more negative values indicate that the sample contains less heavy isotopes in comparison to the standard ($R_x < R_{\text{standard}}$). For this reason there are two inlets one for the sample and one for the standard to the mass spectrometer. The relative proportion is ^{16}O - ^{18}O and ^{12}C - ^{13}C in CO_2 from the samples are compared with the standard gasses. Four different common accepted standard gasses are used in geochemistry: Standard Mean Ocean Water (SMOW) for hydrogen and carbon, Pee Dee Belemnite (PDB) for carbon and oxygen, Mean Atmospheric Air for nitrogen, El Canyon Meteorite (CD) for sulphur. The PDB standard is the isotopic composition of *Belemnitella americana* from the Pee Dee Formation of the Upper Cretaceous of South Carolina, which is completely exhausted, for this reason recently this standard was replaced with an artificial one named Vienna Pee Dee Belemnite (VPDB) created by the International Atomic Energy Agency (IAEA). The VPDB is the standard that was used also in this study, therefore all the results are reported in this manner. To compare the oxygen isotopic content of fossil carbonate samples and seawater the following conversions are needed:

$$\delta^{18}\text{O}_{\text{VSMOW}} = 1.03091 \times \delta^{18}\text{O}_{\text{VPDB}} + 30.91 \quad \text{Equation 3.7 (Coplen et al., 1983)}$$

$$\delta^{18}\text{O}_{\text{VPDB}} = 0.97002 \times \delta^{18}\text{O}_{\text{VSMOW}} - 29.98 \quad \text{Equation 3.8 (Coplen et al., 1983)}$$

The GMS laboratory at the BCCR calibrates its own Carrera Marble (CM03) standards for mass spectrometry, and uses NBS 19 and NBS 18 to convert the measured values to the VPDB scale.

3.6.2. Inductively coupled plasma spectrometer

The mass spectrometer used for the Mg/Ca analysis is an Inductively Coupled Plasma Optical Emission Spectrometer (ICP-OES) in radial view TJA IRIS. Each element emits specific wavelength light. The ICP spectrometer recording and reading the wavelengths light analyses the isotopic content of certain liquid samples. The ICP Spectrometers works on the same bases, the normal working process is here described. IPC hardware generates plasma, a gas that contains ionized atoms, as explained below.

Three inlets bring the gas where the torch is situated. Three concentric tubes reach the torch that is placed within a water-cooled coil of a radio frequency generator. When the gas flows through the tubes and enters into the torch the radio frequency field is activated and the gas in the coil region becomes electrically conductive. The formation of the plasma is dependent to the strength of the magnetic field and the rotation pattern of the gas flow. The plasma is maintained by inductive heating of the incoming gasses. The magnetic field generates a high frequency electric current within the conductor. The conductor is warmed by the ohmic resistance. The plasma is insulated from the rest of the instrument to avoid short-circuiting and meltdown. Insulation is obtained by the simultaneous flux of gasses through the tubes: outer gas, intermediate gas and inner gas. The outer gas is Argon and it has the functions of maintaining and stabilizing the plasma, and isolating the plasma. Argon is the gas used also in the inner tube to carry the gas to the plasma. When the instrument is started it needs a couple of hours to stabilize plasma and temperature, when these are stable the analyses can start. If the plasma is not stable the results of the analyses will be affected by errors. When the sample reaches the torch the heat excites the atoms that after resting cools down to emit a photon. A detector detects the wavelength of the emitted photons. Through a digital detector intensity and wavelength are detected. After each run with the sample a run with the blank is done, so that a calibration curve to avoid the background noises can be build after the analyses. This curve has also the function to find the correspondence between wavelength results to the content in ppm of the analysed atomic species. The reproducibility of the analyses is 2,07% RSD for a Mg/Ca standard solution at 1 mmol/mol.

4. RESULTS

4.1. Carbon isotopes

The $\delta^{13}\text{C}$ record shows increasing values throughout the Holocene. The curve in figure 4.1A evidence a more marked increase of $\delta^{13}\text{C}$ during the early Holocene - beginning of mid Holocene interval, whereas the late Holocene shows a more stable pattern with a slightly increase.

From an overall observation of the curves three major minimum values are visible in the $\delta^{13}\text{C}$: ~10 ka BP, ~7.9 ka BP, and 1.8 ka BP. High variability is seen throughout the whole considered period, however the period 4-6 ka BP seems to have a less variable pattern.

4.2. Oxygen isotopes

The oxygen isotope curve (Fig. 4.1B) shows a main trend, since $\delta^{18}\text{O}$ slightly decreases in values from the older to the youngest part of the analysed section core. Since the observed $\delta^{18}\text{O}$ is mainly temperature dependent, a decrease of $\delta^{18}\text{O}$ mainly corresponds to an increase in temperatures. Focusing on *Globigerina bulloides* $\delta^{18}\text{O}$ trend the early Holocene and the first part of the mid-Holocene are characterised by a decrease in values. Whereas the late Holocene is characterised by a slowly increasing values. For the last 6 ka the trend seems constantly stable, although the variance is very high mostly in the last 4 ka. Five main negative values occurred at about 1.1, 1.8, 3.7, 7.4, 7.9 ka BP (Fig 4.1B). The peak at 3.7 ka BP highlights the longest period with low values of this section: from 3.4 to 3.8 ka BP. Also the high values present a certain variance, however no minimum values stand out as for the low values. In the most recent part of the Holocene the values seem to change the trend and the $\delta^{18}\text{O}$ increases.

4.3. Mg/Ca ratios

The results of the ICP-OES analyses are Mg, Ca, Sr, Li, Fe, Mn average intensity and concentration per sample. The values obtained from the analyses have been calibrated against the standards and the values of the blank solution. The concentration in ppm was recalculated from the intensity values, to make sure that no error affected the values. The data were converted in Mg/Ca, Sr/Ca, Fe/Ca and Mn/Ca mmol/mol. All the raw data in mmol/mol are listed in the Table 3.2. The minor elements (Al, Fe, Si, Mn) ratios provide the evidence of the presence of contaminants in the samples. Clay and silicate contamination is related to high values of Al/Ca, Fe/Ca and Si/Ca (Barker *et al.*, 2003). The content of Al in ICP-OES analysis

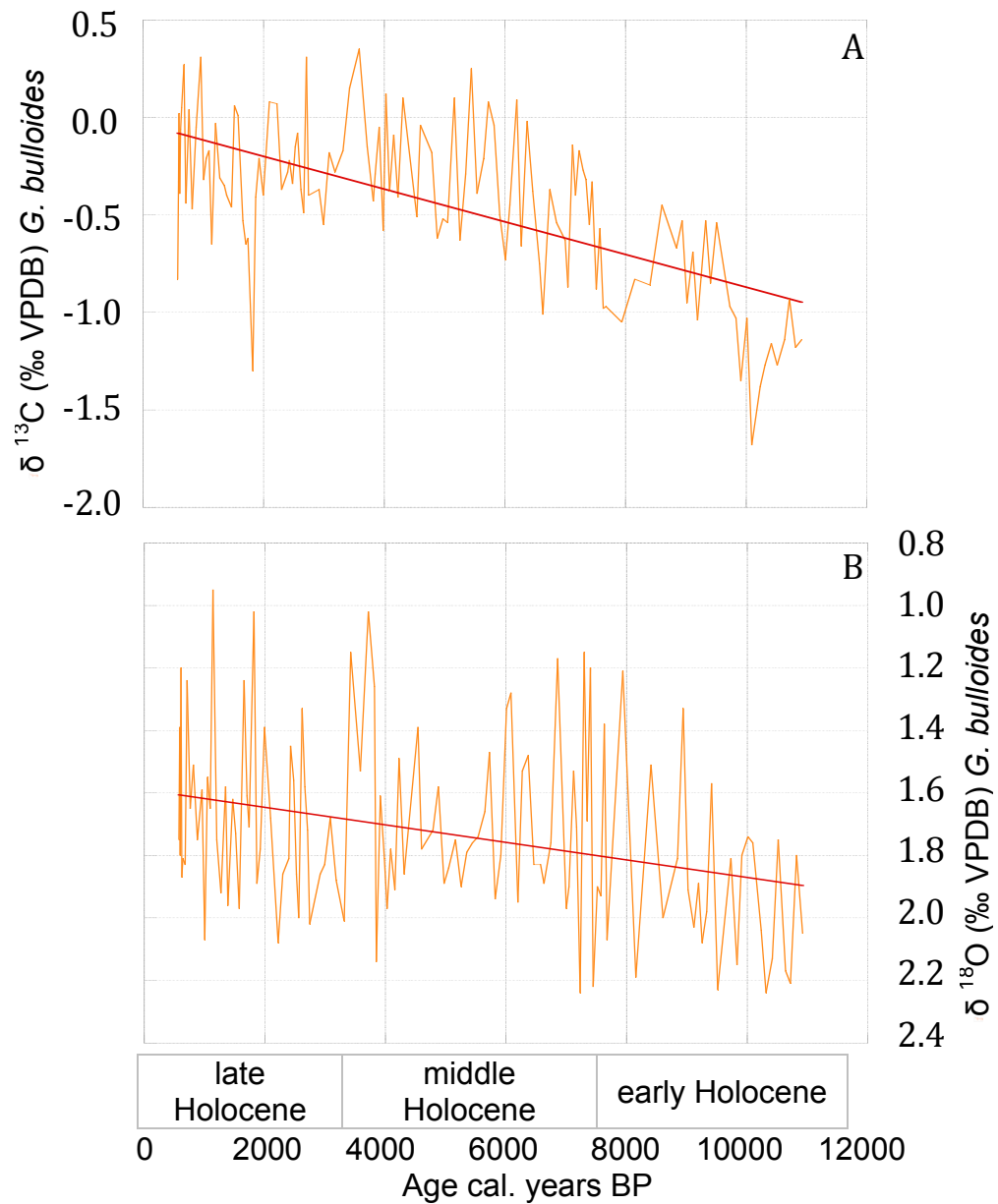



Fig. 4.1. Holocene variation in surface water conditions in the Norwegian Sea from MD95-2011. A, carbon isotopic composition; B, oxygen isotopic composition. Red line indicates the linear regression calculated with the program KaleidaGraph. 

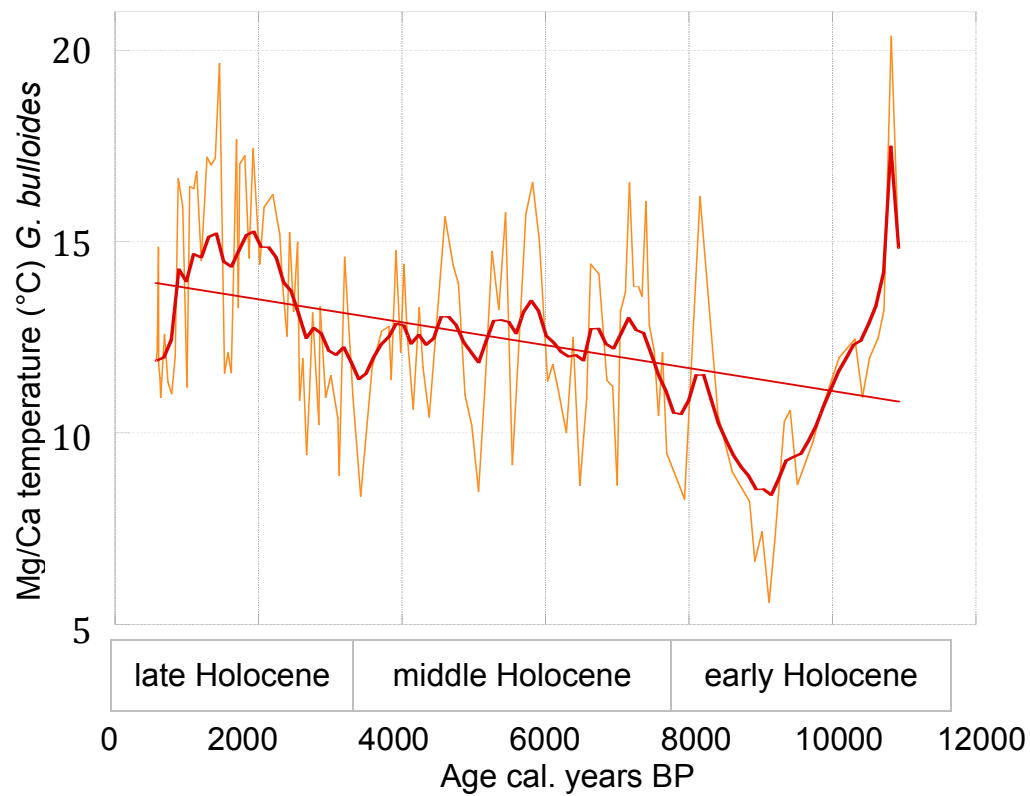


Fig. 4.2. Holocene variation in surface water conditions in the Norwegian Sea from core MD95-2011. Mg/Ca temperatures show in orange, smoothed curve seen in red. A geometric weight is applied to the points and $\pm 10\%$ of the data range is smoothed in the final curve. The red straight line indicates the linear regression during the Holocene (obtained with KaleidaGraph).

is usually under detection limit, for this reason Mn/Ca and Fe/Ca ratios have been examined. The Fe/Ca and Mn/Ca ratios indicate the possible contamination by Mn and Fe.

The calculated Mg/Ca temperatures (Fig. 4.2) show high frequency variability, for this reason a smoothed curve was used for the comparison with other records. Smoothing was performed using a Stineman function in KaleidaGraph. A geometric weight is applied to the points and $\pm 10\%$ of the data range is smoothed in the final curve. The youngest data point in the record has a temperature of $\sim 12^{\circ}\text{C}$. This value is close to the modern conditions, in fact the modern temperature at the Vøring Plateau at 10 m water depth is about 11°C for July-August-September (NODC WOA98, 1998). The similarity with the modern temperature confirms the general reliability of the data. The average Mg/Ca temperature is 12.6°C , which is slightly higher than the modern temperature at the site. From a general overview of the data two main warm periods and two main cooling periods can be observed. The two main warm periods are centred respectively at 1.5 ka and 6.3 ka BP. The latest warm period shows relatively high temperatures ($\sim 15^{\circ}\text{C}$ mean value). A discrete cooling centred at 3 ka BP separates these two warm periods. The most evident and long lasting cooling in this record is the 8.4-10 ka BP cold event (Fig. 4.2). This cooling event is centred at 9.5 ka BP and has the lowest peak at 9.1 ka BP. The highest temperature present in the record is 20°C at about 10.8 ka BP.

5. DISCUSSION

5.1. Carbon isotopes

Carbonates are unequally distributed in the ocean: marine carbonates have a mean composition $\delta^{13}\text{C}$ of about 0‰, organic matter has a $\delta^{13}\text{C}$ composition of about 25‰ (Hoefs, 2009). Accordingly two reservoirs and isotope mass balance exist:

$$\delta^{13}\text{C}_{\text{input}} = f_{\text{org}} \delta^{13}\text{C}_{\text{org}} + (1 - f_{\text{org}}) \delta^{13}\text{C}_{\text{carb}} \quad \text{Equation 5.1 (Hoefs, 2009)}$$

Where f_{org} is the fraction of organic carbon entering the sediment, it is defined in terms of global mass balance. Large f_{org} values can result from high productivity and high levels of preservation. The variables that affect the $\delta^{13}\text{C}$ ratio are still not well understood (Sharp *et al.*, 2007) and interpreting the $\delta^{13}\text{C}$ record is difficult and brings to uncertain conclusions. In general the $\delta^{13}\text{C}$ is inversely correlated with the nutrient concentration, thus it changes with the degree of incorporation of ^{12}C by phytoplankton and ^{12}C exchanges with the atmospheric CO_2 . However, *Globigerina bulloides* is known for showing decreasing values with increasing nutrient content and with enhanced primary productivity (Ganssen and Kroon, 2000). Thus the large fluctuations in the $\delta^{13}\text{C}$ record (Fig. 4.1A) can be interpreted as *G. bulloides* calcification changes in response to variations in the primary productivity within the photic zone. From an overall observation of the results a constant increase in values is seen throughout the whole Holocene. This trend correlates well with the temperatures increase trend seen in the $\delta^{18}\text{O}$ and Mg/Ca records in this study. A trend towards increasing $\delta^{18}\text{O}$ and decreasing $\delta^{13}\text{C}$ in planktic foraminifera from shallow to thermocline waters was seen in many studies (e.g. Curry and Crowley, 1987; Fairbanks *et al.*, 1980) and proves the existence of a correlation between $\delta^{18}\text{O}$ and $\delta^{13}\text{C}$ (Katz *et al.*, 2010 and references therein). Very low values are seen at the base of the analysed period at ~10 ka BP and a minimum is seen at 1.8 ka. These minima can reflect a low primary production, thus no such changes are seen in the other records from the same core. Considered the complexity of factors and relations that influence the $\delta^{13}\text{C}/^{12}\text{C}$ content, it is complicated to evaluate the influence of each single component on the final $\delta^{13}\text{C}/^{12}\text{C}$ values.

5.2. Oxygen isotopes

The amount and percentage of oxygen contained in marine organisms depends mainly on the water temperature, but also on the salinity and presence of salts dissolved in the water and water pH (see chapter 3.4 above; Hoefs, 2009; Katz *et al.*, 2010 and references therein). The first equation linking water temperature and stable oxygen content of shells of marine organisms (eq. 3.3) established by Epstein *et al.* (1953) shows a simple and direct connection between water temperature and $\delta^{18}\text{O}$ content.

$$T = 16.5 - 4.3 (\delta_{\text{carbonate}} - \delta_{\text{seawater}}) + 0.14 (\delta_{\text{carbonate}} - \delta_{\text{seawater}})^2$$

Equation 5.2 (Epstein *et al.*, 1953)

The oxygen stable isotopes in this study show a main decreasing trend throughout the whole Holocene superimposed by smaller, high-frequency fluctuations (Fig. 4.1B). Since the ice volume does not vary a lot after the last deglaciation (7.5 ka) it does not influence in a significant way the record, so this increasing pattern is interpreted as a warming trend throughout the Holocene. The trend of increasing temperature during the Holocene is seen also in the Mg/Ca records of *Globigerina bulloides* in this core (see section 5.3 Mg/Ca ratios; Fig. 5.1, 5.2 and 5.3), meaning that the temperatures are increasing during the Holocene. This trend is seen in other records in the North Atlantic (Fig. 5.1, 5.2 and 5.3), and reflects an increased winter insolation (Came *et al.*, 2007 and references therein). The trend in the $\delta^{18}\text{O}$ record of *G. bulloides* shows two main periods of decreasing oxygen isotopic values (8-11 ka and 2-0.6 ka BP). The warming trend of the late Holocene is supported by observations of warming periods in other records from the same site (Andersson *et al.*, 2003; Dolven *et al.*, 2002; Risebrobakken *et al.*, 2003), in other sites (Marchal *et al.*, 2002) and terrestrial records (Helama *et al.*, 2002). Risebrobakken *et al.* (2003) suggested that during the late Holocene the Arctic front was further from the Vøring Plateau than in the preceding periods (early and mid- Holocene). This interpretation is supported by the observations that the $\Delta\delta^{18}\text{O}$ values of *N. pachyderma* (dex.) and *N. pachyderma* (sin.) are lower during the late Holocene than in the early and mid-Holocene. This is seen as evidence of an eastward migration of the Arctic front. Moreover, high relative abundance of *Globigerina quinqueloba* (a species strongly connected to the Arctic Front (Johannessen *et al.*, 1994)) between 4-8 ka supports the hypothesis of a more eastward location of the Arctic front. In the early Holocene the decreasing trend of *G. bulloides* $\delta^{18}\text{O}$ record corresponds to the warming event at 10.8 ka seen in the Mg/Ca record in the same core (see section 5.3 below). The $\delta^{18}\text{O}$ values are supported by the evidence that the warm Atlantic water increased its influence at ~10 ka (Hald *et al.*, 2007; Risebrobakken *et al.*, submitted). Andersson, *et al.* (2010), Hald *et al.* (2007) and Risebrobakken *et al.* (submitted) showed that the early Holocene warming was recorded in the whole North Atlantic and caused by an increase in heat in the NwAC and/or by an increase northwards transport. The heat was mainly lost for advection before the NwAC entered the Fram Strait (Risebrobakken *et al.*, submitted). Although before 7ka also the ice volume can have a big effect on the foraminiferal oxygen content. In the $\delta^{18}\text{O}$ record of *G. bulloides* the middle Holocene is in average stable. This stable period from 2 to 8 ka is evident also from the Mg/Ca temperatures recorded in *G. bulloides*. This relatively stable period can be correlated with the evidence in many records in this region of warm stable period between 6 and 9 ka BP (e.g. Risebrobakken *et al.*, submitted). This trend is assumed to be the response to the highest summer insolation during the early

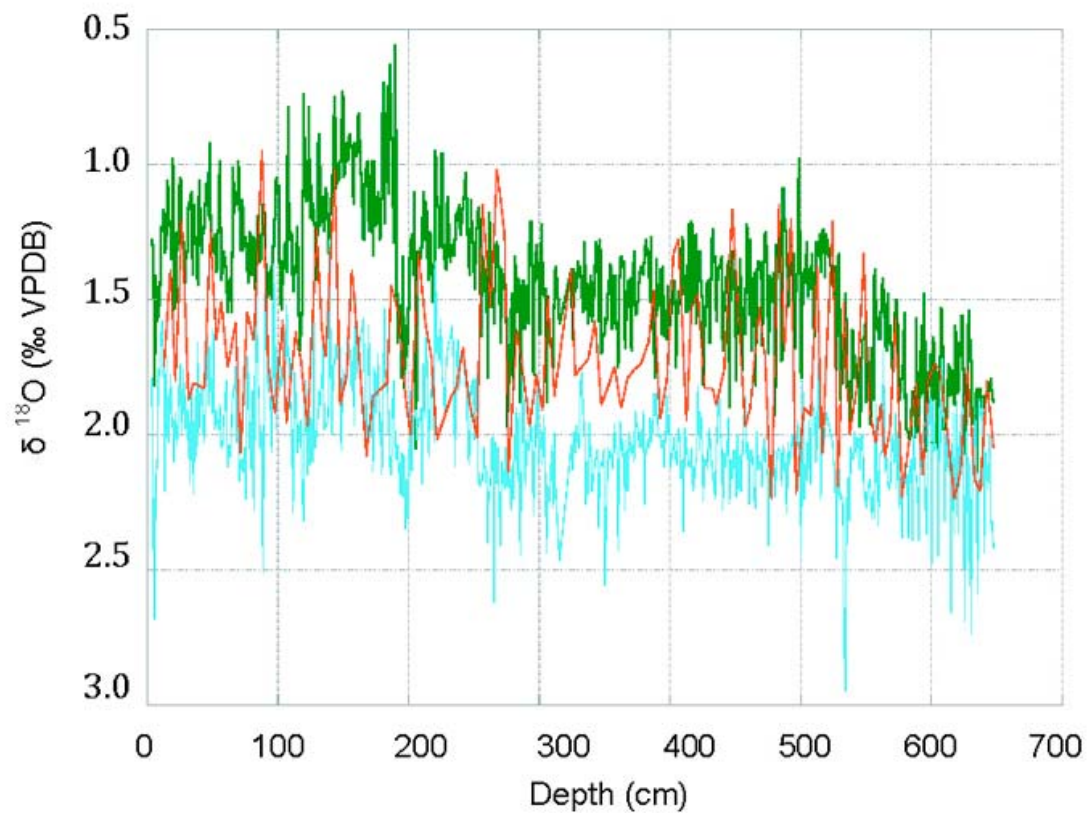


Fig. 5.1. Comparison between oxygen isotopic content of *Globigerina bulloides* in red (this study) and *Neogloboquadrina pachyderma* (dex.) in green, *N. pachyderma* (sin.) in blue (Risebrobakken *et al.*, 2003) from the core MD95-2011. In x-axis depth of the core, in y-axis the oxygen content as $\delta^{18}\text{O}$ vs VPDB.

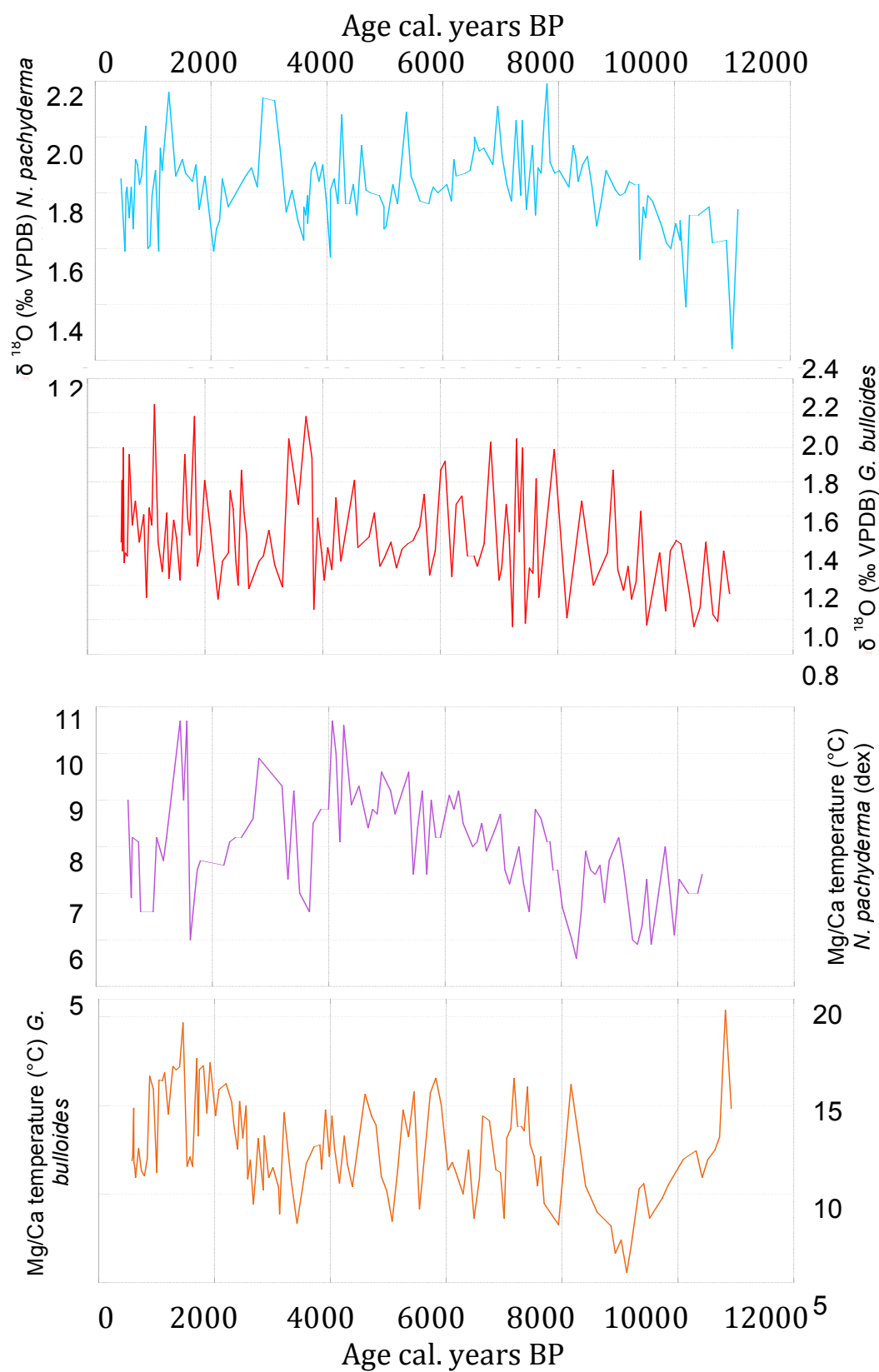


Fig. 5.2. Oxygen isotopic content and Mg/Ca temperatures of *Globigerina bulloides* of the core MD95-2011 are displayed as red and orange lines, and of *Neogloboquadrina pachyderma* (dex.) in the core ODP 984 are shown with blue and violet lines (Came *et al.*, 2007).

Holocene. This pattern is also seen in the Mg/Ca analysis in this study (see section 5.3 below) and in other foraminiferal records from the same core (Fig. 5.1; Andersson *et al.*, 2003; Nyland *et al.*, 2006; Risebrobakken *et al.*, 2003), and from other cores in the North Atlantic (e.g. Thornalley *et al.*, 2009). Five episodes with minimum values are present at about 1.1, 1.8, 3.7, 7.4, 7.9 ka BP in the $\delta^{18}\text{O}$ record (Fig. 4.1B). However, these minimum temperatures do not seem to have any correspondence with other records from the same core, and neither with other records in the North Atlantic. Seven main peaks of high values are seen at 1, 2.2, 3.8, 7.2, 7.4, 8.1, 9.5, 10.3, 10.7 ka in this study (Fig. 4.1B). The ones at 1, 3.8, and 9.5 ka are roughly corresponding to low temperatures values reported in the Mg/Ca temperatures in this study, and also from ODP Site 984 (Came *et al.*, 2007) and from the Greenland record GISP2 (O'Brien *et al.*, 1995).

5.3. Mg/Ca ratios

The reliability of calcite Mg/Ca as paleotemperature proxy was tested in laboratory experiments (Burton and Walter, 1991; Katz, 1973), empirical and culture studies of marine biogenic calcite such as ostracodes (Dwyer *et al.*, 1995), corals (Mitsuguchi *et al.*, 1996) and foraminifera (e.g. Lea *et al.*, 1999).

Some secondary effects can interfere with the Mg/Ca content of foraminiferal tests. The core was drilled at 1048 m water depth; considering that the Carbonate Compensation Depth (CCD) is approximately below 5 km water depth in the North Atlantic (Nichols and Williams, 2008), a partial dissolution of the calcite can be excluded. In addition the plot between Mg/Ca content and average weight shows positive correlation (Fig. 5.4). A negative correlation links heavier test with lower Mg/Ca content and shows that a partial dissolution affected the analysed samples. Few outlier points at the extremes of the range show negative correlation. However, the main trend is positive and any massive dissolution effect can be excluded in the samples.

The function of the minor elements (Al, Fe, Si, Mn) ratios recorded in the spectrometer analysis is to check the presence of contaminants in the samples. If the content of Mn/Ca and Fe/Ca is higher than 0,1 mmol/mol the analyses are considered to be affected by contamination. The Mn/Ca and Fe/Ca content is higher in foraminiferal species with thinner tests, and the accepted limit to exclude contamination is assume to be below 0.1 mmol/mol (Barker *et al.*, 2003). Few samples contained a Fe/Ca ratio higher than 0,1 mmol/mol. However, comparing the Mg/Ca ratios to the Fe/Ca and Mn/Ca ratio indicates any possible contamination. As shown in Figure 5.5, the correlation factor between Mg and Fe is $R^2_{\text{Fe}}=0.7$ and between Mn and Mg is $R^2_{\text{Mn}}=0.3$. The correlation factors are very low therefore no contamination is assumed to have affected the analysis. Mg/Ca data from *Globigerina bulloides* evidence a warm stable period is centred at 5.5 ka. This stable period (7.5-4 ka) almost coincides with the warm steady period

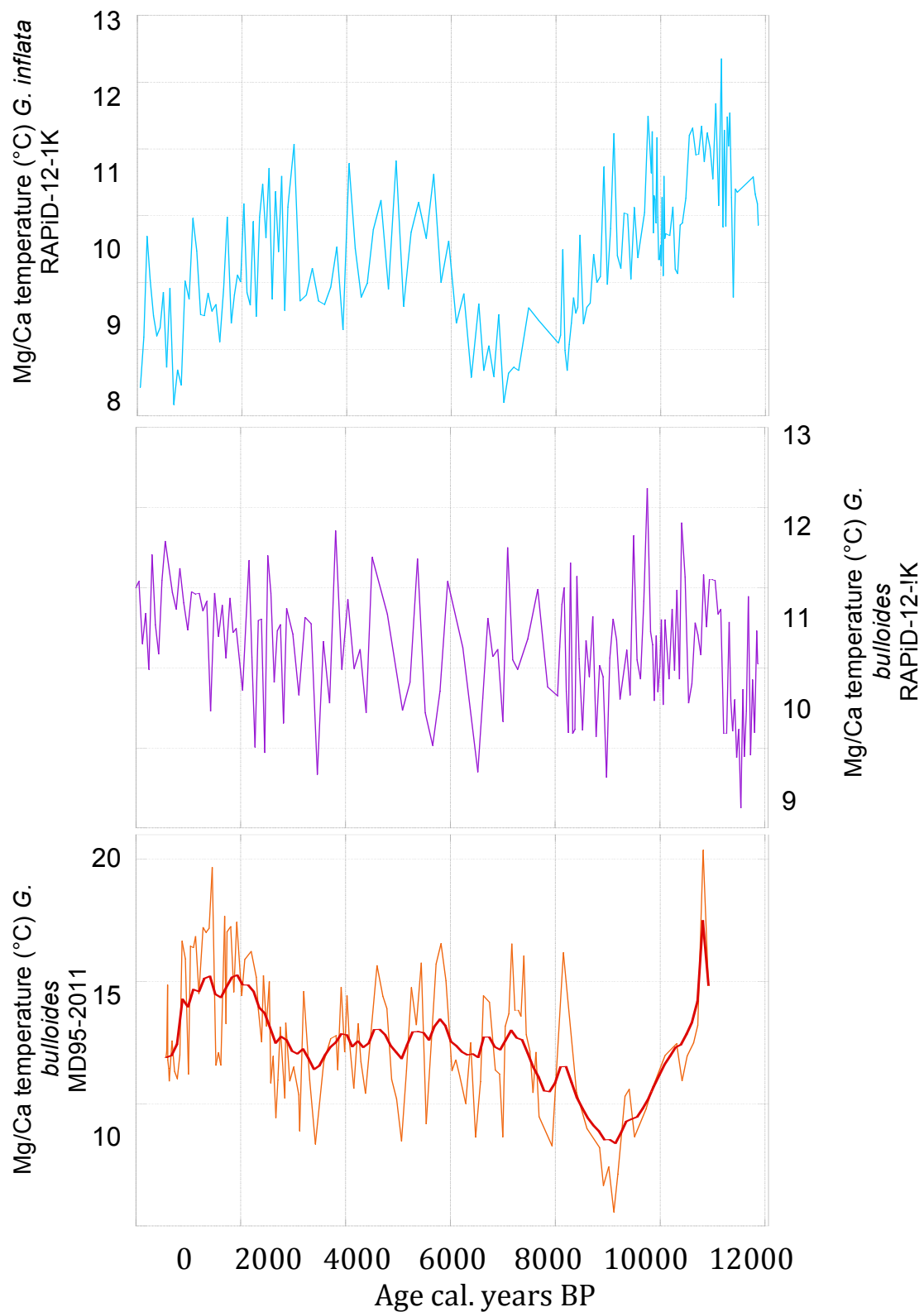


Fig. 5.3. Temperature curves based on Mg/Ca record, the blu line shows *G. inflata* record from core RAPiD-12-1K (Thornalley *et al.*, 2009), the violet line shows *G. bulloides* record from core RAPiD-12-1K (Thornalley *et al.*, 2009), and the orange line shows the record of *G. bulloides* in this study (the red line shows the smoothened values).

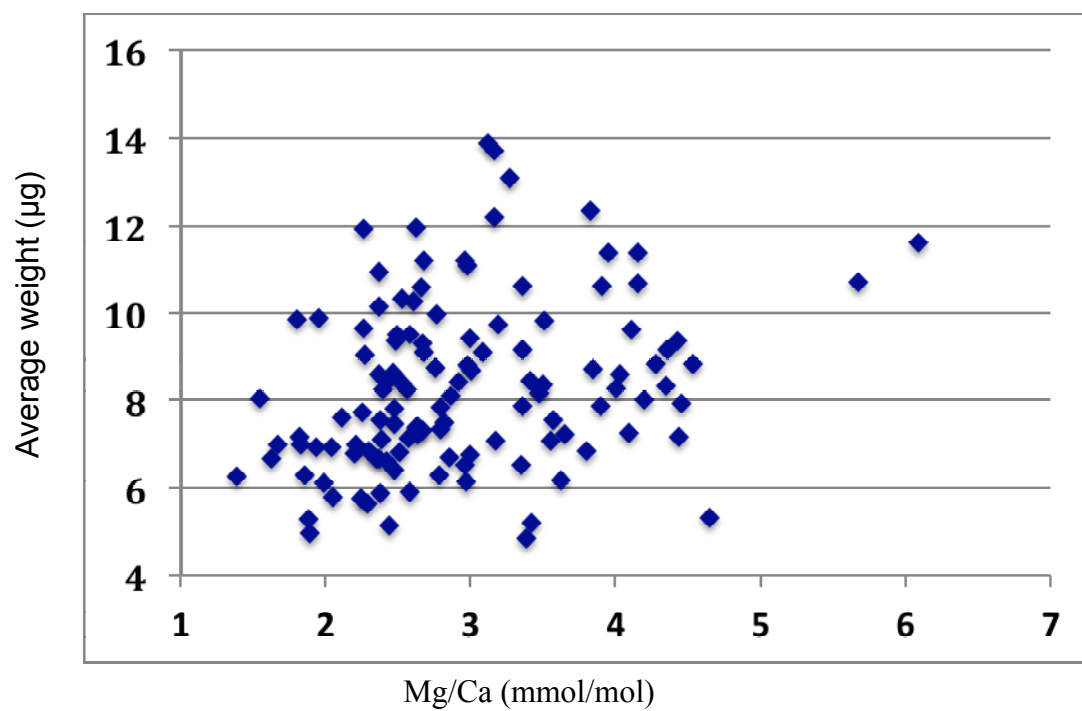


Fig. 5.4. Mg/Ca content plotted versus average weight of the tests of *G. bulloides*. The positive correlation shows that no dissolution affected the samples.

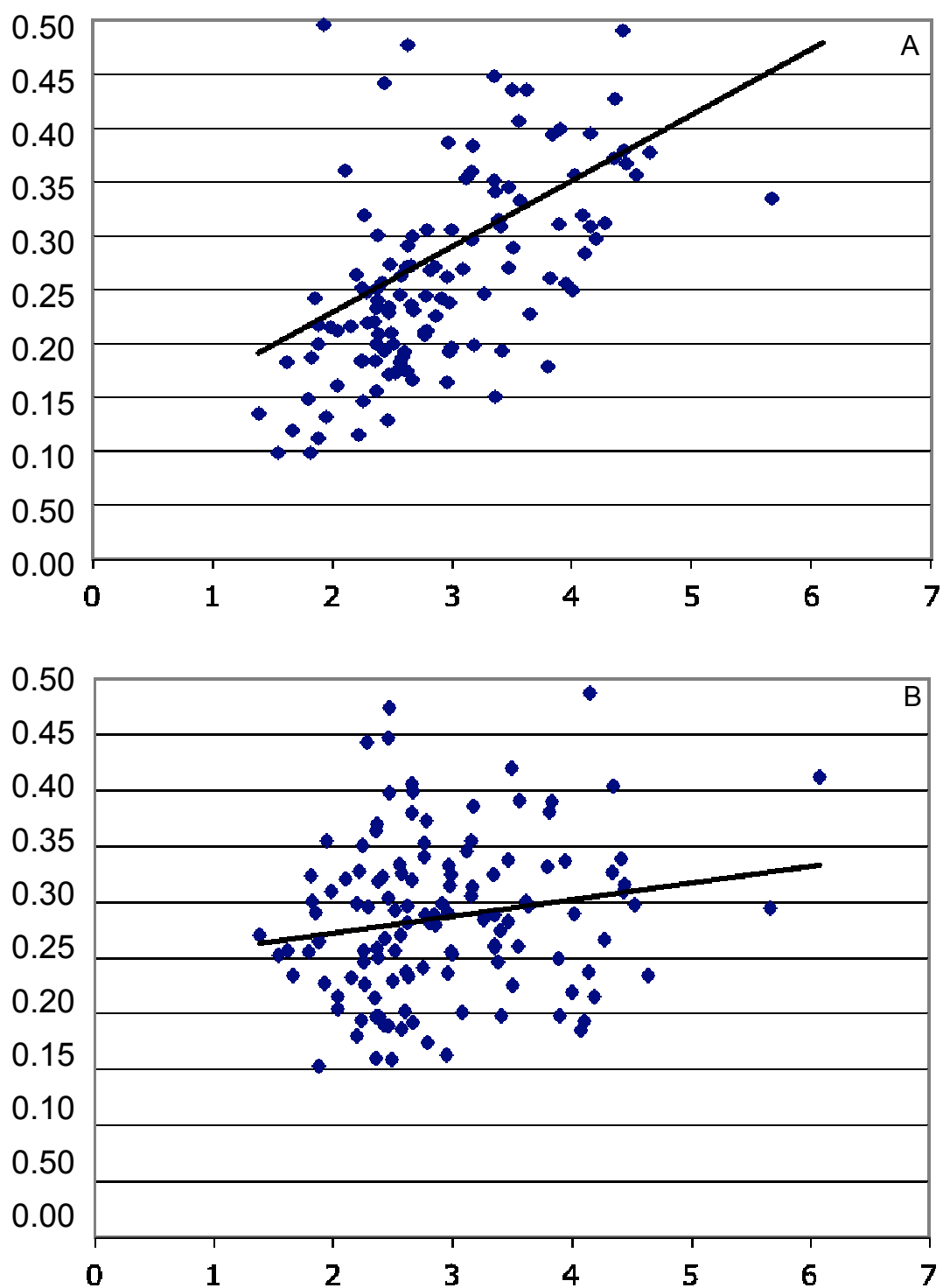


Fig. 5.5. A, correlation between Fe/Ca mmol/mol with correlation factor $R^2_{Fe}=0.7$. B, correlation between Mn/Ca mmol/mol, the correlation factor is $R^2_{Mn}=0.3$.

seen in the $\delta^{18}\text{O}$ record of *G. bulloides* in the same core. This pattern is also seen in other foraminiferal records from the same core (Andersson *et al.*, 2003; Nyland *et al.*, 2006; Risebrobakken *et al.*, 2003; Fig. 5.1), and from other cores in the North Atlantic (e.g. Thornalley *et al.*, 2009; Fig. 5.3). In the core MD95-2011 the SST reconstructions based on alkenones and diatoms record between 9-6 ka show a warm period (Birks and Koç, 2002; Calvo *et al.*, 2002; Risebrobakken *et al.*, submitted). This period is considered to correspond to the HTM in the North Atlantic, and as noted by Risebrobakken *et al.* (submitted), it coincides with the maximum warming of the Summer Mixed Layer (SML). This warming did not affect the water mass below the SML, so that organisms dwelling and calcifying below it did not record in their tests the warming trend. However, other records display warm conditions during the Holocene. In the Greenland borehole temperatures reconstructions and $\delta^{18}\text{O}$ the warmest temperatures of the Holocene are displayed at 5-8 ka and 7-10 ka BP respectively (e.g. Dahl-Jensen *et al.*, 1998; Vinther *et al.*, 2009). The Norwegian glaciers reach their minimum volume during the early and mid-Holocene (e.g. Nesje *et al.*, 2005). The average temperature recorded in the tests of *G. bulloides* during the middle Holocene is 12.5°C (almost 1.5°C higher than the modern mean sea surface temperatures; NODC WOA98, 1998). Warmer temperatures during this period are reported from many studies in the North Atlantic (e.g. Andersson *et al.*, 2010 and references therein; Thornalley *et al.*, 2009). In these studies the temperature during the mid-Holocene was just slightly warmer than the modern one, however the temperatures displayed in this record are not always comparable with other records, since the temperatures in this study are much warmer than what expected (see discussion below). Risebrobakken *et al.* (submitted) in their comparison of various proxies from many cores in the Nordic Seas notice that the HTM did not influence the water temperature below the summer mixed layer (SML), therefore it is not seen in foraminiferal based records. Accordingly with this observation no increased temperatures were seen in *G. bulloides* in this record during the mid-Holocene.

The mid-Holocene stable period is followed by a colder period in the late Holocene in this record. Between 600-800 yr BP a cooling trend is seen in the Mg/Ca temperature record of this study, this cooling overlaps with a period of colder SST and variations in abundance of *N. pachyderma* (sin.) at Vøring Plateau (Andersson *et al.*, 2003). This event was also seen by Jennings and Weiner (1996) in the Nansen Fjord, and compares well with the seen beginning glacier advance at 700-750 yrs BP (Grove and Switsur, 1994). These correlations show that this cooling event affected the Norwegian Sea and the Norwegian coast and should probably be inserted in the Little Ice Age period.

During the late early Holocene the Mg/Ca temperature reconstructions of *Globigerina bulloides* show a cooling event at 7.9 ka is seen (Fig. 4.2). However, this cannot be connected to the 8.2 event in this study (Fig. 5.1), since the 8.2 event in the MD95-2011 core was seen at an interval thinner than 5 cm. Therefore it is difficult to detect with a picking range of 5 cm, moreover the

8.2 event is normally seen as a much bigger cooling event. From other records of the same core (e.g. Risebrobakken *et al.*, 2003; Fig. 5.1) a cool event comparable with the 8.2 event is evident. In this study a cooling is seen at 8.1, although with lower magnitude. This can be seen as the last part of the 8.2 cooling event. Comparable temperature reduction occurred at 9.1 ka (Mg/Ca record, Fig. 4.2). Evidence of this cooling event is also seen in the study of Came *et al.* (2007), which measured foraminiferal Mg/Ca and $\delta^{18}\text{O}$ in the planktic foram *Neogloboquadrina pachyderma* dextral coiled. A contemporaneous cooling is also seen in the GISP2 $\delta^{18}\text{O}$ record, but this cooling event is less evident in this archive. However, the cooling is simultaneous with an excursion in the terrestrial dust concentration in the GISP2, showing increased winds over Greenland (O'Brien *et al.*, 1995), and it is almost concurrent with detrital evidence of an ice-rafting event in the North Atlantic at ~9.5 ka (Bond *et al.*, 2001), it is also coincident with a reduced solar irradiance (Neff *et al.*, 2001). The cooling event in this study (Mg/Ca temperatures record) is the culmination of a long term cooling that lasts from 8.4 to 11 ka. This event can possibly be correlated to a cooling at approximately the same period at ODP 984 (Came *et al.*, 2007; see section 5.4 below, Fig. 5.2). This cold period is also seen in other records in the North Atlantic (Thornalley *et al.*, 2010). The comparison of many cores (Risebrobakken *et al.*, submitted) of the Nordic Seas showed the decrease of relative abundance of *G. bulloides*, *N. pachyderma* (dex.) and *T. quinqueloba* that corresponds to a decrease in temperatures. This cold event has been recognised in the whole Nordic Seas region, and it is seen as the consequence of the diminution of the Atlantic reservoir of surplus heat after the warm event at ~10 ka and the decreased northwards heat advection (Risebrobakken *et al.*, submitted).

Two anomalous warm periods are seen at the end and at the beginning of the Mg/Ca record of *Globigerina bulloides*. The first event is included in the early Holocene: Mg/Ca data from *G. bulloides* display a warm peak (20.4°C) at about 10.8 ka. The absolute temperature recorded by the Mg/Ca seems, however, highly unlikely to reflect the sea temperature of the Norwegian Sea in the Holocene. However, this signal must be considered as it is overlapping with a warming signal in the $\delta^{18}\text{O}$ record of Risebrobakken *et al.* (submitted) study. Warm temperature at this time is supported by data from Risebrobakken *et al.* (submitted) that registered the maximum northward heat advection at around 10 ka, confirming the presence of a warm event in the Nordic Seas. A second anomalous warm period appears more long lasting: it last from 0.8 to 2.4 ka BP (Fig. 4.2) and shows an average temperature of about 15°C. In this study the warm conditions persist for a long time and show an average temperature of almost 4°C warmer than the present situation. An increase in temperature can be explained by a change in calcification depth *G. bulloides* during this period, or by a change in the water condition, and/or by a change in the period of calcification of the tests. It is difficult that a change in the water column was not seen in any other records from the same core, although this possibility cannot be completely

excluded. A change in calcification season and/or depth should be driven by some mechanism, such as a change in the composition of the upper part of the water column, however there are no evidence of such an event in other studies in the North Atlantic (e.g. Farmer *et al.*, 2008; Risebrobakken *et al.*, *submitted*). A warming trend was seen at the Vøring Plateau during the late Holocene in the study of Andersson *et al.* (2003), the warming period lasts from 800 to 1200 years in their study, and the temperatures recorded by *N. pachyderma* in their study are just slightly warmer or as warm as the modern ones. Isotopic record and foraminiferal content in MD95-2011 indicates generally warmer conditions in the late Holocene (Risebrobakken *et al.*, 2003).

The mean Mg/Ca temperature in *Globigerina bulloides* in the whole record is 12.6°C, on average higher than modern temperatures, and it reaches peaks of ~20°C. The record of *G. bulloides* in this study shows higher temperatures than elsewhere in the North Atlantic during the Holocene. Other records from the Norwegian Sea and Nord Atlantic do not show such high values. However, the reasons of these high values are unknown. One possible explanation is that under stress conditions, such as changes in the water conditions (i.e. change from the winter to the summer circulation) *G. bulloides* calcifying patterns changed. The organisms could uptake more Mg than normal, even more than what considered from the vital effect for this species. However, no support for this theory was found, moreover during the same stratigraphic interval investigated in other sites in other studies *G. bulloides* do not show such anomalous calcification.

5.4. Comparison with North Atlantic records

Surface dwelling foraminifera like *Globigerina bulloides* normally calcify above the thermocline, therefore they are supposed to respond to changes in summer insolation and they should show the same Holocene SST tendency as phytoplankton-based SST proxies since the early-middle Holocene (Jansen *et al.*, 2008). However, the connection between SST and foraminifera is not as clear as in phytoplankton records. Radiolarians and foraminiferal record the seawater conditions more than the insolation (e. g. Dolven *et al.*, 2002; Imbrie and Kipp, 1971). For the core MD95-2011 the alkenones (Birks and Koç, 2002) and diatoms (Calvo *et al.*, 2002) records show an increase in temperatures in the early and middle Holocene, and a decrease in the late Holocene (Fig. 1.4). The foraminiferal $\delta^{18}\text{O}$ record of *G. bulloides* (this study) and *N. pachyderma* (dex. and sin.) (Risebrobakken *et al.*, 2003) show slightly decreased temperatures during the whole Holocene (Fig. 5.1). Moreover, the warm conditions present at 5-10 ka BP in the foraminiferal record are not seen in the phytoplanktonic surface dwellers (Fig. 1.4). Moros *et al.* (2004) explained the difference between the phytoplankton and the

zooplankton record as consequent effect of a different dwelling depth (phytoplankton lives in more shallower waters, therefore it records the SST), and differences in blooming seasons.

The oxygen isotopic and Mg/Ca temperature records from *Globigerina bulloides* in this study were compared with earlier studies of cores in the North Atlantic. Calibration issues make species to species comparisons difficult but raw Mg/Ca data can provide valuable information, the warming trend during the Holocene seen in Mg/Ca and $\delta^{18}\text{O}$ records in this study (Fig. 4.1 and 4.2) was measured also on the $\delta^{18}\text{O}$ content of *Neogloboquadrina pachyderma* in the same core (Risebrobakken *et al.*, 2003; Fig. 5.1). On the whole the main trend of $\delta^{18}\text{O}$ record of *G. bulloides* is similar to the $\delta^{18}\text{O}$ record of *N. pachyderma* from the same core (Fig. 5.1). The values of *G. bulloides* record are generally intermediate between the $\delta^{18}\text{O}$ values of *N. pachyderma* (dex.) and *N. pachyderma* (sin.). Generally *N. pachyderma* (dex.) calcifies between 30 and 40 m water depth, and *N. pachyderma* (sin.) usually calcify below the pycnocline at a depth between 70 and 250 m water (Simstich *et al.*, 2003). At these depths the temperatures are generally 2-3°C lower than at the sea-surface (Andersson *et al.*, 2010). This suggests that *G. bulloides* shows intermediate conditions between *N. pachyderma* (sin.) and (dex.). However, the discussion concerning the depth habitat of *Neogloboquadrina pachyderma* is still open. At the North of Iceland, for example, the calcification depth is reported to be the same for both the morphotypes (Andersson *et al.*, 2010). Using a global foraminiferal model (PLAFOM) Fraile *et al.* (2009) calculated the seasonal imprint on the sedimentary record. They found that both the morphotypes of *N. pachyderma* and *G. bulloides* present a positive gap between the expected mean temperature and the annual mean temperature, suggesting that these species mirror the summer temperatures more than other periods of the year. However, recent studies suggest that foraminiferal Mg/Ca temperatures and isotopic reconstructions are mainly influenced by annual average temperature, more than seasonal conditions (Leduc *et al.*, 2010). Johannessen *et al.* (1994) showed that *N. pachyderma* (sin.) mirrors the arctic and polar water, indeed *G. bulloides* and *N. pachyderma* (dex.) are more related to the Atlantic water, since they are more thermophilic species. Andersson *et al.* (2010) temperature reconstructions show that the warming trend during the Holocene is not confined at the Vøring Plateau, but it was seen also in other localities in the North Atlantic.

Other foraminiferal records from the North Atlantic share the same temperature trend of the Vøring Plateau. The foraminiferal abundance of *Globigerina bulloides* and *Globorotalia inflata* was analysed in the core RAPiD-12-1K from the South of Iceland by Thornalley *et al.* (2009). The Mg/Ca record of *G. bulloides* of this study compares well with the Mg/Ca temperature from the RAPiD record (Fig. 5.3). The main trend of *G. bulloides* in both the cores is overlapping; the temperature decreases between 10 ka and 9 ka having the minimum temperature at 9.1 ka BP. The interval between 8 and 4 ka is characterized by abrupt variations in values in both the records, the peaks and the minimum values of *G. bulloides* record in RAPiD-12-1K and MD95-

2011 overlap for the whole period, indicating the same variations in the climatic pattern of the North Atlantic. In the late Holocene warming pattern is seen in the RAPiD-12-1K record. A similar trend is seen also in the studied core, but the increasing trend starts at about 3 ka BP whereas in the study of Thornalley *et al.* (2009) it starts at about 2 ka BP.

Hald *et al.* (2007) compared six Holocene sediment cores in the eastern Norwegian Sea, below the path of the Norwegian Current. They reported stable or weak warming during the mid and late Holocene between 60 and 69°N: the same conditions are seen in the record of *G. bulloides* of this study. Hald *et al.* (2007) also noticed many abrupt climatic events superimposed on this main trend. They reported four major cooling periods between 8-9 ka, 5.5-3 ka, at around 1 ka and around 400 years BP. The same abrupt cooling can be seen also in the *G. bulloides* Mg/Ca record in this core with the exception of the cooling at 1 ka. The cooling at 400 years BP cannot be seen because the analysed period in this study stops at 600 years BP. In the study of Hald *et al.* (2007) other marked cooling events were observed (9-8, 7.5, 6.5, 5.5-3 and 1 ka BP) in the northernmost sites and according to Hald *et al.* (2007) these are related to an increased influence of the Arctic waters. A long lasting cool period is evident between 8.4-10 ka in the Mg/Ca record of *G. bulloides* in this study. Most of the cores analysed by Hald *et al.* (2007) show a cooling period between 8-9 ka BP, according to these authors this cool period incorporates the 8.2 event. Smaller cooling events are seen at about 5.5 and 3 ka BP. In the Hald *et al.* (2007) comparison and also in this record a warming peak around 2 ka BP follows the cold period at 3-5.5 ka BP. In general, the Mg/Ca record of this study compares well with the overview comparison on the North Atlantic Holocene climatic evolution made by Hald *et al.* (2007).

The core from ODP Site 984 was drilled on the Björn Drift on the Reykjanes Ridge at 61°N 25°W and 1648 meters water deep (Came *et al.*, 2007). Came *et al.* (2007) have analysed the Mg/Ca content and the oxygen isotopes of this core. Generally, the Mg/Ca record from MD95-2011 (this study) compares well with the Mg/Ca record based on *N. pachyderma* (dex.) from ODP 984 (Fig. 5.2). The main trend is the same for both the records throughout the whole period, apart from the exceptionally high temperature recorded at 10.8 ka in MD95-2011. There is an offset in timing of about a century between the two records, however this can be explained by uncertainties in the age-models used. There are two major cool events at about 9.3 ka and 8.2 ka (8.1 ka in the MD95-2011 record) that correlate well. A global stable steady warm period follows the 8.2 event. Another cool event at about 3.4 ka correlates well between the two records. There is also a weak warming seen at ODP 984 between 1.5 and 1 ka, which is also present in the *G. bulloides* record from the Vøring Plateau.

5.5. High frequency variability

Both the stable isotopes and Mg/Ca data show a high-frequency variability throughout the records. The observed variability in the *Globigerina bulloides* record from MD95-2011 is unusually high compared to other published records (Andersson *et al.*, 2003, 2010; Risebrobakken *et al.*, 2003 and submitted; Thornalley *et al.*, 2009). However, in previous Mg/Ca analysis of *Neogloboquadrina pachyderma* (dextral coiled) from the same core (Nyland *et al.*, 2006) similar variability was observed. Nyland *et al.* (2006) suggested that this can be the result of uncertainties in the Mg/Ca temperature calibration for the species. However, it is difficult to follow the same argumentation in the case of *G. bulloides* since available Mg/Ca calibration curves have been successfully used in many paleotemperatures reconstructions from different latitudes including the Nordic Seas (e.g. Came *et al.*, 2007; Thornalley *et al.*, 2009). Moreover, this study demonstrated that not only *N. pachyderma* (dex.) shows high variability, but also *G. bulloides*, so that high variability is not species-specific, but it is seen in all the Mg/Ca analyses at the Vøring Plateau.

A possible explanation for the high-variability, in this study is that the size range of the picked specimens could have been too large. In the size fraction smaller than 150 μm juvenile specimens occur. About 15 samples taken from different depth in the core had size fraction 125-500 μm , those were not further sieved, therefore they were analysed and may contained young specimens. Anand *et al.* (2003) showed that differences in specimen size can result in small differences in the isotopic and Mg/Ca values. Furthermore, it is experimentally demonstrated that the oxygen isotopic composition of *Globigerina bulloides* increases with increasing size fraction, to a lesser extent $\delta^{13}\text{C}$ and Mg/Ca increase with increasing size fraction (Elderfield *et al.* 2002). According to Katz *et al.* (2010) small specimen calcify faster than larger ones, and larger specimen dwell at warmer, shallower waters where light intensity is higher and the photosymbionts activity is higher. These two factors force the Mg/Ca content to be higher in larger specimens, so that larger specimens should have warmer signals in their Mg/Ca ratios. Nyland *et al.* (2006) suggested that it is possible to decrease the variability changing the B constant in the Mg/Ca equation (Eq. 3.3). Many different equations have been tested, but the one used by Thornalley *et al.* (2009) appears to be the most appropriate, also because it respects the limits registered in the laboratory tests on living specimens. However, 15 samples of a total of 126 analysed samples cannot explain such a high variability throughout the whole analysed period. 15 samples containing a couple of specimen with the size fraction 125-150 μm cannot be considered the explanation of this problem. However, the large size fraction (125-500 μm) can partly explain the variability seen in the analyses. The $\delta^{18}\text{O}$ ratio increases with increasing size fraction, reaching a plateau at 300-350 μm (Elderfield *et al.*, 2002). This size fraction assures that no ontogenetic effect affects the specimens. However, to explain such a high variability the content of the samples should have alternately large size fraction samples and

small ones. This unequal distribution of foraminiferal size fraction was not seen in the samples. So the size fraction range cannot explain the high variability.

Ganssen and Kroon (2000) show that *Globigerina bulloides* does not reflect the summer temperature as assumed by Duplessy *et al.* (1991). Indeed its calcification is affected by a latitudinal effect: it starts in February-March at medium latitudes (30-40°N) and it reaches its maximum in April-June at higher latitudes (~60°N; Ganssen and Kroon, 2000). It is assumed that the pattern of shifting calcification in time with the latitude reflects the movements of the spring bloom (Wolf and Woods, 1988). At the Vøring Plateau *G. bulloides* is assumed to calcify between April and June (Ganssen and Kroon, 2000). Such a large time span in calcification between April and June could explain the presence of specimen that calcified in different time of the year, and for this reason have different tests compositions. Moreover, at latitudes higher than 57°N in the same period (late spring-early summer) a deep mixing of the water affects the whole water column down to 200 m depth (Ganssen and Kroon, 2000). In such conditions of change between the winter and the summer circulation the mixing in the water column results in differences in isotopic composition of the water and temperature even at the same water depth. Changes in the water composition at the same depth are reflected in the composition of the tests of the organisms that calcify in this period. As a consequence these organisms will show high frequency variability in the paleotemperatures reconstructions. Although at the present state this is just a theory, but new studies in the biology and physiology of this species and further studies on the fossil specimens will help understanding the reasons of such a high variability.

6. CONCLUSIONS

The early Holocene as recorded in the core MD95-2011 is characterized by a warm peak at 10.8 ka in the Mg/Ca analysis. During this period the influence of the Atlantic warm water increased, as supported by the investigations of Hald *et al.* (2007) and Risebrobakken *et al.* (submitted). During this period an increase in heat or/and an increased northwards transport took place in the North Atlantic. The Mg/Ca temperatures show a cold period between 8-10 ka. The results of this work suggest that the 8.2 was not the only cooling event during the Holocene. The Mg/Ca temperatures displays a cooling event at 7.9 ka not correlated with the 8.2 event. A cooling event at 8.1 ka represents the end of the minimum of the 8.2 event in this study. Comparable temperature reduction occurred at 9.1 ka, this event is comparable with the ones reported from other microfossil records from cores of the North Atlantic (Bond *et al.*, 2001; Came *et al.*, 2007, Risebrobakken *et al.*, submitted; Thornalley *et al.*, 2009), and overlap with increased dust content and a cooling event seen in the GISP2 (O'Brien *et al.*, 1995). This event is confirmed by a reported decrease in solar irradiance in the Northern Hemisphere (Neff *et al.*, 2001).

The middle Holocene (2-8 ka) is characterized by stable temperatures, seen in both Mg/Ca and $\delta^{18}\text{O}$ records of this study. In the same core (MD95-2011) during the same period phytoplanktonic surface dwelling species show warm temperatures that slowly decrease towards the late Holocene. The warm period seen in the phytoplanktonic records well compares with the higher summer SST and higher summer insolation seen in this period. As noticed by Risebrobakken *et al.* (submitted), this warm trend is not seen in foraminiferal record because the increased temperatures influenced barely the upper part of the water column, interesting only the summer mixed layer (SML).

The late Holocene in Mg/Ca record of the MD95-2011 core in this study shows a long warm period (800-2400 yr BP) that partly overlaps with a warm period (800-1200) seen in other records from the same core (Andersson *et al.*, 2003). Between 600-800 yr BP a cooling period, that interrupts the warm trend, is seen in the Mg/Ca temperatures dataset. This period overlaps with colder foraminiferal SST in the Norwegian Sea (Andersson *et al.*, 2003) and well overlaps with the Little Ice Age period. The oxygen isotopic record of the late Holocene indicates a warming trend. The same warming trend is seen in the whole North Atlantic in different archives. This warming period is thought to be connected with an east-northward shift in the Arctic front.

In summary the stable isotopes and Mg/Ca records of *G. bulloides* from the Vøring Plateau show a long term temperature increase during the Holocene in the Norwegian Sea. This general trend is in agreement with the observations reported from previously studies on cores of the

North Atlantic, suggesting that this warming trend affected the whole North Atlantic region. The observed trend in the North Atlantic region relates to the influence of Atlantic and Arctic water masses. The Atlantic-Arctic influence can be related to changes in the dynamics of the subpolar gyre (Hátún *et al.*, 2005), since the subpolar gyre dynamics influence the north Atlantic water masses circulation, however this influence has been verified just on decadal timescale. In general the abrupt climatic events seen in this study compare well with terrestrial and marine records of the Norwegian Sea and North Atlantic, showing a common climatic pattern.

Globigerina bulloides analysis results give some uncertain data such as very high temperatures values (e.g. 20°C at 10.8 ka), and high variability, that are difficult to interpret. The high variability values can partly be caused by calcification of the specimens during spring, when changes from the winter to the summer circulation take place. The high variability affects all the reconstructed records (Mg/Ca, $\delta^{18}\text{O}$ and $\delta^{13}\text{C}$ record) for this species in this study and for *Neogloboquadrina pachyderma* (dex.) (Nyland *et al.*, 2006) in the same core. This suggests that the observed variability is not a peculiarity of *G. bulloides*. Therefore the source of the variability may be a variation in the sea conditions during the calcification season, so that in the same month in different years the recorded water conditions can be very different. The high temperatures recorded in the Mg/Ca record throughout the whole analysed period shows that the concentration of Mg in the tests is much higher than what expected to be. However, the main trend and most of the data well correlate with other records from the North Atlantic. Therefore the trend in the record reflects the water conditions and temperature variations, but some kind of vital effect is needed to explain such high Mg values. Vital effect can have affected the calcification process, however other records of *G. bulloides* did not show such pattern.

In summary *Globigerina bulloides* record compares well with other foraminiferal records from the north Atlantic, demonstrating that this species reflects the changes in the water conditions more than the insolation. *Globigerina bulloides* can be used as paleotemperatures proxy, but new studies in the biology and physiology of this species and further studies of fossil specimens are needed to better understand its calcification patterns and explain the high Mg content in the tests.

BIBLIOGRAPHY

- Alley, R. B., and A. M. Ágústadóttir (2005). The 8k event: Cause and consequences of a major Holocene abrupt climate change. *Quaternary Science Reviews*, **24**: 1123-1149.
- Alley, R. B., J. Marotzke, W. D. Nordhaus, J. T. Overpeck, D. M. Peteet, R. A. Pielke Jr., R. T. Pierrehumbert, P. B. Rhines, T. F. Stocker, L. D. Talley and J. M. Wallace (2003). Abrupt climate change. *Science*, **299**: 2005–2010 (DOI: 10.1126/science.1081056).
- Alley, R. B., P. A. Mayewski, T. Sowers, M. Stuiver, K. C. Taylor, and P. U. Clark, Holocene climatic instability (1997). A prominent, widespread event 8200 yr ago. *Geology*, **25**(6): 483–486.
- Anand, P., H. Elderfield, and M. H. Conte (2003). Calibration of Mg/Ca thermometry in planktonic foraminifera from a sediment trap time series. *Paleoceanography*, **18**(2): 1050 (DOI: 10.1029/2002PA000846).
- Andersson, C., F. Pausata, E. Jansen, B. Risebrobakken, and R. J. Telford (2010). Holocene trends in the foraminifer record from the Norwegian Sea and the North Atlantic Ocean. *Climate of the Past*, **6**: 179-193.
- Andersson, C., B. Risebrobakken, E. Jansen, and S. O. Dahl (2003). Late Holocene surface ocean conditions in the Norwegian Sea (Vøring Plateau). *Paleoceanography*, **18**(2): 1044 (DOI: 10.1029/2001PA000654).
- Armstrong, H. A., and M. D. Brasier (2005). Microfossils, second edition. *Foraminifera*, Blackwell Publishing: 142-187.
- Barker, S., and H. Elderfield (2002). Foraminiferal calcification response to glacial-interglacial changes in atmospheric CO₂. *Science*, **297**(5582): 833–836 (DOI: 10.1126/science.1072815).
- Barker, S., M. Greaves, and H. Elderfield (2003). A study of cleaning procedures used for foraminiferal Mg/Ca paleothermometry. *Geochemistry Geophysics Geosystems*, **4**(9): 8407 (DOI: 10.1029/2003GC000559).
- Barreiro, M., A. Fedorov, R. Pacanowski, and S. G. Philander (2008). Abrupt Climate Changes: How Freshening of the Northern Atlantic Affects the Thermohaline and Wind-Driven Oceanic Circulations. *Annual Review of Earth and Planetary Sciences*, **36**: 33 -58.
- Birks, C. J. A., and N. Koç (2002). A high-resolution diatom record of late-Quaternary sea-surface temperatures and oceanographic conditions from the eastern Norwegian Sea. *Boreas*, **31**(4): 323–344.
- Blindheim, J., V. Borovkov, B. Hansen, S. A. Malmberg, W. R. Turrell, and S. Østerhus (2000). Upper layer cooling and freshening in the Norwegian Sea in relation to atmospheric forcing. *Deep Sea Research Part I*, **47**(4): 655–680.
- Blindheim, J., and S. Østerhus (2005). The Nordic seas, main oceanographic features. In: H. Drange *et al* (Eds.), The Nordic Seas: an Integrated Perspective. *Geophysical Monograph Series*, **158**. American Geophysical Union: 11–38.
- Bond, G., B. Kromer, J. Beer, R. Muscheler, M. N. Evans, W. Showers, S. Hoffmann, R. Lottibond, I. Hajdas, and G. Bonani (2001). Persistent Solar Influence on North Atlantic Climate During the Holocene. *Science*, **294**(5549): 2130-2136. (DOI: 10.1126/science.1065680).
- Bond, G., W. Showers, M. Cheseby, R. Lotti, P. Almasi, P. deMenocal, P. Priore, H. Cullen, I. Hajdas, and G. Bonani (1997). A Pervasive Millennial-Scale Cycle in North Atlantic Holocene and Glacial Climates. *Science*, **278**(5341): 1257–1266. (DOI: 10.1126/science.278.5341.1257).
- Boyle, E. A. (1981). Cadmium, zinc, copper, and barium in foraminifera tests. *Earth and Planetary Science Letters*, **53**: 11–35.
- Boyle E. A., and L. D. Keigwin (1985). Comparison of Atlantic and Pacific paleochemical records for the last 250,000 years: changes in deep ocean circulation and chemical inventories. *Earth and Planetary Science Letters*, **76**: 135–150.
- Broecker, W. S. (1997). Thermohaline circulation, the Achilles heel of our climate system: Will man-made CO₂ upset the current balance? *Science*, **278**(5343): 1582 – 1588 (DOI: 10.1126/science.278.5343.1582).

- Brown, S. J., and H. Elderfield (1996). Variations in Mg/Ca and Sr/Ca ratios of planktonic foraminifera caused by postdepositional dissolution: Evidence of shallow Mg- dependent dissolution. *Paleoceanography*, **11**: 543–551.
- Burrows, M., S. A. Thorpe, and D. T. Meldrum (1999). Dispersion over the Hebridean and Shetland shelves and slopes. *Continental Shelf Research*, **19**: 49–55.
- Burton E. A., and L. M. Walter (1991). The effects of pCO₂ and temperature on magnesium incorporation in calcite in seawater and MgCl₂-CaCl₂ solutions. *Geochimica et Cosmochimica Acta*, **55**: 775–785.
- Calvo, E., J. Grimalt, and E. Jansen (2002). High resolution U37 K sea surface temperature reconstruction in the Norwegian Sea during the Holocene. *Quaternary Science Reviews*, **21**: 1385–1394.
- Came, R. E., D. W. Oppo, and J. F. McManus (2007). Amplitude and timing of temperature and salinity variability in the subpolar North Atlantic over the past 10 k.y. *Geology*, **35**: 315–318.
- Carlson, A. E., A. N. LeGrande, D. W. Oppo, R. E. Came, G. A. Schmidt, F. S. Anslow, J. M. Licciardi, and E. A. Obbink (2008). Rapid early Holocene deglaciation of the Laurentide ice sheet. *Nature Geoscience*, **1**: 620–624 (DOI: 10.1038/ngeo285).
- CCSP (2008). *Abrupt Climate Change*. A report by the U.S. Climate Change Science Program and the Subcommittee on Global Change Research (Clark, P.U., A.J. Weaver (coordinating lead authors), E. Brook, E.R. Cook, T.L. Delworth, and K. Steffen (chapter lead authors)). U.S. Geological Survey, Reston, VA, 459 pp.
- Chapman, M. R., and N. J. Shackleton (2000). Evidence of 550-year and 1000-year cyclicity in North Atlantic circulation patterns during the Holocene. *The Holocene*, **10**: 287–291.
- Clark, P. U., N. G. Pisias, T. S. Stocker, and A. J. Weaver (2002). The role of the thermohaline circulation in abrupt climate change. *Nature*, **415**: 863–869.
- Clarke, G. K. C., D. W. Leverington, J. T. Teller, and A. S. Dyke (2004). Paleohydraulics of the last outburst flood from glacial Lake Agassiz and the 8200 BP cold event. *Quaternary Science Reviews*, **23**: 389–407.
- Coplen, T. (1996). New guidelines for reporting stable hydrogen, carbon, and oxygen-ratio data. *Geochimica et Cosmochimica Acta*, **60**(17): 3359–3360.
- Coplen, T. B., C. Kendall, and J. Hopple (1983). Comparison of stable isotope reference samples. *Nature*, **302**(5905): 236–238.
- Cronin, T. M., G. S. Dwyer, T. Kamiya, S. Schwede, and D. A. Willard (2003). Medieval Warm Period, Little Ice Age and 20th century temperature variability from Chesapeake Bay. *Global and Planetary Change*, **36**: 17–29.
- Curry, W. B., and T. J. Crowley (1987). C-13 in equatorial Atlantic surface waters: Implications for ice age pCO₂ levels. *Paleoceanography*, **2**: 489–531.
- Crutzen, P. J. (2002). Geology of mankind. *Nature*, **415**(3): 23.
- Dahl, S. O., and A. Nesje (1994). Holocene glacier fluctuations at Hardangerjokulen, central-southern Norway: a high-resolution composite chronology from lacustrine and terrestrial deposits. *The Holocene*, **4**: 269–277.
- Dahl-Jensen, D., K. Mosegaard, N. Gundestrup, G. D. Clow, S. J. Johnsen, A. W. Hansen, and N. Balling (1998). Past Temperatures Directly from the Greenland Ice Sheet. *Science*, **282**: 268–271.
- Dekens, P. S., D. W. Lea, D. K. Pak, and H. J. Spero (2002). Core top calibration of Mg/Ca in tropical foraminifera: Refining paleotemperature estimation. *Geochemistry, Geophysics, Geosystems*, **3**(4): 1022, (DOI: 10.1029/2001GC000200).
- Delaney, M. L., A. W. H. Be, and E. A. Boyle (1985). Li, Sr, Mg and Na in foraminiferal calcite shells from laboratory culture, sediment traps and sediment cores. *Geochimica et Cosmochimica Acta*, **49**: 1327–1341.
- Delworth, T. L., P. U. Clark, M. Holland, W. E. Johns, T. Kuhlbrodt, J. Lynch-Stieglitz, C. Morrill, R. Seager, A. J. Weaver, and R. Zhang (2008). The potential for abrupt change in the Atlantic Meridional Overturning Circulation. In: *Abrupt Climate Change*. A report by the U.S. Climate Change Science Program and the Subcommittee on Global Change Research. U.S. Geological Survey, Reston, VA, 258–359.

- Denton, G. H., and W. Karlén (1973). Holocene climate variations—Their pattern and possible cause. *Quaternary Research*, **3**: 155–205.
- Dickson, R. R., and J. Brown (1994). The production of North Atlantic Deep Water: Sources, rates and pathways. *Journal of Geophysical Research*, **99**(C6): 12,319–12,341, (DOI: 10.1029/94JC00530).
- Dolven, J. K., G. Cortese, and K. R. Bjørklund (2002). A high-resolution radiolarian-derived paleotemperature record for the Late Pleistocene-Holocene in the Norwegian Sea. *Paleoceanography*, **17**(4): 1072 (DOI: 10.1029/2002PA000780).
- Drange H, T. Dokken, T. Furevik, R. Gerdes, W. Berger, A. Nesje, K. A. Orvik, Ø. Skagseth, I. Skjelvan, and S. Østerhus (2005). The Nordic Seas: an overview. In: H. Drange *et al.* (Eds.), *The Nordic Seas: An integrated perspective*. AGU Monograph 158. *American Geophysical Union*, Washington DC: 1-10.
- Duplessy, J. C., L. Labeyrie, A. Juillet-Leclerc, F. Maitre, J. Duprat, and M. Sarnthein (1991). Surface salinity reconstruction of the North Atlantic Ocean during the last glacial maximum. *Oceanologica Acta*, **14**: 311-324.
- Dwyer G. S., T. M. Cronin, P. A. Baker, M. E. Raymo, J. S. Buzas, and T. Corregge (1995). North Atlantic deepwater temperature change during late Pliocene and late Quaternary climatic cycles. *Science*, **270**: 1347–1351.
- Elderfield, H., and G. M. Ganssen (2000). Past temperature and $\delta^{18}\text{O}$ of surface ocean waters inferred from foraminiferal Mg/Ca ratios. *Nature*, **405**: 442–445.
- Elderfield, H., M. Vautravers, and M. Cooper (2002). The relationship between shell size and Mg/Ca and Sr/Ca ratios of species of planktonic foraminifera. *Geochemistry, Geophysics, Geosystems*, **3**(8): 1052 (DOI: 10.1029/2001GC000194).
- Ellison, C. R. W., M. R. Chapman, and I. R. Hall (2006). Surface and deep ocean interactions during the cold climate event 8200 years ago. *Science*, **312**: 1929–1932.
- Emiliani, C. (1955). Mineralogical and chemical composition of the tests of certain pelagic foraminifera. *Micropaleontology*, **1**: 377-380.
- Epstein, S., R. Buchsbaum, H. A. Lowenstam, and H. C. UREY (1953). Revised carbonate-water isotopic temperature scale. *Geological Society of America Bulletin*, **64**: 1315-1325.
- Fairbanks, R. G., Wiebe, P. H., and A. W. H. Be (1980). Vertical distribution and isotopic composition of living planktonic foraminifera in the western North Atlantic. *Science*, **207**: 61–63.
- Farmer, E. J., M. R. Chapman, and J. E. Andrews (2008). Centennial-scale Holocene North Atlantic surface temperatures from Mg/Ca ratios in *Globigerina bulloides*. *Geochemistry, Geophysics, Geosystems*, **9**: Q12029 (DOI: 10.1029/2008GC002199).
- Fraile, I., M. Schulz, S. Mulitza, U. Merkel, M. Prange, and A. Paul (2009). Modeling the seasonal distribution of planktonic foraminifera during the Last Glacial Maximum. *Paleoceanography*, **24**: PA2216 (DOI: 10.1029/2008PA001686).
- Ganachaud, A., and C. Wunsch (2000). Improved estimates of global ocean circulation, heat transport and mixing from hydrographic data. *Nature*, **408**: 453-457.
- Ganssen, G. M., and D. Kroon (2000). The isotope signature of planktic foraminifera from NE Atlantic surface sediments: implications for the reconstruction of past oceanic conditions. *Journal of the Geological Society of London*, **157**: 693-699.
- Gat, J. R. (1966). Oxygen and hydrogen isotopes in the hydrologic cycle. *Annual Review of Earth and Planetary Sciences*, **24**: 225-262.
- Gervais, P. (1867-9). *Zoologie et paléontologie générales. Nouvelles recherches sur les animaux vertébrés et fossiles*. Paris, 263 pp.
- Gibbard, P., and K. M. Cohen (2008). Global chronostratigraphical correlation table for the last 2.7 million years. *Episodes*, **31**(2): 243-247.
- Gibbard, P., and T. van Kolfshoten (2005). The Pleistocene and Holocene Series. 441-452. In: F. Gradstein *et al.* (Eds). *A Geologic Time Scale 2004*. Cambridge University Press, 589.
- Gleckler, P. J., and B. C. Weare (1997). Uncertainties in global ocean surface heat flux climatologies derived from ship observations. *Journal of Climate*, **10**: 2764-2781.
- Grootes, P. M., M. Stuiver, J. W. C. With, S. Johnsen, and J. Jouzel (1993). Comparison of oxygen isotope records from the GISP2 and GRIP Greenland ice cores. *Nature*, **366**: 552 – 554.

- Grove, J. M., and R. Switsur (1994). Glacial geological evidence for the Medieval Warm Period. *Climate Change*, **26**: 143–169.
- Hald, M., C. Andersson, H. Ebbesen, E. Jansen, D. Klitgaard-Kristensen, B. Risebrobakken, G. R. Salomonsen, M. Sarnthein, H. P. Sejrup, and R. J. Telford (2007). Variations in temperature and extent of Atlantic Water in the Northern North Atlantic during the Holocene. *Quaternary Science Reviews*, **26**(25-28): 3423-3440.
- Helama, S., M. Lindholm, M. Timonen, J. Meriläinen, and M. Eronen (2002). The supra-long Scots pine tree-ring record for Finnish Lapland: Part 2, interannual to centennial variability in summer temperatures for 7500 years. *Holocene*, **12**: 681–687.
- Hemleben C., M. Spindler, and O. R. Anderson (1989). Modern Planktonic Foraminifera. Springer-Verlag New York Berlin Heidelberg London Paris Tokyo: 363 pp.
- Hilbrecht, H., and H. R. Thierstein (1996). Benthic behavior of planktic foraminifera. *Geology*, **24**(3), 200–202.
- Hoefs, J. (2009). Stable isotope geochemistry (6th edition). Springer, Berlin: 1-201.
- Hopkins, T. S. (1991). The GIN sea a synthesis of its physical oceanography and literature review 1972–1985. *Earth-Science Reviews*, **30**: 175–318.
- Houghton, J. T., L. G. Meira Filho, B. A. Callander, N. Harris, A. Kattenberg, and K. Maskell (1995). *Climate Change 1995. The Science of Climate Change*. Contribution of Working Group I to the Second Assessment Report of the Intergovernmental Panel on Climate Change, Cambridge Univ. Press, 584 pp.
- Hurrell, J. W. (1995). Decadal Trends in the North Atlantic Oscillation: Regional Temperatures and Precipitation. *Science*, **269**: 676-679.
- Imbrie, J., and N. G. Kipp (1971). A new micropaleontological method for quantitative paleoclimatology: applications to a late Pleistocene Caribbean core. In: K. K. Turkian (Eds.), *Late Cenozoic Glacial Ages*. Yale University Press, New Haven, 71–191.
- IPCC (2007). *Climate Change 2007. The Physical Science Basis*. Contribution of Working Group I to the Fourth Assessment Report of the Intergovernmental Panel on Climate Change, S. Solomon *et al.* (Eds.), Cambridge Univ Press, Cambridge, UK, 996 pp.
- Jansen, E., C. Andersson, M. Moros, K. H. Nisancioglu, B. F. Nyland, and R. J. Telford (2008.) The early to mid-Holocene thermal optimum in the North Atlantic. In: R.W. Battarbee and H.A. Binney (Eds.), *Natural Climate Variability and Global Warming – A Holocene Perspective*, Wiley-Blackwell: 123–137.
- Jennings, A. E., and N. J. Weiner (1996). Environmental change in eastern Greenland during the last 1300 years: Evidence from foraminifera and lithofacies in Nansen Fjord, 68°N. *Holocene*, **6**: 179–191.
- Johannessen, T., J. Jansen, A. Flatøy, and A. C. Ravelo (1994). The relationship between surface water masses, oceanographic fronts and paleoclimatic proxies in surface sediments of the Greenland, Iceland, Norwegian Seas. In: Zahn *et al.* (Eds.), *Carbon Cycling in the Glacial Ocean: Constraints on the Ocean's Role in Global Change*: 61–85, Springer-Verlag, New York.
- Katz A. (1973). The interaction of magnesium with calcite during crystal growth at 25–90°C and one atmosphere. *Geochimica et Cosmochimica Acta*, **37**: 1563–1586.
- Katz M. E., B. S. Cramer, A. Franzese, B. Hoenisch, K. G. Miller, Y. Rosenthal, and J. D. Wright (2010). Traditional and emerging geochemical proxies in Foraminifera. *Journal of Foraminiferal Research*, **40**(2): 165-192.
- Kaufman, D. S., T. A. Ager, N. J. Anderson, P. M. Anderson, J. T. Andrews, P. J. Bartlein, L. B. Brubaker, L. L. Coats, L. C. Cwynar, M. L. Duvall, A. S. Dyke, M. E. Edwards, W. R. Eisner, K. Gajewski, A. Geirsdottir, F. S. Hu, A. E. Jennings, M. R. Kaplan, M. W. Kerwin, A. V. Lozhkin, G. M. MacDonald, G. H. Miller, C. J. Mock, W. W. Oswald, B. L. Otto-Bliesner, D. F. Porinchu, K. Ruhland, J. P. Smol, E. J. Steig, B. B. Wolfe (2004). Holocene thermal maximum in the western Arctic (0-180 W). *Quaternary Science Reviews*, **23**: 529–560.
- Kennett, J. P., and M. S. Srinivasan (1983). *Neogene Planktonic Foraminifera: A phylogenetic atlas*. Hutchinson Ross Publishing Company, Stroudsburg, Pennsylvania, 265 pp.
- Kerr, R. A. (2000). A North Atlantic Climate Pacemaker for the Centuries. *Science*, **288**(5473): 1984-1985.

- Klitgaard-Kristensen, D., H. P. Sejrup, H. Haflidason, S. Johnsen, and M. Spurk (1998). A regional 8200 cal. yr BP cooling event in northwest Europe, induced by final stages of the Laurentide ice-sheet deglaciation?, *Journal of Quaternary Science*, **13**(2): 165–169.
- Koç, N., and E. Jansen (1992). A high-resolution diatom record of the last deglaciation from the SE Norwegian Sea: Documentation of rapid climatic changes. *Paleoceanography*, **7**: 499–520.
- Kuhlbrodt, T., A. Griesel, M. Montoya, A. Levermann, M. Hofmann, and S. Rahmstorf (2007). On the driving processes of the Atlantic meridional overturning circulation. *Reviews of Geophysics*, **45**: RG2001 (DOI: 10.1029/2004RG000166).
- Kutzbach, J. E., and T. Webb III (1993). Conceptual understanding of climate change. In H. E. Wright *et al.* (Eds.), *Global Climates Since the Last Glacial Maximum*. University of Minnesota Press, Minneapolis: 5-11.
- Lamb, H. H. (1977). *Climate: present, past and future*. Volume 2: *Climatic History and the Future*. Methuen and Co. Ltd., London, XXX + 835 pp.
- Lamb, H. H. (1982). *Climate, History and the Modern World*. Methuen and Co. Ltd., London, 382 pp.
- Lea, D. W., and Boyle, E. (1991). Barium in planktonic foraminifera. *Geochimica et Cosmochimica Acta*, **55**: 3321–3331.
- Lea, D. W., T. A. Mashiota, and H. J. Spero (1999). Controls on magnesium and strontium uptake in planktonic foraminifera determined by live culturing. *Geochimica et Cosmochimica Acta*, **63**: 2369–2379.
- Lear, C. H., Y. Rosenthal, and N. Slowey (2002). Benthic foraminiferal Mg/Ca-paleothermometry: A revised core-top calibration. *Geochimica et Cosmochimica Acta*, **66**: 3375–3387.
- Leduc, G., *et al.* (2010). Holocene and Eemian sea surface temperature trends as revealed by alkenone and Mg/Ca paleothermometry. *Quaternary Science Reviews*, **29**: 989-1004.
- Linden, M., P. Møller, B. Svante, and P. Sandgren (2006). Holocene shore displacement and deglaciation chronology in Norrbotten, Sweden. *Boreas*, **35**: 1-22 (DOI: 10.1080/03009480500359160).
- Litt, T., A. Brauer, T. Goslar, J. Merkt, K. Balaga, H. Müller, M. Ralska-Jasiewiczowa, M. Stebich, and J. F. W. Negendank (2001). Correlation and synchronisation of Lateglacial continental sequences in northern central Europe based on annually laminated lacustrine sediments. *Quaternary Science Reviews*, **20**: 1233–1249.
- Liu, Z., E. Brady, and J. Lynch-Stieglitz (2003). Global ocean response to orbital forcing in the Holocene. *Paleoceanography*, **18**: 1041.
- Loeblich, A.R., and H. Tappan (1988). *Foraminiferal Genera and their Classification*. Van Nostrand Reinhold, New York, 2 vols. 970 pp.
- Lund, D. C., J. Lynch-Stieglitz, and W. B. Curry (2006). Gulf Stream density structure and transport during the past millennium. *Nature*, **444**: 601-604.
- Lyell C. (1839). *Elements of Geology*, Pitois-Levrault, Paris, 648 pp.
- Mangerud, J., S. T. Andersen, B. E. Berglund, and J. J. Donner (1974). Quaternary stratigraphy of Norden, a proposal for terminology and classification. *Boreas*, **3**: 109–128.
- Mangerud, J., S. Bondevik, S. Gulliksen, A.K. Hufthammer and T. Høisæter (2006). Marine ¹⁴C reservoir ages for 19th century whales and molluscs from the North Atlantic. *Quaternary Science Reviews*, **25**: 3228–324.
- Mann, M. E. (2002). Medieval Climatic Optimum, *in* Volume 1, The Earth system: physical and chemical dimensions of global environmental change. In: M. C. MacCracken and J. S. Perry (Eds.), *Encyclopedia of Global Environmental Change*, John Wiley & Sons, Ltd, Chichester: 514-516.
- Mann, M. E., and P. D. Jones (2003). Global surface temperatures over the past two millennia. *Geophysical Research Letters*, **30**(15): 1820-1823.
- Marchal, O., I. Cacho, T. F. Stocker, J. O. Grimalt, E. Calvo, B. Martrat, N. J. Shackleton, M. Vautravers, E. Cortijo, S. van Kreveld, C. Andersson, N. Koç, M. R. Chapman, L. Saffi, J.-C. Duplessy, M. Sarnthein, J.-L. Turon, J. Duprat, and E. Jansen (2002). Apparent long-term cooling of the sea surface in the northeast Atlantic and Mediterranean during the Holocene. *Quaternary Science Reviews*, **21**: 455–483.

- Martin, P. A., and D. W. Lea (2002). A simple evaluation of cleaning procedures on fossil benthic foraminiferal Mg/Ca. *Geochemistry, Geophysics, Geosystems*, **3**(10): 8401 (DOI: 10.1029/2001GC000280).
- McCrea, J. M. (1950). On the Isotopic Chemistry of Carbonates and a Paleotemperature Scale. *The Journal of Chemical Physics*, **18**(6): 849-857.
- Meland, M. Y., E. Jansen, H. Elderfield, T. M. Dokken, A. Olsen, and R. G. J. Bellerby (2006). Mg/Ca ratios in the planktonic foraminifer *Neogloboquadrina pachyderma* (sinistral) in the northern North Atlantic/Nordic Seas. *Geochemistry, Geophysics, Geosystems*, **7**, Q06P14 (DOI: 10.1029/2005GC001078).
- Mitsuguchi T., E. Matsumoto, O. Abe, T. Uchida, and P. J. Isdale (1996). Mg/Ca thermometry in coral skeletons. *Science*, **274**: 961-963.
- Morel, A., and D. Antoine (1994). Heating rate within the upper ocean in relation to its bio-optical state. *Journal of Physical Oceanography*, **24**: 1652-1665.
- Moros, M., K. Emeis, B. Risebrobakken, I. Snowball, A. Kuijpers, J. F. McManus, and E. Jansen (2004). Sea surface temperatures and ice rafting in the Holocene North Atlantic: Climate influences on northern Europe and Greenland. *Quaternary Science Reviews*, **23**: p. 2113-2126.
- Naidu, P. D., and N. Niitsuma (2004). Atypical ¹³C signature in *Globigerina bulloides* at the ODP site 723A (Arabian Sea): implications of environmental changes caused by upwelling. *Marine Micropaleontology*, **53**(1-2), 1-10.
- Neff, U., S. J. Burns, A. Mangini, M. Mudelsee, D. Fleitmann, and A. Matter (2001). Strong coherence between solar variability and the monsoon in Oman between 9 and 6 kyr ago. *Nature*, **411**: 290-293 (DOI: 10.1038/35077048).
- Nesje, A., S. Dahl, T. Thun, and Ø. Nordli (2007). The 'Little Ice Age' glacial expansion in western Scandinavia: summer temperature or winter precipitation?. *Climate dynamics*, **30**(7): 789-801.
- Nesje, A., E. Jansen, H. J. B. Birks, A. E. Bjune, J. Bakke, C. D. Andersson, S. O. Dahl, D. Klitgaard-Kristensen, S-E. Lauritzen, Ø. Lie, B. Risebrobakken, and J. I. Svendsen (2005). Holocene climate variability in the Northern North Atlantic region: a review of marine and terrestrial evidence. In: H. Drange *et al.* (Eds.), *The Nordic Seas: An Integrated Perspective*, AGU Monograph 158, American Geophysical Union, Washington DC 289-321.
- Nichols, R. C., and R. G. Williams (2008). *Enciclopedia of marine science*. (Eds.) Facts on file.
- Nilsen, J. E. Ø., and E. Falck (2006). Variations of mixed layer properties in the Norwegian Sea for the period 1948-1999. *Progress in Oceanography*, **70**: 58-90.
- NODC WOA98 (1998): <http://iridl.ldeo.columbia.edu/SOURCES/.NOAA/NODC/WOA98/>.
- Nordli, P. Ø., Ø. Lie, A. Nesje, S. O. Dahl (2003). Spring-summer temperature reconstruction in western Norway 1734-2003: a data-synthesis approach. *International Journal of Climatology*, **23**: 1821-1841.
- Norris, R. D. (1996). Symbiosis as an evolutionary innovation in the radiation of Paleocene planktic foraminifera. *Paleobiology*, **22**(4): 461-480.
- Nürnberg, D. (1995). Magnesium in tests of *Neogloboquadrina pachyderma* sinistral from high northern and southern latitudes. *Journal of Foraminiferal Research*, **25**(4): 350-368.
- Nyland, B. F., E. Jansen, H. Elderfield, and C. D. Andersson (2006). *Neogloboquadrina pachyderma* (dex. and sin.) Mg/Ca and $\delta^{18}\text{O}$ records from the Norwegian Sea. *Geochemistry, Geophysics, Geosystems*, **7**: Q10P17 (DOI: 10.1029/2005GC001055).
- O'Brien, S.R., P. A. Mayewski, L. D. Meeker, D. A. Meese, M.S. Twickler, and S. I. Whitlow (1995). Complexity of Holocene climate as reconstructed from a Greenland ice core. *Science*, **270**: 1962-1964.
- Orvik, K. A., and P. Niiler (2002). Major pathways of Atlantic water in the northern North Atlantic and Nordic Seas towards Arctic. *Geophysical Research Letters*, **29**(19): 1896.
- Sala, O. E., F. S. Chapin, J. J. Armesto, E. Berlow, J. Bloomfield, R. Dirzo, E. Huber-Sanwald, L. F. Huenneke, R. B. Jackson, A. Kinzig, R. Leemans, D. M. Lodge, H. A. Mooney, M. Oesterheld, N. L.R. Poff, M. T. Sykes, B. H. Walker, M. Walker, and D. H. Wall (2000). Global Biodiversity Scenarios for the Year 2100. *Science*, **287** (5459): 1770-1774. (DOI: 10.1126/science.287.5459.1770)

- Paillard, D., L. Labeyrie and, P. Yiou (1996). Macintosh program performs time-series analysis, *Eos Trans. AGU*, **77**: 379. (http://www.agu.org/eos_elec/96097e.html)
- Pedersen, O. P., M. Zhou, K. S. Tande, and A. Edvardsen (2005). Eddy formation on the coast of North Norway-evidence by synoptic sampling. *ICES Journal of Marine Science*, **62**: 615-628.
- Peeters, F. J. C., G. J. A. Brummer, and G. Ganssen (2002). The effect of upwelling on the distribution and stable isotope composition of *Globigerina bulloides* and *Globigerinoides ruber* (planktic foraminifera) in modern surface waters of the NW Arabian Sea. *Global and Planetary Change*, **34**: 269–291.
- Peltier, W (2004). Global glacial isostasy and the surface of the ice-age Earth: The ICE-5G (VM2) model and GRACE. *Annual Review of Earth and Planetary Sciences*, **32**: 111-149.
- Pflaumann, U., M. Sarnthein, M. Chapman, L. d'Abreu, B. Funnell, M. Huels, T. Kiefer, M. Maslin, H. Schultz, J. Swallow, S. van Kreveld, M. Vautravers, E. Vogelsang, and M. Weinelt (2003). Glacial North Atlantic Sea-surface conditions reconstructed by GLAMAP 2000. *Paleoceanography*, **18**: 1.
- Porter S. C., G. H. Denton (1967). Chronology of neoglaciation in the North American Cordillera. *American Journal of Science*, **265**: 177–210.
- Rahmstorf S. (1995). Bifurcation of the Atlantic thermohaline circulation in response to changes in the hydrological cycle. *Nature*, **378**:145–49.
- Rahmstorf, S. (2006). Thermohaline Ocean Circulation. *Encyclopedia of Quaternary Sciences*. S. A. Elias, Elsevier, Amsterdam.
- Rasmussen, S. O., K. K. Andersen, A. M. Svensson, J. P. Steffensen, B. M. Vinther, H. B. Clausen, M-L. Siggaard-Andersen, S. J. Johnsen, L. B. Larsen, D. Dahl-Jensen, M. Bigler, R. Röthlisberger, H. Fischer, K. Goto-Azuma, M. E. Hansson, and U. Ruth (2006). A new Greenland ice core chronology for the last glacial termination. *Journal of Geophysical Research*, **111**: D06102 (DOI: 06110.01029/02005JD006079).
- Renssen, H., H. Seppä, O. Heiri, D. M. Roche, H. Goosse, and T. Fichefet (2009). The spatial and temporal complexity of the Holocene thermal maximum. *Nature Geoscience*, **2**(6): 410-413.
- Risebrobakken, B., E. Jansen, C. Andersson, E. Mjelde, and K. Hevrøy (2003). A high-resolution study of Holocene paleoclimatic and paleoceanographic changes in the Nordic Seas. *Paleoceanography*, **18**(1): 1017 (DOI: 10.1029/2002PA000764).
- Risebrobakken, B., Dokken T., Smedsrud L. H., Andersson C., Jansen E., Moros M., and Ivanova E. V. (submitted). Distinguishing early Holocene temperatures changes caused by northward oceanic heat advection from the ocean temperature response to changes in orbital forcing. *Paleoceanography*.
- Rosenthal, Y., E. A. Boyle, and N. Slowey (1997). Temperature control on the incorporation of magnesium, strontium, fluorine, and cadmium into benthic foraminiferal shells from Little Bahama Bank: Prospects for thermocline paleoceanography. *Geochimica et Cosmochimica Acta*, **61**: 3633–3643.
- Sautter, R.L., and R. C. Thunell (1991). Planktonic foraminiferal response to upwelling and seasonal hydrographic condition: sediment trap results from San Pedro Basin, Southern California Bight. *Journal of Foraminiferal Research*, **21**: 347–363.
- Sharp, Z. (2007). Chapter 2: Terminology, standards, and mass spectrometry. *Stable Isotope Geochemistry*, Pearson Prentice Hall, Pearson Education, Inc., U. S, 334pp.
- Simstich J, M. Sarnthein, and H. Erlenkeuser (2003). Paired $\delta^{18}\text{O}$ signals of *Neogloboquadrina pachyderma* (s) and *Turborotalita quinqueloba* show thermal stratification structure in Nordic Seas. *Marine Micropaleontology*, **48**: 107-125.
- Spero, H. J., I. Lerche, and D. F. Williams (1991). Opening the carbon isotope “vital effect” black box, 2, Quantitative model for interpreting foraminiferal carbon isotope data. *Paleoceanography*, **6**: 639–655.
- Spero, H. J., and D. W. Lea (1996). Experimental determination of stable isotope variability in *Globigerina bulloides*: implications for paleoceanographic reconstructions. *Marine Micropaleontology*, **28**(3-4): 231-246.

- Stouffer R. J., J. Yin, J. M. Gregory, K. W. Dixon, M. J. Spelman, W. Hurlin, A. J. Weaver, M. Eby, G. M. Flato, H. Hasumi, A. Hu, J. H. Jungclaus, I. V. Kamenkovich, A. Levermann, M. Montoya, S. Murakami, S. Nawrath, A. Oka, W. R. Peltier, D. Y. Robitaille, A. Sokolov, G. Vettoretti, and S. L. Weber (2006). Investigating the causes of the response of the thermohaline circulation to past and future climate changes. *Journal of Climate*, **19**: 698–722.
- Stuvier, M., P. J. Reimer, E. Bard, J. W. Beck, G. S. Burr, K. A. Hughen, B. Kromer, G. McCormac, J. van der Plicht, and M. Spurk (1998). INTCAL98 radiocarbon age calibration, 24,000–0 cal BP. *Radiocarbon*, **40**: 1041–1083.
- Széréméta, N., F. Bassinot, Y. Balut, L. Labyrie, and M. Pagel (2004). Oversampling of sedimentary series collected by giant piston corer: Evidence and corrections based on 3.5–kHz chirp profiles. *Paleoceanography*, **19**: PA1005 (DOI: 10.1029/2002PA000795).
- Thornalley, D. J. R., H. Elderfield, and I. N. McCave (2009). Holocene oscillations in temperature and salinity of the surface subpolar North Atlantic. *Nature*, **457**: 711–714.
- Thornalley, D. J. R., I. N. McCave, and H. Elderfield (2010). Freshwater input and abrupt deglacial climate change in the North Atlantic. *Paleoceanography*, **25**: PA1201 (DOI: 10.1029/2009PA001772).
- Urey, H. C. (1947). The thermodynamic properties of isotopic substances. *Journal of Chemical Society*: 562–581.
- Vinther, B. M., S. L. Buchardt, H. B. Clausen, D. Dahl-Jensen, S. J. Johnsen, D. A. Fisher, 929 R. M. Koerner, D. Raynaud, V. Lipenkov, K. K. Andersen, T. Blunier, S. O. Rasmussen, J. P. Steffensen, and A. M. Svensson (2009). Holocene thinning of the Greenland ice sheet. *Nature*, **461**: 385–388.
- Walker, J.D., and J. W. Geissman compilers, (2009). Geologic Time Scale: Geological Society of America (DOI: 10.1130/2009.CTS004R2C).
- Walker, M., S. Johnses, S. O. Rasmussen, J. P. Steffensen, T. Popp, P. Gibbard, W. Hoek, J. Lowe, S. Björck, L. C. Cwynar, K. Hughen, P. Kershaw, B. Kromer, T. Litt, D. J. Lowe, T. Nakagawa, R. Newnham, and J. Schwander (2008). The Global Stratotype Section and Point (GSSP) for the base of the Holocene Series/Epoch (Quaternary System/Period) in the NGRIP ice core. *Episodes*, **31**: 264–267.
- Walker, M., S. Johnsen, S. O. Rasmussen, J-P. Steffensen, T. Popp, P. Gibbard, W. Hoek, J. Lowe, J. Andrews, S. Björck, L. C. Cwynar, K. Hughen, P. Kershaw, B. Kromer, T. Litt, D. J. Lowe, T. Nakagawa, R. Newnham, J. Schwander (2009). Formal definition and dating of the GSSP (Global Stratotype section and Point) for the base of the Holocene using the Greenland NGRIP ice core, and selected auxiliary records. *Journal of Quaternary Science*, **24**(1): 3–17.
- Wolf, K. U. and C. M. Tang (1988). Lagrangian simulation of primary production in the physical environment- the deep chlorophyll maximum and nutricline. In: Rothschild, B. J. (ed.) *Towards a Theory on Biological-Physical Interactions in the World Ocean*. Kluwer, Dordrecht, 51–70.
- Wolff, E. W. (2008). What is the “present”? *Quaternary Science Reviews*, **26**: 3023–2024.
- <http://www.eol.org/pages/489860>
- www.noaa.gov

APPENDIX I

Followed Mg/Ca and Sr/Ca Foraminiferal Cleaning Procedure

1. Foraminifera Cleaning Procedure for Mg

2. Reagents

1. Foraminifera Cleaning Procedure for Mg

The procedure is written assuming moderately difficult (e.g. *bulloides*), cold (< 2 mmol/mol Mg/Ca) samples and includes transfer to low Mg blank vials before stages involving acid.

N.B. It is important to assess the cleaning requirements of each particular set of samples and modify the stages in the procedure accordingly.

(e.g. for high Mg/Ca samples with little clay infill it may be appropriate to shorten some stages, whereas for cold samples containing IRD it will be necessary to be more rigorous.)

Clean in batches of about 10 samples at a time. Expect to take about 4 hours for the complete procedure.

Weighing:

The method is sensitive enough to analyse as few as one or two foraminifera but for best statistics use at least 20 individuals per sample. Select clean tests and try to keep all the samples approximately the same size. Record details of core, depth, species, size fraction, number of tests and the sample weight if required.

Weigh samples using the microbalance in room S417. Transfer the foraminifera to a stainless steel weighing boat using a glass suction pipette, record the weight and number of individuals. Transfer back to the picking slide after weighing. It is very important to accurately count the number of individuals weighed; an incorrect count of 1 in 20 represents a 5% weighing error.

Crushing:

Foraminifera tests are gently crushed using two clean glass plates - the aim here is to crack open the test chambers to allow any chamber fill to escape during subsequent cleaning, while avoiding over-crushing which will lead to excessive sample loss.

1. Place the tests in a single layer on the lower glass slide. Keep the sample moist with excess water.

2. In a controlled manner, lower the second plate onto the sample and apply gentle pressure in order to open every shell chamber.

3. Remove the upper glass plate and transfer all particles to the lower plate.

At this time, a piece of light coloured paper should be positioned beneath the sample whilst under a microscope. This will reveal the presence of any larger silicate grains that may not be removed during the following clay removal steps. It is not necessary to remove such grains at this stage but only to note their presence so that action may be taken later on.

Clay removal:

During this stage, all samples should be treated individually in order to maximize cleaning effectiveness (batch treatment for ultrasonication is appropriate). It is important to use separate pipette tips for adding and removing reagents.

Having opened the test chambers during crushing, much of the test fill will be loosened and easily brought into suspension.

1. Squirt 500 µl of UHQ H₂O onto the crushed sample (trapped air bubbles may be freed by flicking the tube end with a fingernail).
2. Ultrasonic bath for 30 seconds, in order to remove the possible bubbles of gas between the fragments and the H₂O.
3. Centrifuge the vials for 1 and ½ min at 10000 rpm.
4. Allow the sample to settle for 30 seconds or so.
5. Remove the overlying solution (supernatant) with a separate pipette – the size of a 1000 µl pipette tip is suitable for removing most of the overlying liquid from the tube without risk of sample loss.

At this stage, all tubes should still contain about 10-20 µl of H₂O.

6. Place the sample rack in an ultrasonic bath for 2 minutes - this will encourage separation of more tightly bound clays from the test surfaces.

Suspended clays will appear as a milky residue in the liquid just above the sample.

7. Squirt 500 µl of UHQ H₂O onto each sample - this will agitate the sample and bring loose clays into suspension.
 8. Briefly allow the sample to settle (minimal settling technique) - sufficient settling will only take a number of seconds (long enough for the distinct carbonate grains to reach the bottom). After this period the remaining settling material will mainly comprise unwanted silicate particles.
 9. Remove the overlying solution.
 10. Repeat steps (4) to (7) a further 4 times. More repetitions may be necessary for as long as clays are being visibly brought into suspension by ultrasonication.
- After the water cleaning steps, ethanol is used for further clay removal - the lower viscosity of this reagent should dislodge material still attached to the carbonate tests.
11. Squirt 250 µl of Aristar ethanol into each tube.
 12. Ultrasonicate the tubes for 2 minutes.
 13. Use the vortex mixer for some second with couplets of vials to bring clays into suspension.
 14. Allow sample to settle for a few seconds and remove the ethanol.
 15. Repeat steps (11) to (14).
 16. Repeat steps (7) to (9) in order to remove any remaining methanol (further ultrasonication may be applied if desired).

Removal of organic matter:

1. Add 250 µl of alkali buffered 1% H₂O₂ solution to each tube and secure the rack with a lid to prevent tubes popping open whilst under pressure.
2. Place the sample rack in a boiling water bath for 10 minutes. At 2.5 and 7.5 minutes remove the rack momentarily and rap on the bench top to release any gaseous build-up. At 5 minutes place the rack in an ultrasonic bath for a 30 seconds and return to the water bath after rapping on the bench – the aim of these interim steps is to maintain contact between reagent and sample.
3. Centrifuge the sample tubes (1 minute at 10000 rpm) to remove gas bubbles and ensure the samples have settled then remove the oxidizing reagent using a pipette.
4. Repeat steps (1) to (3).
5. Remove any remaining oxidizing reagent by filling the tube with 500 µl and the lids with UHQ H₂O and removing after settling. This step should be repeated 2 times.

Dilute acid leach:

A dilute acid is used to remove any adsorbed contaminants from the test fragments.

1. Add 250 µl of 0.001M HNO₃ to each sample.
2. Ultrasonicate all samples for 30 seconds.
3. Remove acid from each sample.
4. Squirt 500 µl of UHQ H₂O into each tube.

It is important to replace the leach acid with H₂O as soon as possible for all samples in order to prevent excess dissolution.

5. Remove the overlying H₂O.
 6. Repeat steps (4) and (5).
 7. Using a 10 µl pipette, carefully remove any remaining solution from each sample.
- Samples should be stored after this stage, then dissolved and diluted on the day they are to be run.

Dissolution:

This has to be done the same day of the measurements.

In order to ensure accurate dilutions, it is important that all volumes are accurately pipetted from this stage onwards.

1. Add 350 µl of 0.1 M HNO₃ to each sample (for large samples 500 µl may be used).
2. Ultrasonicate to aid dissolution for at least 5 minutes.
3. Every few seconds, flick each tube to allow any build-up of CO₂ to escape and the reaction to continue.
4. As soon as the production of CO₂ ceases, vortex the samples to mix.
5. Centrifuge (10000 rpm for 5 minutes) to settle any remaining small silicate particles.
6. Immediately transfer 300 µl of solution to a clean sample tube, leaving any particles to be discarded in the residual 50 µl

If the dissolution acid is left on a sample containing any silicate or other non-carbonate material for longer than is necessary to dissolve the sample, there is a high risk of contamination by elemental leaching.

Dilution:

After cleaning and dissolution, 20 planktonic foraminifera should give Ca concentrations in the range 100 – 200 ppm, depending on the species and sample loss during cleaning.

The method for Mg/Ca & Sr/Ca determinations using the Vista ICP-AES requires, for best precision and accuracy, solutions containing known Ca concentrations of typically either 60 or 100 ppm and uses ~250 µl solution per analysis.

Two runs of each sample are required; an initial concentration determination followed by a second run at optimum Ca concentration for Mg/Ca and Sr/Ca determinations.

For samples contained in 350 µl of 0.1 M HNO₃ after centrifuging, a 5 fold dilution should be done for the initial concentration determination, followed by dilution of the remaining concentrate as required.

1. Set up a series of clean 0.5ml thin walled vials for the dilutions.
2. Add 280 µl of 0.1 M HNO₃ to each.
3. Add 70 µl sample to give a 5 fold dilution.

It is important that volumes are accurately pipetted to ensure correct concentration calculations and subsequent dilutions.

Run the diluted samples on the Vista to determine Ca concentrations. Calculate dilutions required to give optimum Ca for the intensity calibration of Mg/Ca & Sr/Ca ratios.

Dilute the remaining 230 µl of sample concentrates as calculated and run on the Vista using the intensity ratio calibration at the appropriate Ca concentration.

2. Reagents

Tip rinse

Acid (10% HNO ₃)	125 ml
Elga UHQ H ₂ O	125 ml

Removal of fine clays

Elga UHQ H ₂ O	125 ml
Methanol (Aristar)	125 ml

Oxidising reagent (to remove organic matter)

Alkali buffered 1% H₂O₂ solution
250 µl oxidising solution used per sample.
Prepare fresh mixture for each batch of samples.
Prepared from:-

Hydrogen peroxide	8 ml
30% w/v Aristar grade. (stored in fridge)	

0.1M sodium hydroxide (Aristar grade) water	500 ml in UHQ
0.1M NaOH = 4g / litre. (NaOH = 40.00g g mol ⁻¹)	

Add 100 µl H ₂ O ₂ to ~10 ml 0.1 M NaOH, sufficient for ~ 20 samples.	15 ml
--	-------

Dilute acid leach

QD 0.001 M HNO ₃	500 ml
250 µl used from 1 - 5 times per sample.	30 ml
75 fold dilution of 0.075 M HNO ₃	
1ml 0.075M HNO ₃ in 75ml UHQ H ₂ O or	
6ml 0.075M HNO ₃ in 450ml UHQ H ₂ O	

Dissolution

QD 0.075 M HNO ₃	1000 ml
500 µl used per sample.	30 ml
200 fold dilution of QD concentrated HNO ₃ (15M)	
5 ml concentrated HNO ₃ in 1 litre UHQ H ₂ O	